UNIVERSIDADE ESTADUAL DE CAMPINAS
Faculdade de Engenharia Elétrica e de Computação

Lucas Lugnani Fernandes

Study of Coherency and Inertia Impacts on Power Systems after Ring-down events using Typicality Data Analysis and Synchrophasors

Estudo de Coerência e Impactos da Inércia em Sistemas de Potência Após Perturbações Severas utilizando Análise de Tipicalidade de Dados e Sincrofasores

Campinas

2022

UNIVERSIDADE ESTADUAL DE CAMPINAS
Faculdade de Engenharia Elétrica e de Computação

Lucas Lugnani Fernandes

Study of Coherency and Inertia Impacts on Power Systems after Ring-down events using Typicality Data Analysis and Synchrophasors

Estudo de Coerência e Impactos da Inércia em Sistemas de Potência Após Perturbações Severas utilizando Análise de Tipicalidade de Dados e Sincrofasores

Thesis presented to the School of Electrical and Computer Engineering of the University of Campinas in partial fulfillment of the requirements for the degree of Doctor in Electrical Engineering, in the area of Electrical Energy

Tese apresentada à Faculdade de Engenharia Elétrica e de Computação da Universidade Estadual de Campinas como parte dos requisitos exigidos para a obtenção do título de Doutor em Engenharia Elétrica, na Área de Energia Elétrica.

Supervisor: Prof. Dr. Daniel Dotta

Co-orientador Prof. Dr. Mario Roberto Arrieta Paternina

Este exemplar corresponde à versão final da tese defendida pelo aluno Lucas Lugnani Fernandes, e orientada pelo Prof. Dr. Daniel Dotta

---

Campinas

2022

Ficha catalográfica
Universidade Estadual de Campinas
Biblioteca da Área de Engenharia e Arquitetura
Rose Meire da Silva - CRB 8/5974

Fernandes, Lucas Lugnani, 1992-
F391s Study of coherency and inertia impacts on power systems after ring-down events using typicality data analysis and synchrophasors / Lucas Lugnani Fernandes. – Campinas, SP : [s.n.], 2022.

Orientadores: Daniel Dotta e Mario Roberto Arrieta Paternina.
Coorientador: Mario Roberto Arrieta Paternina.
Tese (doutorado) – Universidade Estadual de Campinas, Faculdade de Engenharia Elétrica e de Computação.
Em cotutela com: Universidad Nacional Autonoma de Mexico.

1. Coerência (ótica). 2. Resposta em frequência (Dinâmica). 3. Inércia (Mecânica). I. Dotta, Daniel, 1978-. II. Arrieta Paternina, Mario Roberto. III. Arrieta Paternina, Mario Roberto. IV. Universidade Estadual de Campinas. Faculdade de Engenharia Elétrica e de Computação. VI. Título.

Informações para Biblioteca Digital

Título em outro idioma: Estudo de coerência e impactos da inércia em sistemas de potência após perturbações severas utilizando análise de tipicalidade de dados e sincrofasores
Palavras-chave em inglês:
Coherency
Frequency response
Inertia
Área de concentração: Energia Elétrica
Titulação: Doutor em Engenharia Elétrica
Banca examinadora:
Daniel Dotta [Orientador]
Marcos Julio Rider Flores
Guido Rosseto Moraes
Denisson Queiroz Oliveira
Alejandro Zamora Mendez
Data de defesa: 26-08-2022
Programa de Pós-Graduação: Engenharia Elétrica

Identificação e informações acadêmicas do(a) aluno(a)
- ORCID do autor: https://orcid.org/0000-0002-4934-5662
- Currículo Lattes do autor: http://lattes.cnpq.br/2774977052467186

COMISSÃO JULGADORA — TESE (DOUTORADO)

Candidato: Lucas Lugnani Fernandes **RA:** 190725
Data da Defesa: 26/08/2022

Título da Dissertação/Tese: "Study of Coherency and Inertia Impacts on Power Systems after Ring-down events using Typicality Data Analysis and Synchrophasors

Estudo de Coerência e Impactos da Inércia em Sistemas de Potência Após Perturbações Severas utilizando Análise de Tipicalidade de Dados e Sincrofasores"

Prof. Dr. Daniel Dotta (presidente, FEEC/UNICAMP)
Prof. Dr. Marcos Julio Rider Flores (FEEC/UNICAMP)
Prof. Dr. Guido Rosseto Moraes (UFSC)
Prof. Dr. Denisson Queiroz Oliveira (UFMA)
Prof. Dr. Alejandro Zamora Mendez (UMSNH)

A ata de defesa, com as respectivas assinaturas dos membros da Comissão Julgadora, encontra-se no SIGA (Sistema de Fluxo de Dissertação/Tese) e na Secretaria de Pós-Graduação da Faculdade de Engenharia Elétrica e de Computação.

Acknowledgements

This study was financed in part by CNPq, Conselho Nacional de Desenvolvimento Científico e Tecnológico - Brasil, grant 170100/2018-9; this study was also financed in part by grants 2016/08645-9, 2018/07375-3, 2018/20104-9 e 2019/10033-0 for equipment purchases, São Paulo Research Foundation (FAPESP). This work was also partially financed from ENGIE Brasil, under research and development project PD-00403-0053/2021.

Further, my work is not just my own, where the help from my advisors, prof. Dr. Daniel Dotta and prof. Dr. Mario Paternina, was and still is fundamental for my research, which culminated in this thesis, but also career advisement. To lab colleagues, I also leave my thanks for the help within the lab and outside it, making this 4 year trip more bearable and even enjoyable from time to time. Thank you Raul, Marciano, Luigi, Bruno, Marcelo, Maique, Orlem, Filipe, João, Andres, and many others which have helped one way or another throughout these years. I also must be much grateful for all the help and precious comments and data given to me by my research colleagues: Dr. Christoph Lackner, prof. Dr. Morgan Jones, Bruno Pinheiro, prof. Dr. Mario Paternina , prof. Dr. Mathew Peet, prof. Dr. Luis Alberto, prof. Dr. Antonio Aquino, prof. Dr. Joe Chow and prof. Dr. Yilu Liu. I think my work was made more distinct by the help of each of you.

Finally I must thank my family which supported me in my career choice and the moments I doubted myself, all of them, but specially my wife, Yasmim, who was there for me, by phone, internet or shoulder and hug, to push me forward. Thank you all for sharing all the good and bad moments with me, I expect to share more of them with you (hopefully the better ones the most!). With you and God utmost gift, I can say I can always try my best to move forward.

“It’s a dangerous business, Frodo, going out your door. You step onto the road, and if you don’t keep your feet, there’s no knowing where you might be swept off to”

(J.R.R. Tolkien, The Lord of the Rings)

Abstract

This thesis presents a study of the coherency and inertial response of power systems with special focus on application of data-driven methods, using synchrophasor measurements of disturbances extracted from Wide Area Measurement Systems (WAMS), statistical clustering technique Typicality Data Analysis (TDA) and Auto-Regressive Moving-Average eXogenous input (ARMAX) model parametric identification. The overall concepts regarding the physical phenomena and tools of this work are presented and discussed. The methodology proposed for region detection using TDA is first presented, developed and tested using benchmark test systems and validated using real measurements from the Eastern Interconnection. Further, the pilot-bus representative of the Center of Inertia of the regions is identified using TDA and the regional inertial response of each region is estimated using ARMAX parametric model, considering the participation of the load inertial response, the pilot-bus frequency and the region interconnection power flows. The methodology is tested and validated using the benchmark IEEE 68 bus test system.

Keywords: Coherency; Clustering; WAMS; TDA; Pilot-bus; Inertia; Load inertia; TDA.

Resumo

Esta tese apresenta um estudo de coerência e resposta inercial de sistemas de potência com foco especial na aplicação de metodologias baseada em dados, utilizando medidas de sincrofasores de distúrbios extraídos de Sistemas de Medição Fasorial Sincronisada (WAMS, em inglês), técnica estatística de clusterização Análise de Tipicalidade de Dados (TDA, em inglês) e modelo de identificação paramétrico Auto-Regressivo de Média-móvel e entrada eXógena (ARMAX, em inglês). Os conceitos gerais relativos aos fenômenos físicos e ferramentas deste trabalho são apresentados e explicados. A metodologida proposta para detecção de áreas elétricas utilizando TDA é apresentada primeiramente, desenvolvida e testada utilizando modelos de bancada testes e validado utilizando medições reais da Interconexão Leste norte-americana. Ademais, a barra-piloto representatica do Centro de Inércia das regiões é identificada utilizando TDA e a resposta inercial regional estimada utilizando modelo paramétrico ARMAX, considerando a participação da resposta inercial da carga, a frequência da barra-piloto e fluxos de potência de interconexões regionais. A metodologia é testada e validada com os sistema teste de bancada IEEE 68 barras.

Palavras-chave: Coerência; Clusterização; WAMS; TDA; Barra-piloto; Inércia; Inércia da carga; TDA.

Figures List

Figure 1.1 – The transition of modern pwoer systems. 19
Figure 1.2 – Evolution of global installed capacity per primary source, extracted from (GLOBAL. . . , 2021) 20
Figure 1.3 – Archtecture example of a centralized WAMS, extracted from (GORE; KANDE, 2015) 21
Figure 1.4 – Evolution of Blackouts through the last 5 decades, extracted from (NAGLIC, 2022) 22
Figure 1.5 – Available methodologies for Regional Inertia estimation. 24
Figure 1.6 – Thesis methodology proposal. 26
Figure 2.1 – Classification of Power System Stability considering IBR, extracted from (HATZIARGYRIOU et al., 2021) 27
Figure 2.2 – Power system time scales for dynamics, data, and control functions. Special protection schemes (SPS), special protection schemes; Voltage Regulator (VR), voltage regulator; Power System Stabilizer (PSS), power system stabilizer; State estimation (SE), state estimation; Contingency analysis (CA), contingency analysis; Real time market (RTM), real-time market; Day ahead market (DAM), day-ahead market. Extracted from (CHOW; SANCHEZ-GASCA, 2020) 28
Figure 2.3 – Typical frequency response after a disturbance, ... 30
Figure 2.4 – Time-invariant linear system 34
Figure 2.5 – Time-invariant linear system with noise 35
Figure 2.6 – The ARX model structure 43
Figure 2.7 – Slow Coherency Algorithm 54
Figure 2.8 – Slow coherency aggregation steps. 57
Figure 2.9 – Slow-coherency aggregation method 59
Figure 3.1 – Clustering validity example. 73
Figure 3.2 – Correlation map for *Case S1.C1*, for **TDA - Stage II**. 80
Figure 3.3 – *Case S1.C1*: Stages III and IV of the **TDA Algorithm 1**. 80
Figure 3.4 – Areas by the TDA method for *Case S1.C1*. 81
Figure 3.5 – Frequency signals of Areas 6 and 7 during transitory period. 81
Figure 3.6 – Areas by the TDA method for *Case S1.C2*. 83
Figure 3.7 – Areas 2 and 7 generators responses for *Case S1.C2*. 85
Figure 3.8 – WPPs frequency responses to fault at bus 27. 86
Figure 3.9 – Generators from Areas 1, 2 and 7 of *Case S1C1* in *Case S1.C3w*. . . . 87

Figure 3.10–Generator 9 frequency response: connected and islanded with speed regulator. . . . 89
Figure 3.11–Stages III and IV of the TDA for the sixth case in the EI system. . . . 90
Figure 3.12–FNET/GridEye groups for the sixth event. . . . 91
Figure 3.13–Geographical distribution of groups in the EI. . . . 92
Figure 4.1 – Pilot-bus detection and regional inertia estimation. . . . 106
Figure 4.2 – IEEE 68-Bus with 6 areas determined by the TDA method. . . . 110
Figure 4.3 – Metrics Region 5. . . . 112
Figure 4.4 – Cumulative proximities Region 5. . . . 113
Figure 4.5 – Frequency response comparison of f_{coi}, f_{pb}, f_g and f_b for Region 5. . . . 114
Figure 4.6 – Typicalities for S1.m. . . . 115
Figure 4.7 – Input signal - active power of Region 5 tie-lines. Output signal - pilot-bus frequency deviation of Region 5 . . . 117
Figure A.1 – Recursive TDA methodology . . . 140
Figure A.2 – Size controlled window . . . 142
Figure A.3 – KundurTestSystem . . . 142
Figure A.4 – Frequency response of the Kundur test system to 100 MW step at bus 9. 143
Figure A.5 – First set of typicalities. . . . 144
Figure A.6 – Evolution of typicalities. . . . 145
Figure A.7 – Variance of typicalities. . . . 146

Tables List

Table 2.1 – SISO Model Structures 44
Table 2.2 – Model-based methods comparison 56
Table 3.1 – Comparison of requirements for coherency methods 66
Table 3.2 – Areas identified by the TDA method for *Case S1.C1.* 79
Table 3.3 – Correlation statistics for Case 1 (*S1.C1*) 82
Table 3.4 – Clustering results with different time windows 83
Table 3.5 – Areas identified by the TDA method, *Case S1.C2.* 84
Table 3.6 – WPPs for *S1.C3w* 85
Table 3.7 – Areas identified by the TDA method, *Case S1.C3w.* 88
Table 3.8 – Execution time for *Cases S1.C1, S1.C2, and S2* and comparison methods. 92
Table 3.9 – Slow modes Comparison - S1.C1. 94
Table 4.1 – Dynamic load for of NETS/NYPS system. 109
Table 4.2 – Regions and their respective buses for Figure 4.2. 109
Table 4.3 – Regions, detected pilot-buses and NRMSE of frequency responses, with respect to f_{coi} for S1.w. 111
Table 4.4 – Regions, detected pilot-buses and NRMSE of frequency responses, with respect to f_{coi} for S1.m. 113
Table 4.5 – Regional Inertia Estimates for Case 4.6.1.1 116
Table 4.6 – Regional Inertia Estimates for Case 4.6.1.2 116
Table A.1 – Groups in the 2-area Kundur system. 142

Acronyms and Abbreviations List

AC Alternating Current

AHC AAgglomerative hierarchical clustering

AR Autoregressive

ARMAX Autoregressive Moving Average eXogenous input

ARX Autoregressive eXogenous input

AP Affinity propagation

CA Contingency analysis

COI Center of Inertia

CRITIC Criteria importance through inter-criteria correlation

DAM Day ahead market

DBSCAN Density-based spatial clustering of applications with noise

DDM Data-driven methods

DFR Digital Fault Recorders

DFA detrended fluctuation analysis

DFT Discrete Fourier Transform

DREM Dynamic regressor and mixing

DTW Dynamic time warping

EDA Empirical Data Analysis

ESS Electrical storage systems

FCMdd Fuzzy medoids algorithm

FFDD Fast frequency domain decomposition

FIR finite impulse response

GB Great Britain

GPS Global Positioning System

HDBSCAN Hierarchical density-based spatial clustering of applications with noise

IBR Inverter Based Resources

iid independent identically distributed

KPCA Kernel principal component analysis

LQR Linear quadratic regulator

LTI Linear Time-Invariant

MAP Maximum a Posteriori

MBA Model-based approaches

ML Machine learning

MPM Microperturbation method

MRFR Multivariate random forest regression

PDF Probability Density Function

PMU Phasor Measuring Unit

PPCC Pearson product-moment correlation coefficient

PSO Particle swarm optimization

PSS Power System Stabilizer

PV Photovoltaic

RLS Recursive least-squares

ROA Region of Attraction

RoCoF Rate of Change of Frequency

RTE Réseau de Transport d'Électricité

RTM Real time market

SCADA Supervisory Control and Data Acquisition

SE State estimation

SPS Special protection schemes

TDA Typicality Data Analysis

VR Voltage Regulator

WAMS Wide Area Measuring Systems

WAMPAC Wide Area Monitoring Protection and Control

WECC Western Electricity Coordinating Council

ZIP Constant Impedance, constant current, constant power load model

Summary

1 Introduction . . . **18**

1.1 Motivation . . . 23

1.1.1 Objectives . . . 23

1.1.2 Contribution . . . 24

2 Fundamentals . . . **27**

2.1 Stability Classification . . . 27

2.1.1 Frequency response . . . 29

2.2 System Identification . . . 33

2.2.1 Types of Models . . . 34

2.2.1.1 Time-invariant linear systems . . . 34

2.2.1.1.1 Periodic Inputs and Frequency Function . . . 37

2.2.2 Mutivariable Systems . . . 39

2.2.3 Prediction . . . 40

2.2.4 One-step ahead Prediction of v . . . 40

2.2.4.1 Models of Linear Time-Invariant Systems . . . 41

2.2.4.1.1 Equation Error Model Structure . . . 42

2.2.4.1.2 ARMAX Model Structure . . . 43

2.3 Coherency of generators in power systems . . . 45

2.3.1 Overview . . . 45

2.3.2 Slow modes coherency theory . . . 46

2.4 Clustering techniques . . . 50

2.4.1 Slow-coherency algorithm . . . 51

2.4.2 Tolerance based grouping algorithm . . . 53

2.4.3 Comparison between Tolerance-based and Slow-coherency grouping for the NPCC . . . 55

2.5 Aggregation of Machines . . . 56

2.5.1 Slow-coherency method . . . 56

2.5.2 Next Chapters . . . 61

3 A meaningful area to estimate inertia . . . **62**

3.1 State-of-the-art . . . 62

3.2 Problem statement . . . 65

3.3 Contributions . . . 67

3.4 Fundamentals . . . 67

3.4.1 Coherency . . . 67

3.4.2 The Euclidean norm . . . 68
3.4.3 The distance metric: correlation . . . 69
3.5 Typicality-Based Data Analysis . . . 69
3.5.1 Cumulative proximity . . . 69
3.5.2 Standardized eccentricity . . . 70
3.5.3 Discrete local density . . . 71
3.5.4 Discrete typicality . . . 71
3.5.5 Proof of the clustering concept of TDA . . . 71
3.6 TDA Application for Coherency Detection . . . 72
3.6.1 Stage I. Pre-processing . . . 73
3.6.2 Stage II. Metric (correlation) computation . . . 74
3.6.3 Stage III. Properties calculation . . . 74
3.6.4 Stage IV. Typicality ranking . . . 74
3.6.5 Stage V. Cluster formation and filtering . . . 75
3.7 Performance of the Typicality-Based Data Analysis . . . 75
3.7.1 68-bus System (*S1*) - Comparison to DCD . . . 77
3.7.1.1 Application on Case S1.C1 . . . 77
3.7.1.2 Application on Case S1.C2 . . . 82
3.7.2 Application on Case S1.C1, with presence of wind generation (S1.C3w) 85
3.7.3 Application on Case S1.C4i - Islanding detection . . . 88
3.7.4 Eastern Interconnection (S2) . . . 89
3.7.5 Processing time . . . 90
3.7.6 Discussion . . . 92
3.8 TDA validation . . . 93
3.8.1 Validation against existing methods for Case S1.C1 . . . 94
3.9 Discussion . . . 94
3.10 Conclusion . . . 95
4 Where in the area to measure the inertia? . . . 96
4.1 Literature Review . . . 96
4.2 Contribution . . . 99
4.3 Fundamentals . . . 100
4.3.1 Pilot-bus detection using TDA . . . 100
4.3.2 Regional Inertia Estimation . . . 103
4.4 Methodology: ARMAX-based regional inertia estimation . . . 105
4.4.1 Signals pre-processing . . . 105
4.4.2 Pilot-bus detection . . . 105
4.4.3 Regional inertia estimation . . . 107
4.5 IEEE Test Benchmark System . . . 108

4.6 Performance of the COI and Regional Inertia Estimation with Load Contribution . . . 109
4.6.1 Application of the TDA method for pilot-bus detection . . . 109
4.6.1.1 S1.w - Detection of pilot-bus per Region without motor contributions . . . 109
4.6.1.2 S1.m - Detection of pilot-bus per Region including motors 111
4.6.2 Regional inertia estimation using the detected pilot-bus . . . 115
4.6.2.1 ARMAX Regional inertia estimation for case 4.6.1.1 . . . 115
4.6.2.2 ARMAX Regional inertia estimation for case 4.6.1.2 . . . 116
4.7 Discussion . . . 117
Conclusion . . . 118

Bibliography . . . 126
APPENDIX A Appendix: Recursive TDA . . . 136
A.1 Fundamentals . . . 136
A.1.1 Coherency . . . 136
A.1.2 TDA . . . 137
A.2 Methodology . . . 140
A.3 Results . . . 141
A.4 Conclusion . . . 145

1 Introduction

Electrical power systems are the most complex systems created by mankind. Hundreds of complex generators, synchronously connected by thousands of transformers and kilometers of high voltage transmission lines, operating with thousands of coordinated switches and protection equipments on a real time basis. Simulations of the condition of the system, with thousands of variables, must be carried out and several predictions must be done regarding load demand curves, states and stability requirements of voltage, angle and frequency, for the contingency of all the aforementioned components, at every new operating condition, usually under a 15 minute basis (KUNDUR et al., 1994).

The operation and planning of such large and complex systems has being iteratively improved along the last century, with several contributions from both industry and academy alike, albeit some important jumps occurred, such as the introduction of Power System Stabilizers (CHOW, 2013) or the opening of energy markets (SIOSHANSI; PFAFFENBERGER, 2006). Traditional power systems were (usually) operated on a 10 to 5 to 1 year planning, followed by seasonal, trimestral and monthly, weekly, daily and hourly planning (some cases go as far as 15 minutes updates of load demand curves), in order to predict primary resources availability to generators and load demand curves, so hundreds of synchronous generators are dispatched in an optimal manner. Operator control rooms dispatched said hundreds of machines in semi-hour periods, following the demand curve, while calculating a large dimensional problem, the power flow solution of the system dispatch, to determine the equilibrium point, the static condition of the system, for that 30 minute period. Along that power flow solution, with limited availability of measurements, the state variables of the systems were estimated, oscillations on power flows in interconnections monitored and contingencies simulated for the initial condition of the system in the following 30 minutes period, all to assess the stable operation of the system. This laborious routine, performed diligently 48 times a day by shift teams of technicians and engineers was developed along the decades of learning how to handle these enormous systems that are essential to modern societies (CHOW, 2013).

However, as time progressed, some key changes took place (and are still taking place, actually), that kick-started a considerable transition to everything related to power systems, from its constituent parts, to the monitoring tools, to the way they are operated. Some of these changes came from outside the power systems, like the societal and political push for a more sustainable and less carbon dependent generation fleet due to climate changes, which lead to the acceleration in the development of wind and

Photovoltaic (PV) sources and the earlier retirement of fossil fuel-based synchronous generators. Additionally, concerns from society regarding the risk of nuclear power plants also enforced the deactivation of several of these synchronous generators globally, as seen in Figure 1.1. Other changes came from within the power system community as ways to explore new generation sources, enhance the visibility of the system from the control rooms and optimize the control and protection of the system (MILANO et al., 2018).

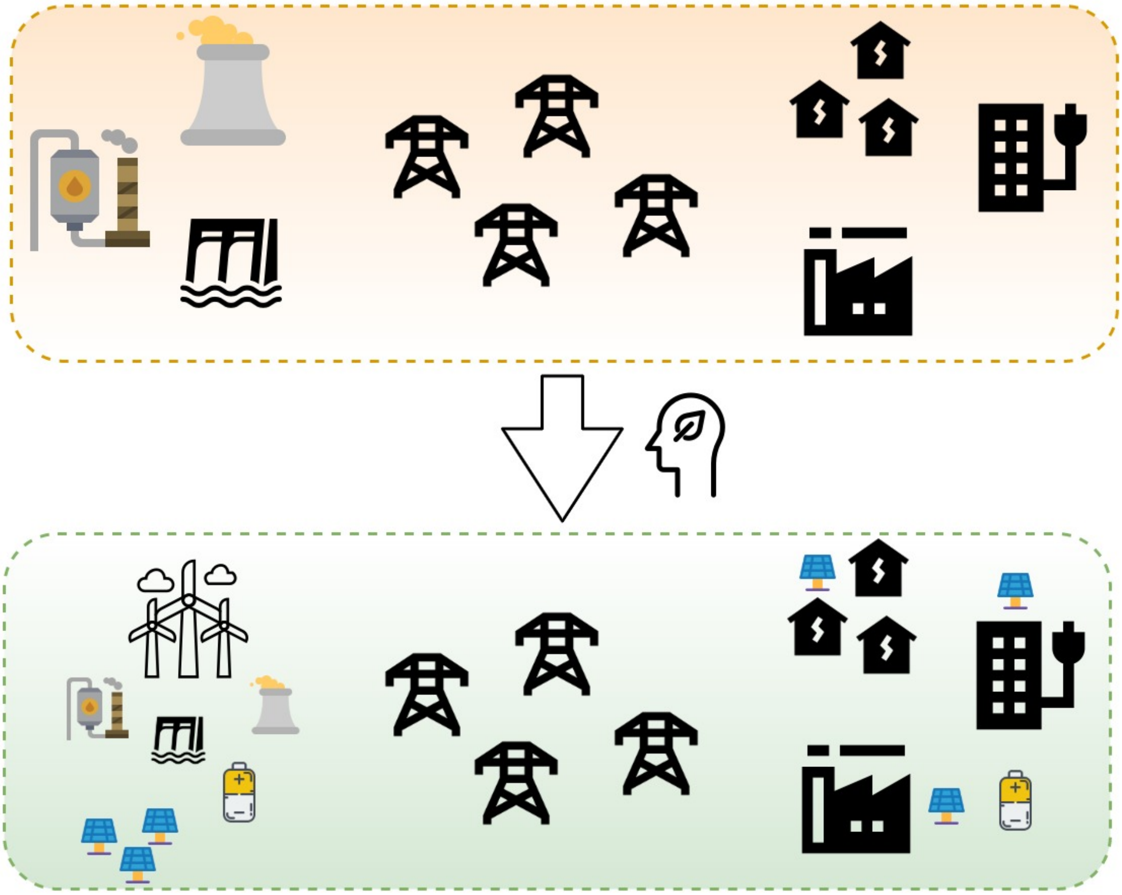

Figure 1.1 – The transition of modern pwoer systems.

Regarding the exploitation of new generation sources, the rapid development of power electronics associated with the push for sustainable sources brought the introduction of wind and PV generation to systems. PV from the start and wind as the power electronics technology progressed, are becoming more prominent in the systems, with some cases of instantaneous generation covered exclusively by these sources in some systems and ever increasing average generation penetration annually, as can be seen in Figure 1.2.

Both PV and newer wind generators are constructed using power electronic inverters that make possible to extract the maximum energy from their intermittent primary sources and inject it in the power system with the Alternating Current (AC) form and

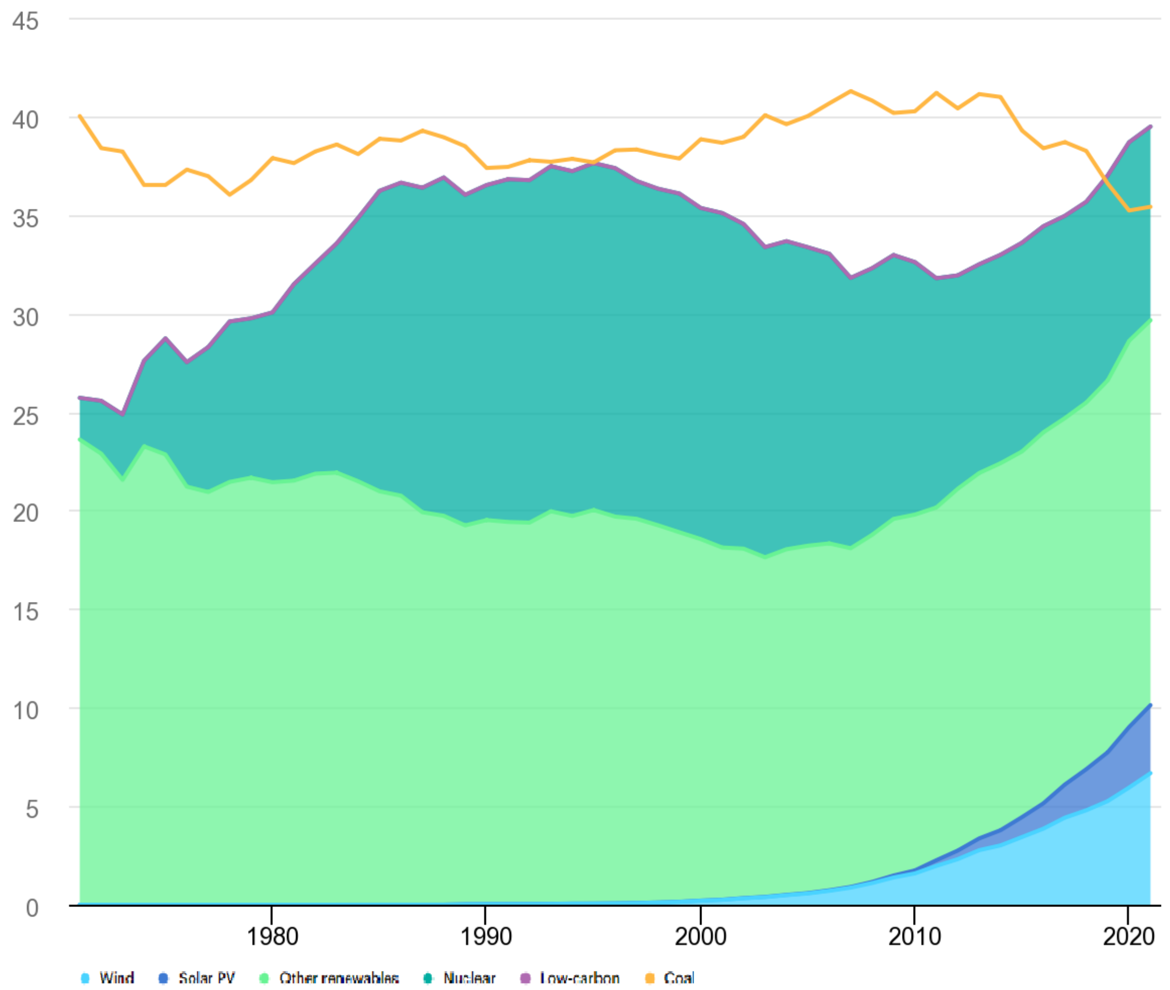

Figure 1.2 – Evolution of global installed capacity per primary source, extracted from (GLOBAL. . . , 2021)

adequate voltage profile levels. These generators, called Inverter Based Resources (IBR) have grown in nominal power capacity up to tens of MW making it possible for PV and wind farms to be comparable in dependable power injection with large traditional power plants with multiple synchronous generators. However, the technology that permit this deep exploitation of solar and wind energy is also responsible for the isolation of these renewable generators from the electromechanical phenomena that occur in the system, besides having little or no spinning mass which is associated with stability standards that are relevant for system operation and will be further explained in the next sections. This new context, while moving towards the direction of social demands, makes operators face a new set of obstacles for daily operation of systems and their security assessment.

Additionally, the development of measuring tools capable of measuring the positive sequence components of voltage and current with high sampling rates called Phasor Measuring Unit (PMU) which, alongside Digital Fault Recorders (DFR) three phase measurements, increased the observability of the system, as operators gained more comprehension of dynamical phenomena that occur in the system and not possible to be captured by the traditional Supervisory Control and Data Acquisition (SCADA) systems, but were more easily observed in simulations. As information technology also progressed, the creation of Wide Area Measuring Systems (WAMS) took place, where a set of PMU synchronyzed by Global Positioning System (GPS) signal were able to provide measurements of these phenomena with precise time synchronization, as exemplified in Figure 1.3, giving way to a new perspective of fast dynamics evolving throughout the system to the operator (CAI et al., 2005), making way to new analysis, control and protection tools to be developed to enhance the operation scheme.

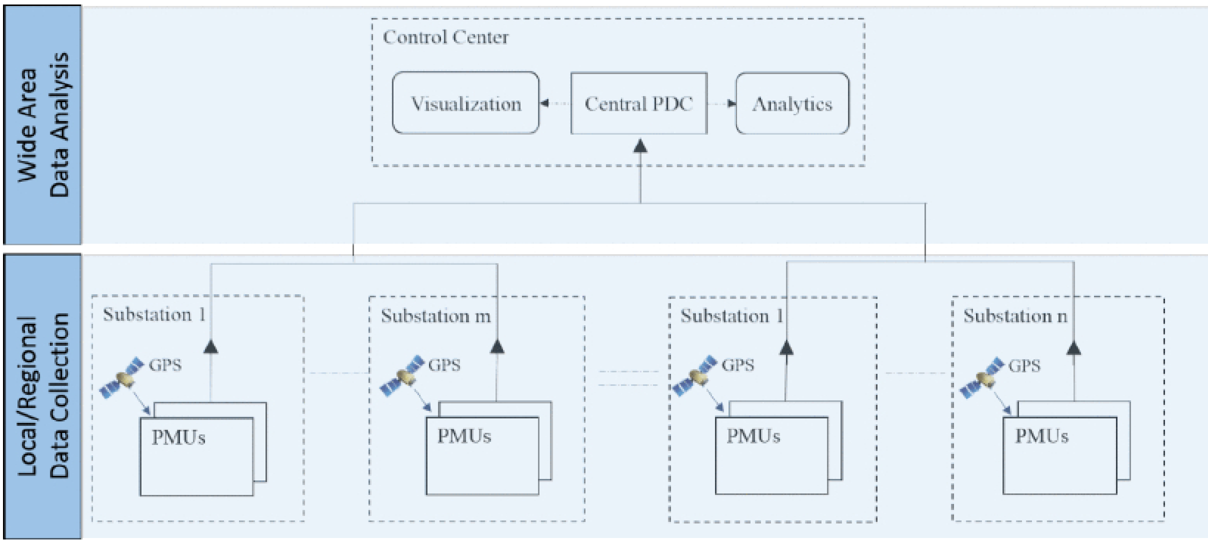

Figure 1.3 – Archtecture example of a centralized WAMS, extracted from (GORE; KANDE, 2015)

Further developments of measuring and information technologies, with the integration of command action that once happened *in situ* at subsation terminals, to the control rooms, and the maturing of WAMS are leading to the development of Wide Area Monitoring Protection and Control (WAMPAC) systems which are an integration of the perspective (measuring) and action (control and protection) processes at faster response times by the operator, integrated with traditional SCADA at the control room, increasing the work load of the operation teams. While these new control rooms provide a never before range of possibilities for predicting, preventing and taking remedial actions to the operator, the concrete application of the new tools is still not well defined, both in its integration to the SCADA system, that is, where it will supplement the existing system (pre-operation planning, operation, *post mortem* analysis) and which supplementary information (like faster state estimation, prediction of contingencies, system parameters estimation, forced oscillations and so forth) it can provide, and which supplementary action it can do (coordinated damping control, interconnection power flow regulation, primary and secondary frequency control re-calibration and so on).

Besides the increase of data collected by WAMS by their faster sampling power, which is hard to manage and merge with current routines, this enormous amount of data must be analyzed and stored with ease of fast consultation making relevant events that occurred in the system of rapid retrieval. Such task is and additional burden to operators of modern power systems that exemplify a non-incremental step in their evolution currently happening.

All these new challenges from generation technologies to control room new context, together with the intermittent nature of IBR make modern power system even more complex and dynamic than ever before. This is attested by the number of severe events that lead to the ultimate failure of the system, a blackout, happening in systems worldwide. Figure 1.4, albeit knowledge of past blackouts is harder to collect/consult, shows that the number and severity of such events is increasing as time passes. This could be the case of more events that routinely take place in systems ending in complete failure without the increase of the actual number of ordinary events. However, the amount of new technological obstacles posed to contemporary power systems and described here, have greatly increased the number of ordinary events and diminished the operator capacity to suppress them. This give way to a great deal of opportunities to improve the way we analyze, operate and control the system.

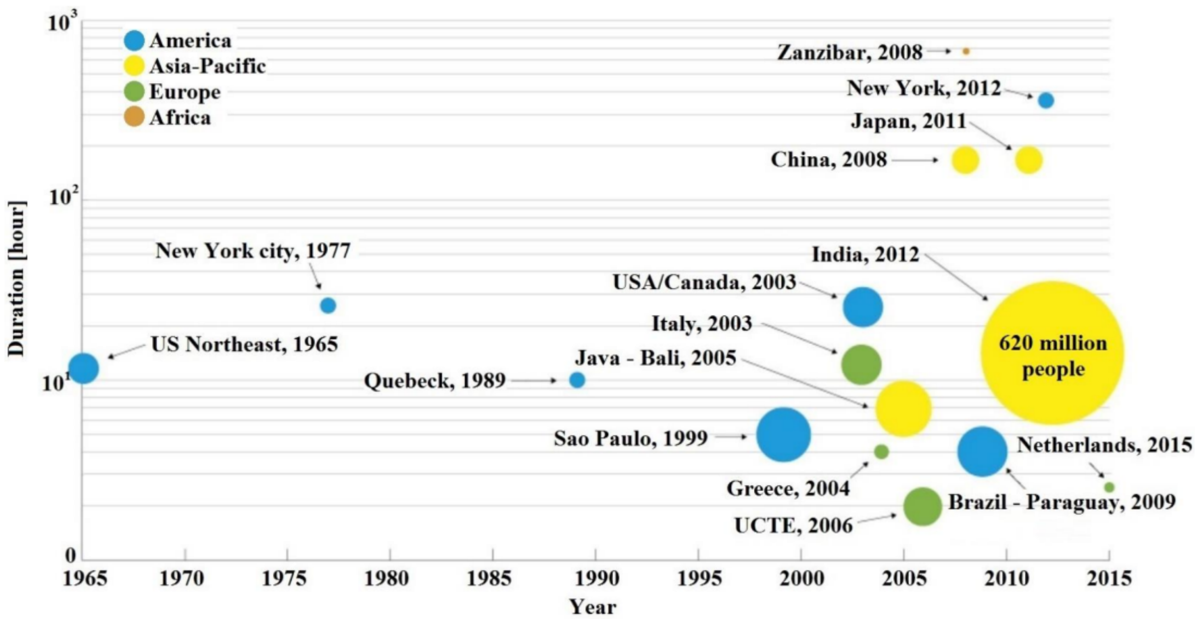

Figure 1.4 – Evolution of Blackouts through the last 5 decades, extracted from (NAGLIC, 2022)

1.1 Motivation

In this particular context power systems currently provide a great set of opportunities for research that can be vastly exploited. Particularly, the opportunity to take advantage of the great amount of new electromechanical dynamics data available to operators to implement new data-driven tools to supplement traditional SCADA systems.

These tools can be developed for analysis of data, protection schemes, identification and estimation purposes, and control. All these approaches can enhance the operator situational awareness, make the decision making process for actions to counter events happen earlier and faster and reduce the work load and human factor error rate, if appropriately developed and applied.

Within the context of the frequency stability and the diminishing inertia of systems worldwide due to IBR constructive characteristics and isolation from the grid, there is a gap to be filled in the appropriate knowledge of system inertia, that can be reached by a method that does not rely exclusively on model information, like traditionally done. This gap can be clearly seen in Figure 1.5, where the estimation of regional inertia currently available is comprised of a combination of partitioned methods for its intermediate steps, with different requirements of inputs and level of model independence.

1.1.1 Objectives

The gap pointed out above can be dealt with using WAMS data to improve frequency stability awareness and must consider that power systems are dynamic systems over time. Thus, the objectives of this thesis are summarized as:

- Proposal of a data-driven way to identify regions of the system after a specific disturbance;
- Proposal of a data-driven methodology to detect a representative point in each region from which the regional frequency response can be observed;
- Estimation of the regional inertial response considering the contribution of the load to give the operator quantitative information of the frequency stability of the system.

In this thesis, fundamental theory and mathematics is revised and the methodological concepts presented necessary to achieve such objectives. Additionally, the methodologies are tested with several simulations of power systems and real data from real WAMS. The overall manuscript encapsules the proposition of a method to achieve the

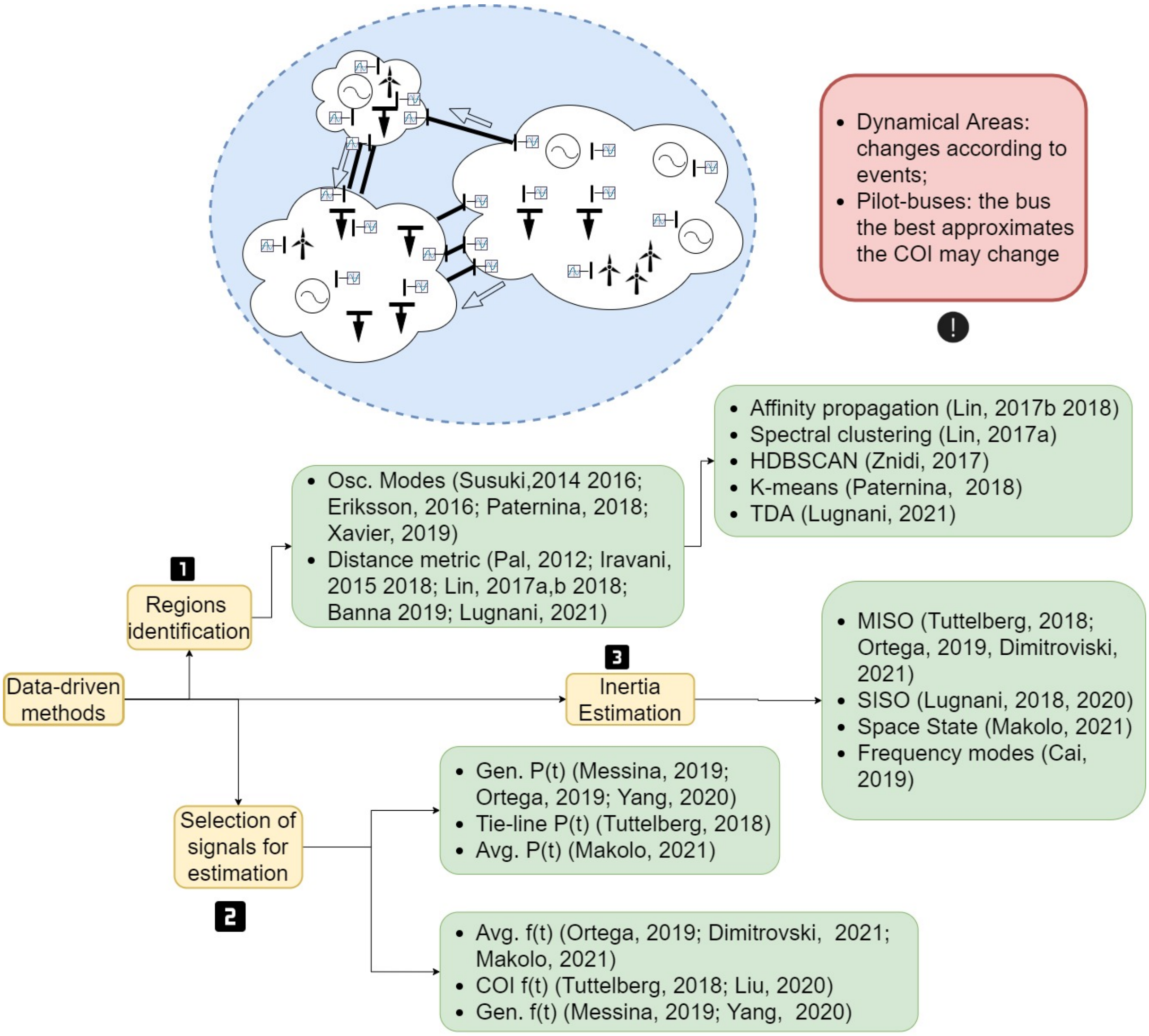

Figure 1.5 – Available methodologies for Regional Inertia estimation.

aforementioned objectives, how this proposition is validated and a discussion of the applicability and limitations faced by the method, so further work could be performed in order to increase its usefulness to power system operators.

1.1.2 Contribution

As previously stated, the confluence of new measuring tools and mathematical methods with the challenges imposed by the penetration of IBR has provided an opportunity for new contributions in the studiees of frequency stability. Figure 1.5 clearly shows that no single proposal has been made to estimate the regional inertia in power systems using a model independent method. This is the aim of this thesis.

In this doctorate research the results the author proposed to achieve are:

- The definition of a method for areas identification in a power system using data-driven method called Empirical Data Analysis (EDA), where:

  - Disturbances data is utilized;
  - A new clustering method for coherent areas is proposed: Typicality Data Analysis (TDA);
  - Statistical guarantee of borderline buses through the Chebyshev inequality;
  - Islanding detection.

- Regional pilot-bus detection after disturbance using EDA, where:

  - The modeling of the inertial response of the region is proposed considering the load contribution;
  - The relation of the Center of Inertia (COI) and the inertia distribution is demonstrated to indicate the validity of the pilot-bus and signal distribution detection;
  - COI pilot-bus detection using the approximation of the data Probability Density Function (PDF) through TDA.

- Additionally, the regional inertia estimation is performed with a data-drive method previously proposed by the author and using data from the pilot-buses identified of the regions detected using the proposed methodology.

An overall illustration of the thesis methodology is presented in Figure 1.6, with the pointed items.

It is important to point out that for sake of the reader, some terms are used interchangeably along the document, e.g. region and area, load and demand, generator and machine, events and disturbances, etc. At any point of the document that such terms appear, among others that are of common knowledge to power system community, and are not explicitly discriminated from each other, they should be considered synonyms.

The remaining parts of this document are organized as follows: Chapter 2 presents theory of frequency stability and concepts related to previous efforts related the estimation of regional inertia, the theory of coherent machines and power system regions, and ways previously used to obtain such regions. Chapter 3 presents the data-driven technique proposed in this thesis to identify such regions, using disturbance data collected by WAMS. Chapter 4 introduces the data-driven identification method proposed to choose the candidate measurement point to represent each region as a equivalent machine. Such point, called pilot-bus, is used to estimate the regional inertial response, using a technique proposed by the author previous to the thesis. Conclusion provides an overall perspective

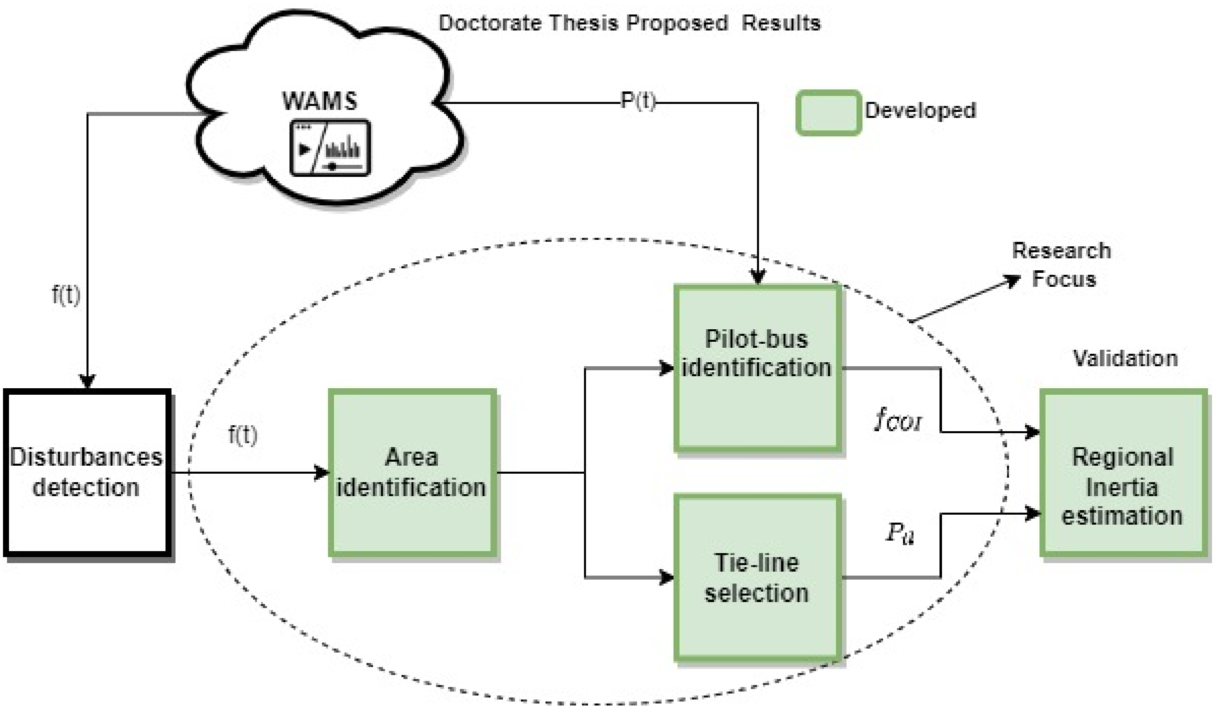

Figure 1.6 – Thesis methodology proposal.

of the results reached within the thesis work. This last chapter also points out subsequential work to the thesis that could be pursued and further contribute with research effort in power systems, and the detailed list of publications and presentations arising from the 4 year research work.

2 Fundamentals

This Chapter presents the main theoretical concepts regarding power system stability, system identification methods, and model-based generator coherency methods. It starts with a review of power system stability, focusing on emerging problems on frequency stability (especially the inertia estimation). A review of system identification methods in the sequence is provided, emphasizing the ARMAX method that is further applied in this work. Finally, a conventional model-based approach for coherency and model-reduction methodology is described. These model-based methods are used to validate the coherent areas find out by the proposed data-driven approach proposed in this work.

2.1 Stability Classification

The stability of power systems divided into fields according to the variable of interest during the analysis, for a given disturbance. Traditional stability comprehends the study of the ability of the system to deal with disturbances related to rotor angle, voltage and frequency (KUNDUR et al., 1994). With the transition imposed by IBR, the study of stability has been further divided to include studies related to resonance and converter-drives phenomena. The classification is illustrated in Figure 2.1 and the time scale of the dynamics related to each of these studies varies greatly and is depicted in Figure 2.2.

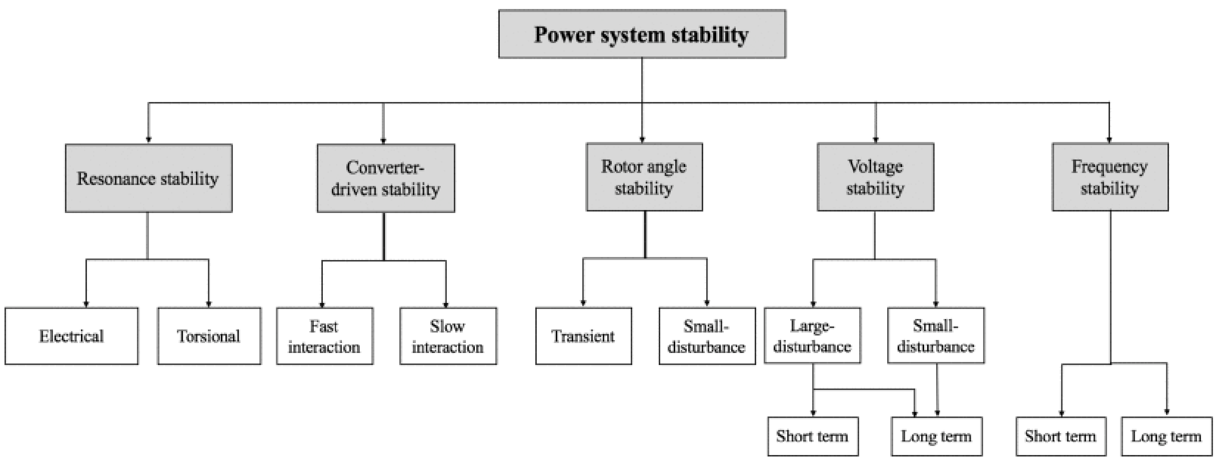

Figure 2.1 – Classification of Power System Stability considering IBR, extracted from (HATZIARGYRIOU et al., 2021)

For these dynamical studies, the system is then represented by a set of differential-algebraic equations, where transmission lines and transformers remain represented by algebraic equations and generators, condensers, converters and their controls and regulators

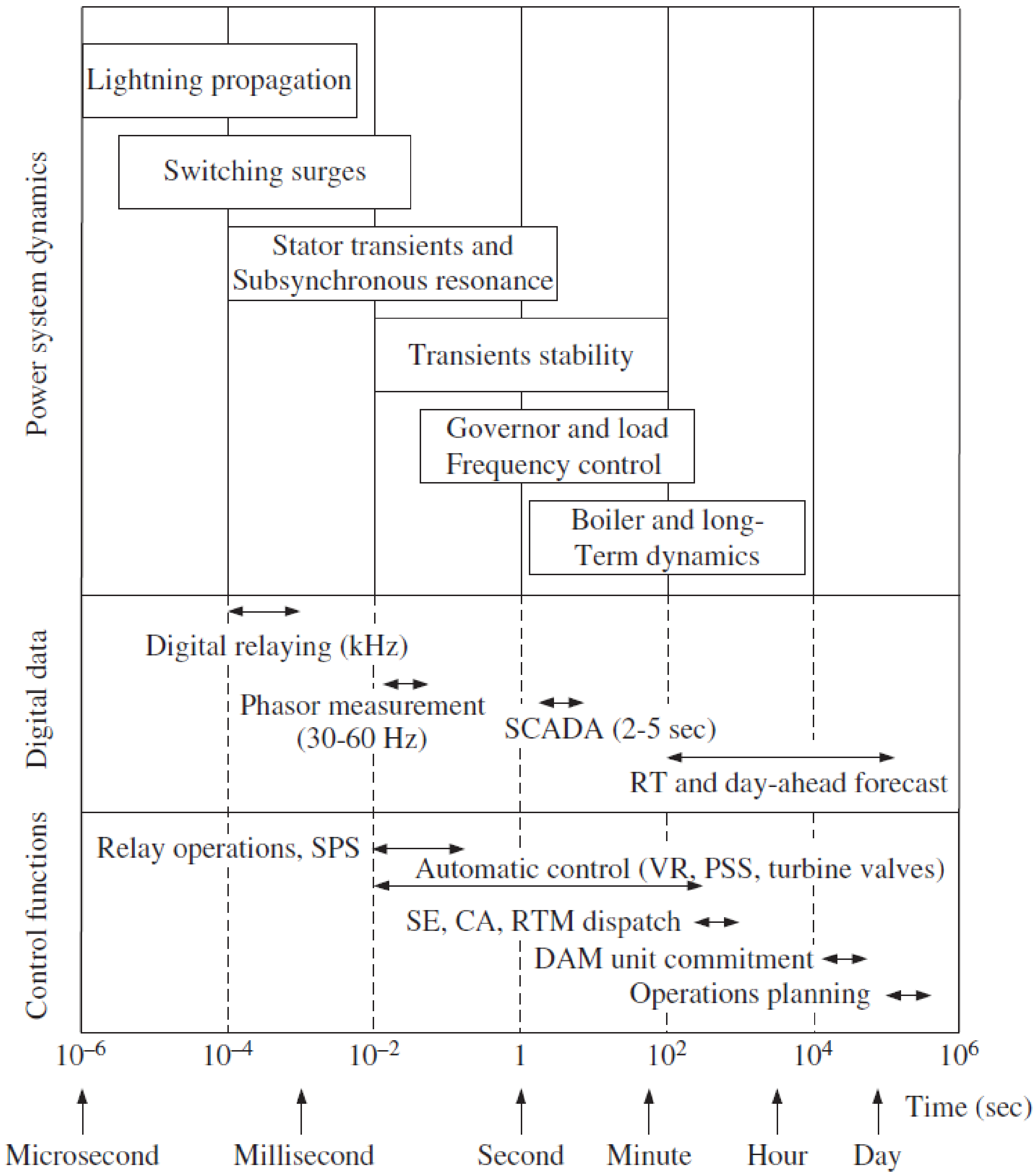

Figure 2.2 – Power system time scales for dynamics, data, and control functions. SPS, special protection schemes; VR, voltage regulator; PSS, power system stabilizer; SE, state estimation; CA, contingency analysis; RTM, real-time market; DAM, day-ahead market. Extracted from (CHOW; SANCHEZ-GASCA, 2020)

are represented by their differential equations. As the sets of events that may occur in the system span a wide variety of disturbances, it is reasonable to consider that their size and rapidness of dynamics may differ, as explained in Figure 2.2.

We will focus on the study of a steam or hydro turbine-synchronous generator, and its interaction with the grid, which can then be extrapolated to multimachine system (KUNDUR et al., 1994). We do not present the modeling of wind generators, although their introduction in the system is driving a renewed study of the frequency stability, because the frequency response is greatly driven by synchronous generators, which have the greatest inertial response of the system.

The time span of the dynamics is roughly in order in Figure 2.1, from left to right, from faster to slower. Hence it is clear to see that for the study of frequency stability the modeling of the system must consider only time constants from tens of milliseconds to minutes. This study is concerned with the ability of the system to maintain the balance between generated active power and demanded active power by the load and is related to the time constants of kinectic energy from the turbine-generator set and the valves that adjust the primary energy source to turbines.

2.1.1 Frequency response

Power system frequency stability concerns the balance of active power between generation and load. In order to study the frequency stability we must study the frequency response model of the system generator. The model considers the interactions of the turbine-generator system with the network, and is described ahead.

The typical disturbance that concerns frequency stability is either the loss of a generator or the rejection of a load block. The unbalance between generated power and demanded power will entail a response of the frequency of the system such as presented in Figure 2.3, for a typical generator, or a typical transmission bus (KUNDUR et al., 1994).

The frequency response is divided into thee stages: the inertial response; primary control and secondary control. A fourth stage, the tertiary control is not addressed here since it is an control based on economic criteria, rather than the power system stability, and it does not affect a disturbance analysis study. The preceding stages are, including the pre-disturbance:

- Pre-disturbance: previous to the occurrence of the disturbance, the frequency remains around the nominal value f_0, indicating the balance between mechanical power provided to the generator by the turbine and the active power requested by the grid;
- Inertial response: Right after the disturbance, when the active power balance is disturbed, there will be a frequency deviation inversely proportional to the inertia of the generator. Besides, given the slow acting nature of speed regulators, during the inertial response the regulators action may be disregarded;
- Primary control: The primary control starts at around 5 to 10 seconds (KUNDUR et al., 1994) after the disturbance (according to the type of machine, hydro, gas,

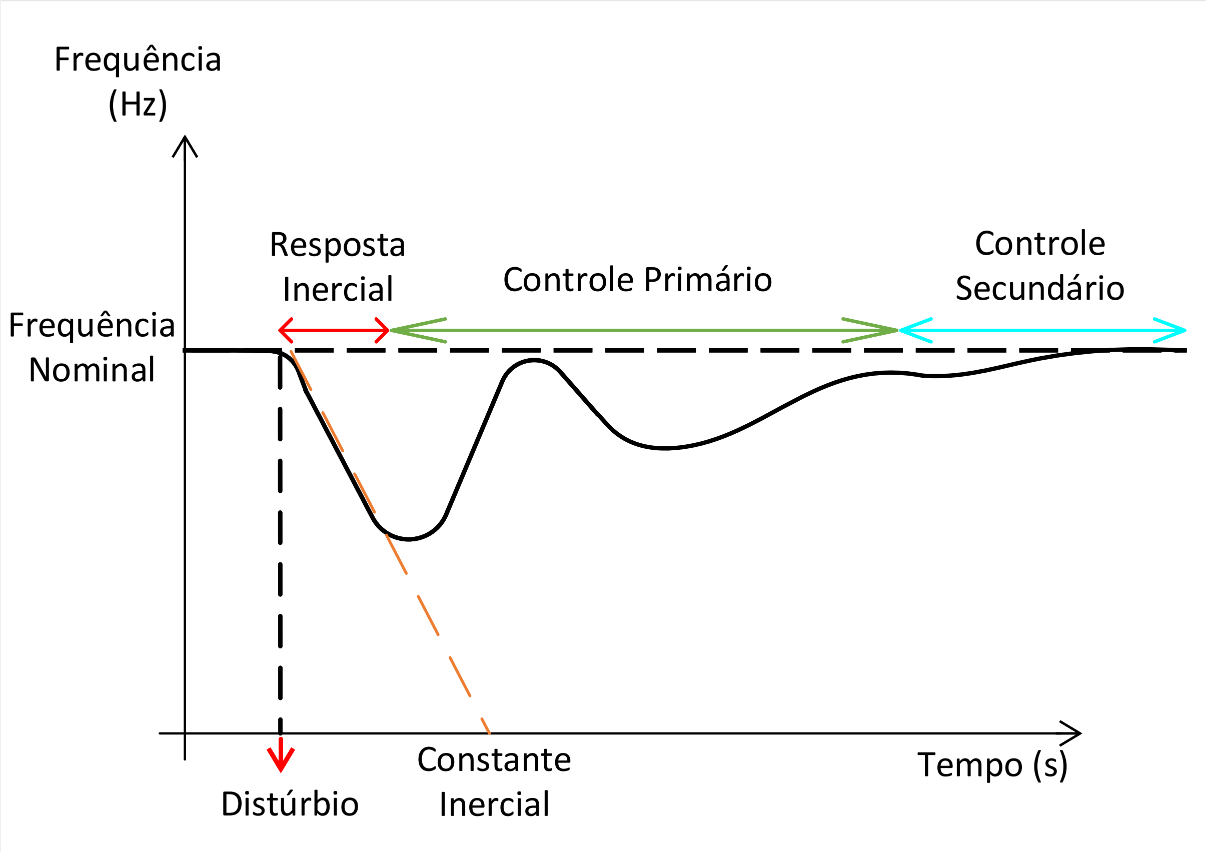

Figure 2.3 – Typical frequency response after a disturbance,

coal or steam):

$$R = \frac{\omega_{SC} - \omega_{CT}}{\omega_0} 100 \quad (2.1)$$

where ω_{SC} is the generator rotor nominal speed without loaD, ω_{CT} is the rotor's instantaneous speed and ω_0 the rotor's nominal speed, which in p.u. is equal to the frequency deviation Δf. The control seeks to arrest the frequency deviation (Δf) and is known as droop, which seeks a equilibrium state not necessarily equal to initial nominal frequency f_0, as a proportional control. For example, a 5% droop meas that a 5% frequency deviation causes a 100% excursion of the turbine admission valve;

- Secondary control: Once the primary control establishes a new equilibrium point with a given permanent regime error, the secondary control, or automatic control, acts via a integral control loop the reinstates the nominal frequency value.

The inverse relation between the frequency response and the inertia, and also the frequency response to a unbalance between generated power and the demanded power is given by the swing equation. which is presented now.

We start presenting the mechanical phenomenon that produces work at the turbine-generator shaft, which is the mechanical torque, elated from the angular acceleration of the turbine rotor and the rotor inertial moment J, which is a function of its constructive parameters:

$$J\frac{d^2\theta}{dt^2} = T \tag{2.2}$$

Where θ is the rotor angular position as a function of time t and $\frac{d^2}{dt^2}$ is the second order derivative. T is the net torque, that is the sum of all torques upon the rotor, considering the primary source generated torque, rotational losses torques and the electromagnetic torque. To facilitate visualization, all torques, except the electromagnetic torque T_e, are summed up into T_m, called the mechanical torque. The final net torque that produces acceleration T_a is then:

$$T_a = T_m - T_e \tag{2.3}$$

At nominal regime the difference should be zero and therefore, no resulting acceleration. For disturbances, the difference will not equal zero and be positive for load rejection events and negative for generation loss events. To solve Equation (2.2) to find the rotor position θ it is more convenient to measure the position and angular speed with respect to a rotating reference. Then:

$$\delta = \theta - \omega_0 \tag{2.4}$$

where, ω_0 is the nominal synchronous speed. Taking the derivative with respect to time:

$$\frac{d\delta}{dt} = \frac{d\theta}{dt} - \omega_0 \tag{2.5}$$

and

$$\frac{d^2\delta}{dt^2} = \frac{d^2\theta}{dt^2} \tag{2.6}$$

With that substitution, Equation (2.2) becomes:

$$J\frac{d^2\delta}{dt^2} = T = T_a = T_m - T_e \tag{2.7}$$

If we multiply Equation (2.7) by the nominal speed ω, we obtain:

$$M\frac{d^2\delta}{dt^2} = P_a = P_m - P_e \tag{2.8}$$

Equation (2.8) is more convenient than Equation (2.7), as it involves the electrical power provided by the machine, instead of the corresponding torque. Equation (2.8) may be referred to as the Swing Equation, which, for frequency stability purposes, may represent each machine in the system.

The angular momentum is not strictly constant as the velocity ω varies along disturbances. In practice, however, the change in speed ω is so small with respect to the reference speed ω_0 that M may be regarded as constant. Thus, it is usual to consider M as constant and equal to the angular momentum at nominal speed $J\omega_0$. M is known as the machines angular momentum quantity.

Usually, the available angular momentum information is given in the form of kinetic energy stored at the spinning mass at nominal speed. From that information and having knowledge of the machine rated power, another representation of the inertia constant of the machine is given H. The inertia constant represents the machine kinetic energy (E_{kin}) [W.s] stored at the moving turbine-generator rotor, at the rated power of the machine (S_B) [VA]. The constant value represents the time quantity during which the machine is able to provide its rated power exclusively from the rotor kinetic energy.

Although we consider disturbances, the frequency deviations are small with respect to the nominal frequency (Δf ≈ 0) and that $P_m - P_e$ is equal to the accelerating power (P_{acc}), given a disturbance to the active power balance (ΔG), the frequency deviation with initial mechanical and electrical powers P_{m0} e P_{e0} is:

$$\Delta f = \frac{1}{2Hs} P_{acc} = \frac{1}{2Hs}[(P_{m0} + \Delta P_m - \Delta G) - (P_{e0} - D\Delta f)] \tag{2.9}$$

During nominal regime $P_{m0} = P_{e0}$, allowing these terms to be disregarded. Considering that during the first seconds after a disturbance there is no primary control action, ΔP_m will be zero. Further, during the first moments of the disturbance the load frequency damping can also be disregarded. So, for the first moments of the frequency response, that is, the inertial response to a disturbance, is described as:

$$\dot{E}_{kin} = \frac{2HS_B}{f_m}\dot{f}_m = (P_m - P_e) \tag{2.10}$$

With this last identity H is related to parameters (f_m e P_e). Equation (2.10) for small deviation becomes:

$$\Delta \dot{f} = -\frac{\Delta G}{2H} \tag{2.11}$$

Where the machine nominal power may be ommitted if the power deviation ΔG is considered at the same rating and $\Delta \dot{f}$ is the Rate of Change of Frequency (RoCoF). In the frequency domain, Equation (2.9) may be rewritten as a transfer function of ΔG to Δf, as:

$$s\Delta f = \frac{1}{2H}(-\Delta G + (\frac{1}{R_D}\frac{1}{1+sT_G} + D)\Delta f) \tag{2.12}$$

During permanent regime, when$P_{acc} = 0$, the frequency deviation will be given by:

$$\Delta f = \frac{1}{D + \frac{1}{R_D}}\Delta G \tag{2.13}$$

Where $D + \frac{1}{R_D} = \beta$ is the frequency response (CHOW; SANCHEZ-GASCA, 2020). Equations (2.11) and (2.13) represent the initial moments of the frequency response, where the primary frequency control and load frequency damping have not yet acted. This model of the frequency response is considered in this thesis for the inertial regional estimation purposes, where each region will be represented by an equivalent machine.

2.2 System Identification

System identification is the set of theory and techniques used to identify a model of the system. This model relates in some quantifiable sense variables of the system (LJUNG, 1999). These representations, or models of the systems may range widely in mathematical formalism, according to the necessary application of the model. Typically, engineering models are represented by differential equations (or difference equations), with several specifics that entail the specific kind of differential equations, e.g. continuous, discrete, deterministic, stochastic, linear or nonlinear, etc (LJUNG, 1999).

The identification of a system must then have the judicious judgment of the user, in most cases an engineer, of the compromise between the information that must be considered in the model and the complexity of the model. This compromise will produce a precise model that reproduces the phenomena observed and predicts theoretical scenarios with efficient computational burden. To achieve such goal the identification of a model (system) requires:

- Data observed (measured) from the system;
- Possible models that may adhere to the data;
- Some mathematical formalism to determine the candidate model to be chosen.

Figure 2.4 – Time-invariant linear system

Once a model is chosen it should be validated using some criterion in such a way the user of the model can have some sort of quantifiable confidence on the model. This is to say, the model is good enough to the particular set of data used for identification of that model or, at max, a set of data similar to the one used.

The general procedure of system identification, regardless of the type of model considered or identification technique used or type of data measured, can be summarized by the following 'conceptual' steps:

- Experiment design or simulation;
- Data collection;
- Model set choice;
  - Model calculation (estimation);
  - Model evaluation (criterion fit);
- Model validation.

This briefly presents the philosophy a identification engineer could follow. Next, we present types of models, model estimation techniques and criterion for evaluation of models available in the literature. This is to provide background of the model used for regional inertia estimation of this thesis.

2.2.1 Types of Models

2.2.1.1 Time-invariant linear systems

Let $u(t)$ be the a input scalar signal and $y(t)$ a output scalar signal of a system, such as in Figure 2.4. The system is said to be **time invariant** if its response output does not depend of the **absolute time**. The system is said to be **linear** if its response to a linear combination of inputs is also the same linear combination of outputs, e.g. $y(u_1(t) + u_2(t)) = y_1(t) + y_2(t)$. If the system output depends only of the previous inputs, the system is said to be **causal**.

An important property of Linear Time-Invariant (LTI) systems is its characterization by the **impulse response** $g(\tau)$:

$$y(t) = \int_{\tau=0}^{\infty} g(\tau)u(t-\tau)d\tau \tag{2.14}$$

If we know the impulse response and corresponding input, we may calculate the output for any given input. This is said to be a **complete description of the system.**

It is most common to observe a system with measuring tools that sample signals at a constant rate. This characterizes discrete time signals, so some considerations must be made. For an **sampling interval** T and natural $k = 1, 2, \ldots$:

$$y(kT) = \int_{\tau=0}^{\infty} g(\tau)u(kT-\tau)d\tau \tag{2.15}$$

For a input, which is kept constant between samplings ($u(t) = U_k \;\; kT \leq t < (k+1)T$), the output of the system will be:

$$y(kT) = \sum_{l=1}^{\infty} \Big[\int_{\tau=(l-1)T}^{lT} g(\tau)d\tau \Big] u_{k-l} \tag{2.16}$$

And it is sufficient to know $g(\tau)$ to calculate the response of the system to the input, Equation (2.16) describes a **sampled-data system**, and $g(\tau)$ is its impulse response.

Additive noise: in reality, it is impossible to isolate the system from all external influence. Most influences can be described as noise[1], and can be represented by a clustered additive term $v(k)$ represented in Equation (2.17) and Figure 2.5.

$$y(t) = \sum_{k=1}^{\infty} g(k)u(t-k) + v(k) \tag{2.17}$$

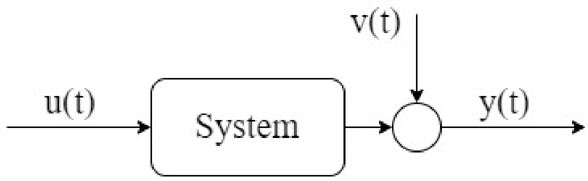

Figure 2.5 – Time-invariant linear system with noise

Noise can also vary widely in magnitude, frequency and variance. The main characteristic of noise is that it is not known until realization. However, previous knowledge of disturbances may help describe the noise in futures samples/signals. The formal description of noise at future moments ($t+k, \;\; k \geq 1$) would be to construct the joint PDF

[1] (LJUNG, 1999) names this phenomena as disturbances, but to avoid confusion in our power system context we define it as noise, although noise is an specific term within disturbance, according to the literature

of noise, which would be event, or signal specific, and thus, burdensome. A compromise approach would be:

$$v(t) = \sum_{k=0}^{\infty} h(k)e(t-k) \tag{2.18}$$

where $e(t)$ is a independent identically distributed (iid) random variables sequence with a given PDF. This representation allow us to make predictions of the identify model with certain confidence levels. The usual assumed PDF for generalization of the process noise is the normal distribution $e(t) \in N(0, \gamma)$, which is well-known to adjust with experimental tries (LJUNG, 1999).

The mean and covariance of (2.18) are:

$$Ev(t) = \sum_{k=0}^{\infty} h(k)Ee(t-k) = 0 \tag{2.19}$$

$$\begin{aligned} Ev(t)v(t-\tau) &= \sum_{k=0}^{\infty}\sum_{s=0}^{\infty} h(k)h(s)Ee(t-k)e(t-\tau-s) \\ &= \sum_{k=0}^{\infty}\sum_{s=0}^{\infty} h(k)h(s)\delta(k-\tau-s)\lambda \\ &= \lambda \sum_{k=0}^{\infty} h(k)h(k-\tau) \end{aligned}$$

This covariance is independent of time t, is called **covariance function of the process** v ($R_v(\tau) = Ev(t)v(t-\tau)$). With this function and the noise mean we describe it up to its second order of statistical properties. Since the mean of $v(t)$ and its covariance are independent of time, it is called **stationary**.

A easy representation of systems is given by the use of transfer functions. In order to introduce these functions it is convenient to define the **forward and backward shift operators** q:

$$qu(t) = u(t+1) \tag{2.20}$$

$$q^{-1}u(t) = u(t-1) \tag{2.21}$$

Then, the impulse response of LTI can be rewritten as:

$$y(t) = \sum_{k=1}^{\infty} g(k)u(t-k) = \sum_{k=1}^{\infty} g(k)q^{-k} = G(q)u(t) \tag{2.22}$$

Where $G(q)$ is called the **transfer operator** or the **transfer function** of the LTI (2.15), relating the sequences u' and y'. Thus, a general representation of a linear system with additive noise is:

$$y(t) = G(q)u(t) + H(q)e(t) \tag{2.23}$$

2.2.1.1.1 Periodic Inputs and Frequency Function

An interesting class of inputs for model identification is the periodic signal inputs. Although there are a myriad of ways to characterize periodic signals, trigonometric functions represent a wide range of inputs within this group, which are a great approach to estimate the model of a system. Lets assume the input:

$$u(t) = cos\omega t = \Re e^{i\omega t} \tag{2.24}$$

The output of a system like (2.15) will be:

$$y(t) = |G(e^{i\omega})|cos(\omega t + \phi) \tag{2.25}$$

where

$$\phi = argG(e^{i\omega}) \tag{2.26}$$

In (2.25) it is assumed the cosine function from minus infinity. If the input is considered zero for $t < 0$, an additional term

$$-\Re e^{i\omega t} \sum_{k=t}^{\infty} g(k)e^{-i\omega k} \tag{2.27}$$

is added, which is dominated by its norm. This is to say that this term will tend to zero as time progresses, or that the term is transient. Either way, the response of the system will also be a cosine function with same frequency. The response being stationary, has complete information for the same frequency ω of the input. Hence:

$$G(e^{i\omega}), \qquad -\pi \leq \omega \leq \pi \tag{2.28}$$

is called a frequency function of the system (2.15). The logarithmic and norm functions of $G(e^{i\omega})$ are usually presented to express the system behavior, as the indicate the excited frequencies by the system, which is valuable information for the identification.

Periodograms of Signals over Finite Intervals

For a function $U_N(\omega)$:

$$U_N(\omega) = \frac{1}{\sqrt{N}} \sum_{t=1}^{N} u(t) e^{-i\omega t} \tag{2.29}$$

For a finite input sequence $u(t), t = 1, 2, \ldots, N$, the values obtained for every period $\omega = 2\pi k/N$ produce the of the sequence of inputs. The input sequence may be represented by the inverse Discrete Fourier Transform (DFT):

$$u(t) = \frac{1}{\sqrt{N}} \sum_{k=1}^{N} U_N(\frac{2\pi k}{N}) e^{i2\pi kt/N} \tag{2.30}$$

Further study of this relation will indicate that $U_N(\omega)$ over $[0, \pi]$ is uniquely defined. The number $U_N(\frac{2\pi k}{N}$ resembles a weight of ω in the decomposition of $u(t)_{t=1}^{N}$. Further, its energy represents the contribution of that frequency to the signal and the values of energies over ω are known as the **periodogram** of the input signal sequence.

A more generalized form of periodograms is the signla spectra, described for the interval $t \in [1, \infty)$. We shall consider signals described as stochastic process with deterministic components, where the input signal is deterministic, with noises, if present in the input propagated through the system and summed at the output, as in Figure 2.5. So, the system response will be:

$$Ey(t) = G(q)u(t) \tag{2.31}$$

non-stationary. Thus, assumptions that should be made for noisy signals $s(t)$:

$$Es(t) = m_s(t), \qquad |m_s(t)| \leq C, \qquad \forall t \tag{2.32}$$

$$Es(t)s(t) = R_s(t, r), \qquad |R_s(t, r)| \leq C \qquad \lim_{N\to\infty} \frac{1}{N} \sum_{t=1}^{N} R_s(t, t-\tau) = R_s(t), \qquad \forall t \tag{2.33}$$

When these affirmations hold, the signal is said **quasi-stationary**. If the signal $s(t)$ is deterministic, the expectation E is a bounded sequence with limits:

$$R_s(\tau) = \lim_{N\to\infty} \frac{1}{N} \sum_{t=1}^{N} s(t)s(t-\tau) \tag{2.34}$$

If the signal is a stochastic process, (2.33) are satisfied. Additionally, two signals $s(t)$ and $w(t)$ are **jointly quasi-stationary** if both are quasi-stationary, and their **cross-variance** function:

$$R_{sw}(\tau) = \overline{E}s(t)w(t-\tau) \tag{2.35}$$

exists, and $\overline{E}s(t) = \lim_{N\to\infty} \frac{1}{N}\sum_{t=1}^{N} Es(t)$. If $R_{sw}(\tau) = 0$, s and w are said to be **uncorrelated**. When the previous assumptions hold, we can define the **spectrum** of $s(t)$ as:

$$\Phi_s(\omega) = \sum_{\tau=-\infty}^{\infty} R_s(\tau)e^{-i\tau\omega} \tag{2.36}$$

$$\Phi_{sw}(\omega) = \sum_{\tau=-\infty}^{\infty} R_{sw}(\tau)e^{-i\tau\omega} \tag{2.37}$$

While $\Phi_s(\omega)$ is always real, $\Phi_{sw}(\omega)$ is generally complex, thus, the representation of the spetrum between signals is done by the **phase spectrum** $arg\Phi_{sw}(\omega)$ and the **amplitude spectrum** $|\Phi_{sw}(\omega)|$.

Signal spectra describe the **second-order properties** of the signals, i.e. the statistical first and second moments for stochastic properties. Although two very different signals can have similar moments, much of the system identification relies on the spectra of the signals.

Further information regarding frequency analysis (periodogram analysis, spectra and proofs) of the signals of the model can be found in (LJUNG, 1999).

2.2.2 Mutivariable Systems

Let the input have m components and output p components, and the system be a **mutivariable** system. Dealing with such systems requires careful track of notation changes and mathematical operations, but most of all, the internal structures of the system which are hard to parameterize.

The description of the system:

$$y(t) = G(q)u(t) + H(q)e(t) \tag{2.38}$$

where $u(t)$ is a vector of m elements and $y(t)$ a vector of p components, and $G(q)$ is a transfer function matrix of dimension $p \times m$ and $H(q)$ a matrix of dimension $p \times p$. The sequence $e(t)$ is a sequence of independent random $p - dimensional$ vector of zero mean and $Ee(t)e^T(t) = \Lambda$ covariance matrices. The presented properties are the same with the careful consideration of matrix algebra, particularly:

- Impulse responses $g(k)$ and $h(k)$, with norms:

$$||g(k)|| = \Big(\sum_{i,j} ||^2\Big)^{1/2} \tag{2.39}$$

- Covariances are defined as:

$$\overline{E}s(t)s^T(t-\tau) = R_s(\tau) \tag{2.40}$$

$$\overline{E}s(t)w^T(t-\tau) = R_{sw}(\tau) \tag{2.41}$$

2.2.3 Prediction

Let a signal $v(t)$ be described as:

$$v(t) = H(q)e(t) = \sum_{k=0}^{\infty} h(k)e(t-k) \tag{2.42}$$

with H being stable, that is?

$$\sum_{k=0}^{\infty} |h(k)| < \infty \tag{2.43}$$

It is essential for estimation to be able to extract the noise of a signal. If $v(s), s \leq t$ are known, $e(t)$ is **invertible** and can be computed by:

$$e(t) = \tilde{H}(q)v(t) = \sum_{k=0}^{\infty} \tilde{h}(k)v(t-k) \tag{2.44}$$

with

$$\sum_{k=0}^{\infty} |\tilde{h}(k)| < \infty \tag{2.45}$$

2.2.4 One-step ahead Prediction of v

Lets assume that we measured $v(s), s \leq -1$ and that we want to predict the value of $v(t)$, with such measurements.

$$v(t) = \sum_{k=0}^{\infty} h(k)e(t-k) = e(t) + \sum_{k=1}^{\infty} h(k)e(t-k) \tag{2.46}$$

Where we assume that H is monic. Since we assume that we know $e(s)$ for $s \leq t-1$ from (2.44), we can denote the second term in (2.46) by:

$$m(t-1) = \sum_{k=1}^{\infty} h(k)e(t-k) \tag{2.47}$$

Supposing that $e(t)$ is iid and the probability of $e(t)$ can be described by the function:

$$P(x \leq e(t) \leq x + \Delta x) \approx f_e(x)\Delta x \tag{2.48}$$

The (posterior) probability density function of $v(t)$, with measurements up to $t-1$ is $f_v(x) = f_e(x - m(t-1))$.

The most probable value of $v(t)$, called Maximum a Posteriori (MAP) prediction is normally subtituted by the conditional expectation of $v(t)$ denoted $\hat{v}(t|t-1)$. Since $e(t)$ is zero mean, we have:

$$\hat{v}(t|t-1) = m(t-1) = \sum_{k=1}^{infty} h(k)e(t-k) = H^{-1}(q)[H(q)-1]v(t) = \sum_{k=1}^{\infty} h(k)v(t-k) \tag{2.49}$$

The prediction of the output follows and is given by:

$$\hat{y}(t|t-1) = H^{-1}(q)G(q)u(t) + [1 - H^{-1}(q)]y(t) \tag{2.50}$$

Further, the prediction error is stated as[2]:

$$y(t) - \hat{y}(t|t-1) = -H^{-1}(q)G(q)u(t) + H^{-1}(q)y(t) - e(t) \tag{2.51}$$

2.2.4.1 Models of Linear Time-Invariant Systems

A LTI model is specified by the impulse response $g(k)_1^{\infty}$, the spectrum $\Phi_v(\omega) = \lambda|H(e^{i\omega})|^2$ of the additive noise and its PDF, if available. A complete model is given as:

$$y(t) = G(q)u(t) + H(q)e(t) \tag{2.52}$$

$$f_e(\dot{}), \text{PDF of e} \tag{2.53}$$

[2] The expressions and formulations for k steps ahead, observers and control can be found on (LJUNG, 1999) and are omitted here as we are focused the **fitting** of models, rather than its predictions.

where:

$$G(q) = \sum_{k=1}^{\infty} g(k)q^{-k}; \qquad H(q) = 1 + \sum_{k=1}^{\infty} h(k)q^{-k} \tag{2.54}$$

Which entails that specifying a model requires defining the infinite sequences H and G and the noise PDF f_e. However it is more convenient to be able to represent the system by finite sequences of numerical values like rational transfer functions or state-space structures and the noise described by its first two statistical moments in detriment of the function f_e.

Additionally, it is usual that besides the structure of the model, it is also necessary to estimate some of the finite sequence values, known as **coefficients**, as parameters of vector θ, hence, the model description becomes:

$$y(t) = G(q,\theta)u(t) + H(q,\theta)e(t) \tag{2.55}$$

$$f_e(x,\theta), \text{PDF of e(t)} \tag{2.56}$$

Since the vector θ is estimated over the $\Re^d$ domain, the estimation is now that of a family of models, instead of a model itself, and the identifying process includes then the choice of the best model within the family. Usual families of models are briefly described ahead.

2.2.4.1.1 Equation Error Model Structure

Probably the most simple input-output relationship is obtained by describing it as a linear difference equation:

$$y(t) + a_1 y(t-1) + \cdots + a_{n_a} y(t-n_a) = b_1 u(t-1_{+} \cdots + b_{n_b} u(t-n_b) + e(t) \tag{2.57}$$

The adjustable parameters in this case are $\theta = [a_1 a_2 \ldots a_{n_a} b_1 \ldots b_{n_b}]^T$, where we can define:

$$A(q) = 1 + a_1 q^{-1} + \cdots + a_{n_a} q^{-n_a} \tag{2.58}$$

$$B(q) = b_1 q^{-1} + \cdots + b_{n_b} q^{-n_b} \tag{2.59}$$

and substituting (2.57) into (2.56), qe have:

$$G(q,\theta) = \frac{B(q)}{A(q)}, \qquad H(q,\theta) = \frac{1}{A(q)} \tag{2.60}$$

This is the Autoregressive eXogenous input (ARX) model, where the AR portion is related to the previous outputs and X portion related to the previous inputs. Figure 2.6 graphically describes the model structure. The zeroth order of this model is known as finite impulse response (FIR).

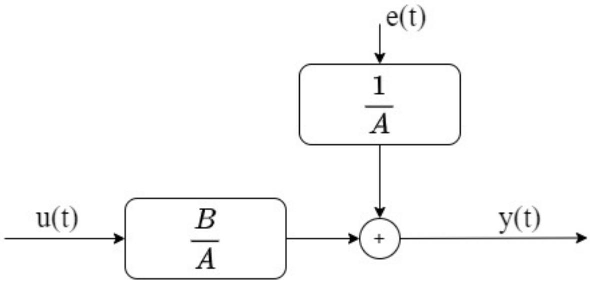

Figure 2.6 – The ARX model structure

To compute the predictor of (2.57), we insert (2.60) into (2.56):

$$\hat{y}(t|\theta) = B(q)u(t) + [1 - A(q)]y(t) \tag{2.61}$$

and introducing the vector $\phi(t) = [-y(t-1)\cdots - y(t-n_a)u(t-1)\ldots u(t-n_b]^T$, the predictions becomes:

$$\hat{y}(t|\theta) = \theta^T\phi(t) = \phi^T(t)\theta \tag{2.62}$$

which is the well known **linear regression**.

2.2.4.1.2 ARMAX Model Structure

This model structure introduces more ability to describe the noise to which the model is subject to. If we add a equation error as a moving average to the model:

$$y(t)+a_1y(t-1)+\cdots+a_{n_a}y(t-n_a) = b_1u(t-1_+\cdots+b_{n_b}u(t-n_b)+e(t)+c_1e(t-1)+\cdots+c_{n_c}e(t-n_c) \tag{2.63}$$

Where

$$C(q) = 1 + c_1q^{-1} + \cdots + c_{n_c}q^{-n_c} \tag{2.64}$$

Table 2.1 – SISO Model Structures

Polynomials of Model	Name of Model Structure
B	FIR
AB	ARX
ABC	ARMAX
AC	ARMA
ABD	ARARX
ABCD	ARARMAX
BF	OE (output error)
BFCF	BF (Box-Jenkins)

we can rewrite as:

$$A(q)y(t) = B(q)u(t) + C(q)e(t) \tag{2.65}$$

and the transfer function polynomial fractions are:

$$G(q,\theta) = \frac{B(q)}{A(q)}, \qquad H(q,\theta) = \frac{C(q)}{A(q)} \tag{2.66}$$

where $\theta = [a_1 a_2 \ldots a_{n_a} b_1 \ldots b_{n_b} c_1 \ldots c_{n_c}]^T$.

Following nomenclature logic, as we added a moving average (MA) term, this is called the Autoregressive Moving Average eXogenous input (ARMAX) model. Its predictor is:

$$\hat{y}(t|\theta) = \frac{B(q)}{C(q)}u(t) + [1 - \frac{A(q)}{C(q)}]y(t) \tag{2.67}$$

The vector of previous measurements becomes $\phi(t,\theta) = [-y(t-1) \cdots - y(t - n_a u((t-1) \ldots u(t-n_b]^T e((t-1) \ldots e(t-n_c, \theta]^T$, and the predictor Equation (2.67) is then:

$$y(\hat{t}|\theta) = \phi^T(t,\theta)\theta \tag{2.68}$$

This form is very similar to the **linear regression**. However, the vector of previous measurements is dependent of the coefficients, thus this is called a **pseudolinear regression**, which is solver iteratively.

This is the model used to describe the inertial response model in this thesis, and will be further explored in Chapter 4. There are however, several other model structures, presented in Table 2.1, with particular application to special cases that are not of interest in this work.

2.3 Coherency of generators in power systems

The following Section introduces the traditional model based coherency theory, that is the slow coherency theory, widely used in power systems. These concepts are important both for understanding the phenomena and inferences done for the data-driven method proposed in the thesis, but also as a validation method, as we present in Section 2.4 the clustering technique based on the slow coherency theory to identify the coherent machines. In Section 2.5 we present model based method with which we can ascertain the areas found the clustering techniques, which we can use to validate the areas found with different clustering methods.

2.3.1 Overview

The coherency phenomenon is the act of a group of generators oscillating in the same direction with each other, upwards or downwards swings of angle and frequency, against one or more group of generators for stress operating conditions and disturbances. It occurs naturally in power systems due to constructive characteristics of the system specially transmission lines limitation between areas of the system (CHOW, 2013).

This phenomenon is interesting in itself, as it can cause or magnify power swings in the system. But it is also a characteristic of the system that can be explored for control and remedial actions. The first obvious exploitation is the damping of such power swings, in order to prevent insecure operation. However, additional use of the coherency phenomenon is found, specially the exploitation of its ability to represent the group of generators, and the region where those generators are located, as a single response. In that sense, the region of **coherent** generators is identified, or **clustered**, and then **aggregated** as a single equivalent machine whose parameters are calculated as the weighted sum of the corresponding individual generators, connected to the rest of the system by an equivalent impedance, or the transmission lines of interest. This equivalent machine representation can be used by operators for simulation of contingency scenarios, as it is quite more computationally efficient to simulate a single machine instead of several, if we can assume this machine represents the region response to the contingency accurately.

The application of the coherency concept is divided into observation of physical properties related to the phenomenon, which are the modes of oscillation that can be observed in the linearized model of the system, through the eigenvalues and eigenvectors of the state-space matrix (slow coherency theory). Next, a clustering method is applied (which is presented in Section 2.4), which is able to gather the most similar generators and remaining buses into groups, based on the characteristics mentioned (slow coherency clustering method). Finally, the generators identified as belonging to the same group are aggregated into a single machine by linear algebra transformation that are guaranteed to preserve the the physical properties of the region response, presented in 2.5.

2.3.2 Slow modes coherency theory

Let the following equations (2.69) and (2.70) represent vectors of differential and algebraic equations of the power system, respectively:

$$M\ddot{\delta} = f(\delta, V) \tag{2.69}$$

$$0 = g(\delta, V) \tag{2.70}$$

where (2.69) represents the motion of the machines' rotor angle (δ), such that, for each machine i:

$$m_i\ddot{\delta}_i = P_{mi} - P_{ei} = P_{mi} - \frac{E_i V_j sin(\delta_i - \theta_j)}{x'_d} \tag{2.71}$$

is the classical electromechanical model of the generator,with $m_i = \frac{2H}{\Omega}$, $\Omega = 2\pi f_0$, P_{mi} is the generator input mechanical power and P_{ei} is the electrical active power expressed in terms of the internal bus voltage behind the transient reactance. (2.70) is the set of equations that represent bus j power-flow balance:

$$P_{ej} - \mathfrak{Re}\left[\sum_{k=1,k\neq j}^{N}(V_{jre} + jV_{jim} - V_{kre} - jV_{kim})\left(\frac{V_{jre} + jV_{jim}}{R_{Ljk} + jX_{Ljk}}\right)^*\right] - V_j^2 G_j = 0 \tag{2.72}$$

and

$$Q_{ej} - \mathfrak{Im}\left[\sum_{k=1,k\neq j}^{N}(V_{jre} + jV_{jim} - V_{kre} - jV_{kim})\left(\frac{V_{jre} + jV_{jim}}{R_{Ljk} + jX_{Ljk}}\right)^*\right] - V_j^2 B_j + V_j^2\frac{B_{Ljk}}{2} = 0 \tag{2.73}$$

In terms of linearized systems, slow-coherency can be observed through eigenvalues and eigenvectors of the slowest modes of oscillation (CHOW, 2013). So, linearizing (2.69) and (2.70) around a equilibrium point (δ_0, V_0), obtained from the power-flow solution of the system:

$$M\Delta\ddot{\delta} = \left.\frac{\partial f(\delta, V)}{\partial \delta}\right|_{\delta_0, V_0} + \left.\frac{\partial f(\delta, V)}{\partial V}\right|_{\delta_0, V_0} = K_1\Delta\delta + K_2\Delta V \tag{2.74}$$

$$0 = \left.\frac{\partial g(\delta, V)}{\partial \delta}\right|_{\delta_0, V_0} + \left.\frac{\partial g(\delta, V)}{\partial V}\right|_{\delta_0, V_0} = K_3 \Delta\delta + K_4 \Delta V \tag{2.75}$$

$\Delta\delta$ is a n-vector (n = # of machines) of the machines angle deviation from δ_0, ΔV is a 2N-vector (N = # of buses) of the real and imaginary parts of load bus deviations from V_0. K_4 is the network admittance matrix and nonsingular, hence, we can solve (2.75) for ΔV:

$$\Delta V = -K_4^{-1} K +_3 \Delta\delta \tag{2.76}$$

substituting (2.76) in(2.74) we get:

$$M\Delta\ddot{\delta} = K_1 \Delta\delta + K_2(-K_4^{-1} K_3 \Delta\delta) = (K_1 - K_2 K_4^{-1} K_3)\Delta\delta = K\Delta\delta \tag{2.77}$$

where $K[i, j] = E_i E_j (B_{ij} cos(\delta_i - \delta_j) - G_{ij} sin(\delta_i - \delta_j))$. E represents machines internal voltages, and $G_{ij} + jB_{ij}$ is the equivalent admittance between generators i and j. Also, the diagonals of K are given by:

$$K_{ij} = -\sum_{j=1, j \neq i}^{n} K_{ij} \tag{2.78}$$

The entries K_{ij} of the matrix are known as the synchronizing torque coefficients between machines i and j. Thus, a linear model of the system is defined.

Lets assume that a power system represented by (2.74) and (2.75) has **r** slow-coherent areas. Let:

- $\Delta\delta_i^\alpha$ = deviation of the rotor angle of machine i in area α from δ_i^0;
- m_i^α = the inertia of machine i in area α.

Also, the order of machines is such that the angle deviations are consecutively order by areas in $\Delta\delta$. The coherency between machines in a given area is attributed in (CHOW, 2013) to the *stiffness* of their connections, caused by:

1. Greater internal admittances in a given area than the admittances to other areas, represented by $\epsilon_1 < 1$, where B_{ij}^E and B_{pq}^I are external and internal suceptances, respectively:

$$\epsilon_1 = \frac{B_{ij}^E}{B_{pq}^I} \tag{2.79}$$

2. The number of internal connections is far greater than the number of external connections, represented by $\epsilon_2 < 1$:
$$\epsilon_2 = \frac{\overline{\gamma^E}}{\underline{\gamma^I}} \tag{2.80}$$
$\overline{\gamma^E} = max_\alpha \gamma_\alpha^E$ is the maximum number of external connections of area α, divided by the number of buses in area α;
$\underline{\gamma^I} = min_\alpha \gamma_\alpha^I$ is the minimum number of internal connections of area α, divided by the number of buses in area α.

For a large power system, a weak connection parameter representing the stiffness of each area can be denoted by:

$$\epsilon = \epsilon_1 \epsilon_2 \tag{2.81}$$

Through this parameter ϵ, we can separate the network admittance matrix K_4 into:

$$K_4 = K_4^I + \epsilon K_4^E \tag{2.82}$$

where ϵ is used as a scale factor smaller than 1 for connections between different areas. Including this factor, the synchronizing torque matrix K is expressed as:

$$K = K^I + \epsilon K^E \tag{2.83}$$

Introducing a transformation such that aggregate and difference variables are obtained, revealing time scales of power systems, with (2.83). The slow motion of an area will be defined as an **inertia wighted aggregate variable:**

$$y^\alpha = \sum_{i=1}^{n_\alpha} \frac{m_i^\alpha \Delta\delta_i^\alpha}{m^\alpha} \tag{2.84}$$

Denoting by $y_{r\times1}$ the vector whose αth entry is y^{alpha}, the matrix form of (2.84) is:

$$y = C\Delta\delta = M_a^{-1} U^T M \Delta\delta \tag{2.85}$$

where,

$$U = blockdiag(u_1, \ldots, u_r) \tag{2.86}$$

is the grouping matrix $(n_\alpha \times 1)$ column vectors

$$u_\alpha = [11 \ldots 1]^T \tag{2.87}$$

$$M_a = diag(m^1, m^2, \ldots, m^r) = U^T M U \tag{2.88}$$

M_a is the $(r \times r)$ diagonal aggregate inertia matrix.

For the difference or local variables, i.e., the fast dynamics, a reference machine is selected in each area, which will be the 'zero' angle machine of that area (or, as we will see further in this Section, the orthogonal base corresponding to this area) for all other machines.

$$z^\alpha_{i-ref} = \Delta\delta^\alpha_i - \Delta\delta^\alpha_{ref} i = 1, 2, \ldots, n_\alpha; i \neq ref; \alpha = 1, 2, \ldots, r \tag{2.89}$$

For simplicity we can choose the first machine of each area or permute the machine area vector such that $ref = 1$. Denoting by z^α the $(n_\alpha - 1 \times 1)$ vector whose $i - th$ entry is Z^α_i and considering z^α as the $\alpha - th$ subvector of the $(n - r \times 1)$ vector z we rewrite (2.89) as:

$$z = G\Delta\delta = blockdiag(G_1, G_2, \ldots, G_r)\Delta\delta \tag{2.90}$$

where G_α is the $(n_\alpha - 1 \times n_{alpha})$ matrix:

$$G_\alpha = \begin{bmatrix} -1 & 1 & 0 & . & 0 \\ -1 & 0 & 1 & . & 0 \\ . & . & . & . & . \\ -1 & 0 & 0 & . & 1 \end{bmatrix} \tag{2.91}$$

Thus, the transformation from original state $\Delta\delta$ into aggregate and local variables y and z is

$$\begin{bmatrix} y \\ z \end{bmatrix} = \begin{bmatrix} C \\ G \end{bmatrix} \Delta\delta \tag{2.92}$$

$$\Delta\delta = [UG^+] \begin{bmatrix} y \\ z \end{bmatrix} \tag{2.93}$$

$$G^{+} = G^{T}(GG^{T})^{-1} \tag{2.94}$$

Applying transformation (2.92) to (2.77), (2.82) we obtain:

$$M_a\ddot{y} = \epsilon K_a y + \epsilon K_{ad} z \tag{2.95}$$

$$M_d\ddot{z} = \epsilon K_{da} y + (K_d + \epsilon K_{dd}) z \tag{2.96}$$

where,

$$\begin{aligned}
M_d &= (GM^{-1}G^{T})^{-1} \\
K_a &= U^{T}K^{E}U \\
K_{ad} &= U^{T}K^{E}M^{-1}G^{T}M_d \\
K_{da} &= M_d G M^{-1}K^{E}U \\
K_d &= M_d G M^{-1}K^{I}M^{-1}G^{T}M_d \\
K_{dd} &= M_d G M^{-1}K^{E}M^{-1}G^{T}M_d
\end{aligned}$$

System (2.96) is in the *standard singularly perturbed form* showing that y is the slow variable and z is the fast variables. Hence, ϵ *is both the weak connection parameter and the singular perturbation parameter, making it possible the observation of slow coherency.*

We now present two model-based techniques used for clustering the generators and other buses using the linearized form of the system, the slow-coherency clustering algorithm and the tolerance-based algorithm. The first is heavily based in the theory shown in this Section, whereas the second introduces a relaxation constant based on a similarity metric. This second one is particularly important for introducing the derivation of data-driven techniques proposed in the next Chapter.

2.4 Clustering techniques

This Section presents the model-based technique that is mostly used in industry for clustering coherent areas, that is, the slow coherency grouping technique. Additionally, another model based method for clustering is presented as this method presents a bridge between model-based methods and data-driven methods due to the approach taken in the clustering technique. The proposed clustering technique of this thesis is compared to the slow coherency method using the aggregation method presented in the next Section.

2.4.1 Slow-coherency algorithm

The transformation (2.92) could also be applied directly to (2.74) and (2.75) (unsolved for ΔV), leading to:

$$M_a\ddot{y} = K_{11}y + K_{12}z + K_{12}\Delta V \tag{2.97}$$

$$M_d\ddot{z} = K_{21}y + K_{22}z + K_{23}\Delta V \tag{2.98}$$

$$0 = K_{31}y + K_{32}z + (K_4^I + \epsilon K_4^E)\Delta V \tag{2.99}$$

$$\tag{2.100}$$

where

$$\begin{aligned}
K_{11} &= U^T K_1 U \\
K_{12} &= U^T K_1 G^+ \\
K_{13} &= U^T K_2 \\
K_{21} &= (G^+)^T K_1 U \\
K_{22} &= (G^+)^T K_1 G^+ \\
K_{23} &= (G^+)^T K_2 \\
K_{31} &= K_3 U \\
K_{32} &= K_3 G^+
\end{aligned}$$

Since the elimination of load buses involves the solution of linear equations (2.76), it follows that eliminating δV variables would reduce (2.100) to (2.96), i.e., **the transformation** (2.92) **and the load bus elimination commute.**

Observe from (2.96) that y (slow variable) is coupled into the fast variable z equation through ϵ. **Thus, as a zero-th order approximation, z can be considered constant and equal to zero. Consequently** (2.100) **reduces to:**

$$M_a\ddot{y} = K_{11}y + K_{13}\Delta V \tag{2.101}$$

$$0 = K_{31}y + K_4\Delta V \tag{2.102}$$

This is the **inertial aggregate model** which is equivalent to linking the internal nodes of the coherent machines by infinite admittances. Since it aggregate the machines by internal nodes, it should be more accurate than machine terminal bus aggregation.

For a model more accurate than the inertial aggregate model, we consider z to vary with y. As a first-order approximation, from (2.100) the quasi-steady-state of z is obtained as:

$$z = -K_{22}^{-1}(K_{21}y + K_{23}\Delta V) \tag{2.103}$$

Eliminating z from (2.100) results in the slow-coherency aggregate model:

$$M_a\ddot{y} = K_{11s}y + K_{13s}\Delta V \tag{2.104}$$

$$0 = K_{31s}y + K_{4s}\Delta V \tag{2.105}$$

where,

$$\begin{aligned}
K_{11s} &= K_{11} - K_{12}K_{22}^{-1}K_{21} \\
K_{13s} &= K_{13} - K_{12}K_{22}^{-1}K_{23} \\
K_{31s} &= K_{31} - K_{32}K_{22}^{-1}K_{21} \\
K_{4s} &= K_{4} - K_{32}K_{22}^{-1}K_{23}
\end{aligned}$$

The main difference between this model and the inertial aggregate model is that in (37) the internal nodes of the coherent machines are no longer connected by infinite admittances. Instead, the singular perturbation method introduces impedances corrections to the matrices K_{11}, K_{13}, K_{31} and K_4. The aggregate models will be discussed in Section 3.

Now, let's consider the linearized system model. From the mode shapes, if machines i and j have similar entries in the eigenvector of mode k, we can conclude that these two machines are coherent with respect to that mode. Thus for a group of machines to be slow coherent, their mode shapes with respect to the low frequency interarea modes must be similar. In other words, if V_s is the matrix of the eigenvectors corresponding to the small eigenvalues of $M^{-1}K$ (2.77), then a slow coherent group of machines must have similar row vectors in V_s. For a system with coherent groups, the row vectors of V_s form r clusters in an r-dimensional space.

Thus a practical algorithm to identify the slow coherent groups is to first find the r most linearly independent vectors w_α from V_s and use them as the reference vectors. Then a machine with the row vector w_i will be grouped in the same area with the reference machine whose row vector w_α is closest to w_i. A coherent machine identification algorithm has been proposed as follows.

1. Choose number of areas r;
2. Compute a basis matrix Vs of the eigensubspace of the r smallest eigenvalues in magnitude of the model (2.77), including the zero eigenvalue;
3. Apply Gaussian elimination with complete pivoting to V_s and obtain the machines used for the pivots as the reference machines.
4. Order the machines such that the rows of V_{s1} correspond to the reference machines and solve for L from
$$V_1^T L^T = V_2^T \tag{2.106}$$
using the LU decomposition of V_{s1} already computed in Step 2;
5. Use L to assign the machines to the coherent areas. That is, if the largest positive entry in a row of L is the αth entry, then the machine corresponding to that row is grouped into area α.

A diagram showing the algorithm is presented in Figure 2.7.

2.4.2 Tolerance based grouping algorithm

In equation (2.105) we eliminate the fast variables vector z from the model. The length of this vector is dependent on the number of areas r set for the reduction of the model. We aim to reduce the model but keeping its capability of adequately representing the modes considered. This representation may be faulted for large power systems, where the reference machine value in L_g is not close to unity, rendering cluster of machines that may not pertain the same area.

A tolerance-based grouping algorithm is presented in (CHOW, 2013) that enhances accuracy and controls the size of areas of coherent machines. **This may be seen as a easier way to obtain the coherent machines groups, as it does not specify the number r of areas. The number of areas will be affected by the number of modes considered and a tolerance constant adjusted by the user based on the desired accuracy.**

The method considers a distance metric for the rows of the matrix V_s (matrix where each column correspond to an eigenvector associated with the modes of the system) for determining 'how coherent' two machines are. This metric is shown in equation (2.107):

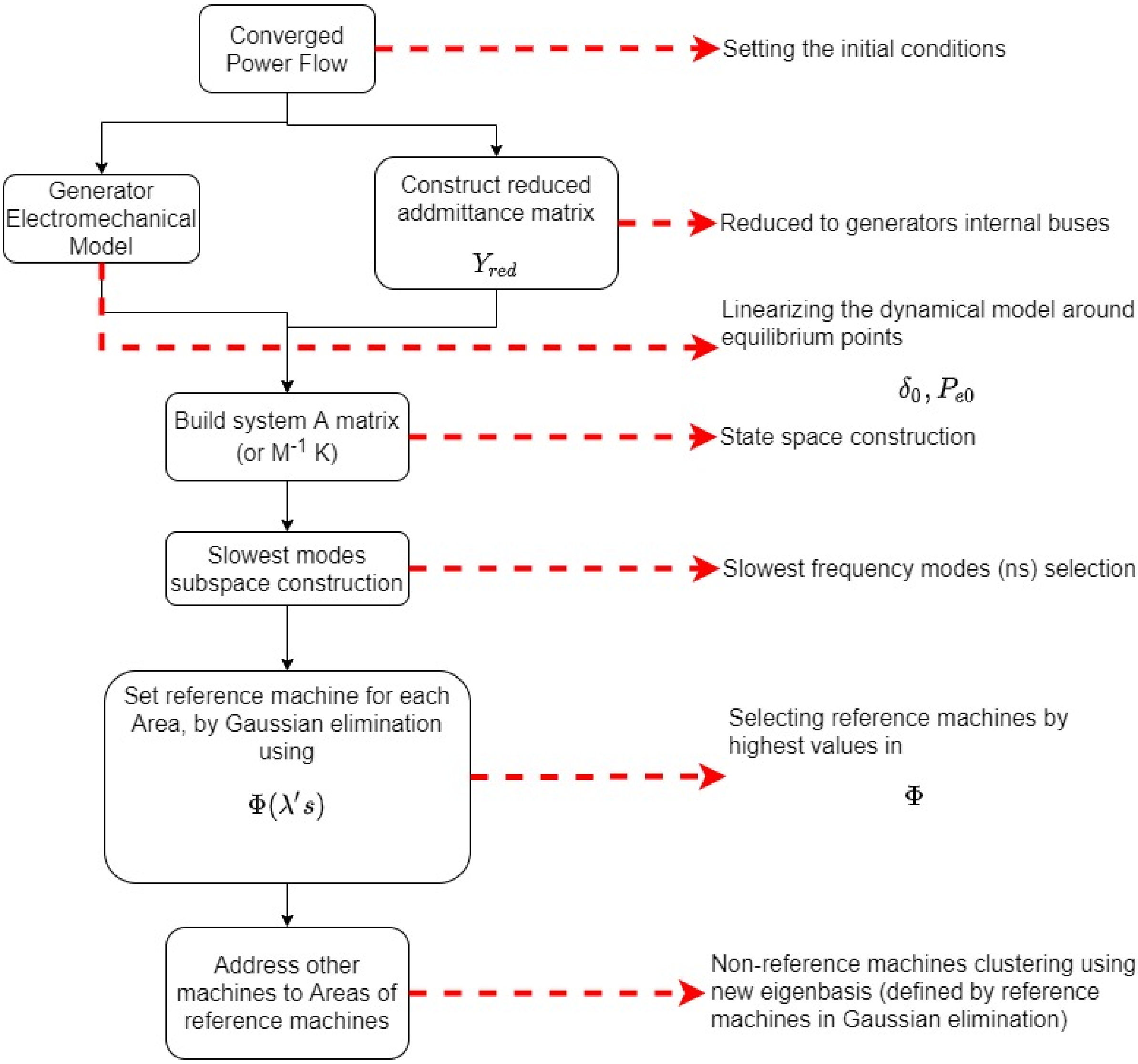

Figure 2.7 – Slow Coherency Algorithm

$$d_{i,j} = \frac{w_i w_j^T}{|w_i||w_j|} \tag{2.107}$$

where $d_{i,j}$ is the cosine between rows w_i and w_j of V_s. Two perfect coherent machines will produce $d_{i,j} = 1$. Hence, a tolerance to 'how coherent' two machines are can be set, namely γ. Let C_m be the matrix, whose elements are defined as:

$$C_m(i, j) = d_{i,j} - \gamma \tag{2.108}$$

Thus, a group of machines can be clustered following the following rules:

1. Machines i and j are coherent if $Cm(i, j) > 0$;
2. If machines i and j are coherent and machines j and k are coherent, then machines i and k are also coherent;

3. A loose coherent area J_α is formed by the machines that are coherent under Rules 1 and 2. Let $(C_m)_\alpha$ be a submatrix of C_m corresponding to J_α;

4. If the column sums of $(C_m)_\alpha$ excluding the diagonal entries are all positive, then J_α is a tight coherent area;

5. If any of the column sums of $(C_m)_\alpha$ excluding the diagonal entries is negative, then J_α should be decomposed into smaller tight coherent areas;

6. The least coherent machine in J_α corresponds to the columns of $(C_m)_\alpha$ with the smallest sum;

7. The coherency of J_α may be improved by removing the least coherent machine and reassigning it to a different area;

8. Given two partitions $I1$ and $I2$ of J_α, $I1$ is tighter than $I2$ if the sum of the offdiagonal entries of $(C_m)_\alpha$ corresponding to $I1$ is larger than that of $I2$.

Sets of tight-coherent generators can be found using the algorithm:

1. Find the loose coherent areas using Rules 1–3;

2. For each loose coherent area J_α;

    a) Use Rule 4 to determine whether it is also a tight coherent area, which requires no further decomposition;

    b) If the area is not tight, decompose the area into tight coherent areas. Start the decomposition by identifying the least coherent machine using Rule 6 and reassigning it using Rule 8. Continue until the loose coherent area has been decomposed into tight coherent areas and no improvement is possible under Rule 8.

2.4.3 Comparison between Tolerance-based and Slow-coherency grouping for the NPCC

(CHOW, 2013) applied the Tolerance-based method to the 48 machine NPCC system, with a tolerance constant $\gamma = 0.95$, and the 9 slowest modes, founding 17 areas. In contrast, using Slow-coherency method with 9 slowest-modes, 9 areas are found. For the Slow-coherency method to obtain the same number of areas, the 17 slowest modes must be considered. However, as can be seen in Table 2.2, different groups were found with each method.

Area	9 slowest modes, $\gamma = 0.95$	Slow-coherency, 17 slowest modes
1	3,4,5,6,7,8	6,3,7,9
2	1,2,9	1,2
3	10	8
4	11,12	11,12
5	13,14,24,25,26	13,10,14,24,25,26
6	15,16,17,18,19,20,21,22,23	16,17,18,19,20,21,22
7	27,28,29,30	29,27,28,30
8	31	15,23
9	32,37,38,40,42	32,31,33,37,38
10	33	40
11	34,35	34,35
12	36	36
13	39	39,42
14	41	41
15	43,44,45,46	44,43,45,46,47
16	47	5,4
17	48	48

Table 2.2 – Model-based methods comparison

2.5 Aggregation of Machines

In order to compare the quality of the resulting groups, the next Section will show an aggregation algorithm that provides a reduced model of the resulting areas. Applying this aggregation method to both sets of groups provided in Table 2.2 we can compare the 9 slowest modes between them and the actual values of the complete model for the NPCC 48 machines system. In this way, we can observe which method provides a better reduced model.

Although linearized models are derived for the inertial and slow-coherency aggregations, aggregates with conventional network and machine models can be reconstructed from the linearized reduced models.

2.5.1 Slow-coherency method

Regarding the slow-coherency aggregation method two must be considered: the model (2.105) is set up for a singular perturbation correction, regarding only the network within the area. The same will not hold for further corrections in (2.105). The second observation is that a nonlinear system must be derived from (2.105).

Starting with the r areas defined with some clustering method, the boundary buses must be identified (bewtween areas). All other load buses are internal to some area. The model dynamical model of that area is linearized and aggregated, having all non-essential load buses eliminated. The reduced models of the areas produced by the aggregation are reconnected and boundary load buses that are unnecessary are eliminated. The remaining linear model is used to reconstruct a network model of line and load parameters. The steps are shown in Figure 2.8 and the following paragraphs will discuss the operations necessary for those steps.

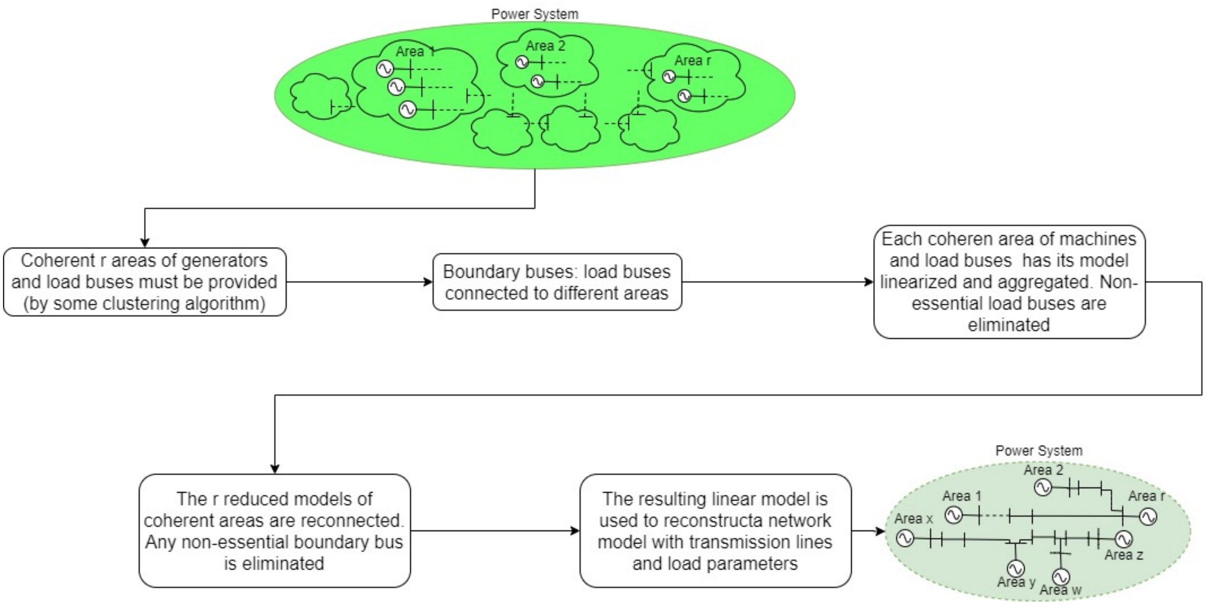

Figure 2.8 – Slow coherency aggregation steps.

Lets say that coherent machines appear consecutively in δ and the load buses as well in V. The nonlinear model for each coherent area $\alpha, \alpha = 1, 2, \ldots\ r$ is given by:

$$M^\alpha \ddot{\delta^\alpha} = f^\alpha(\delta^\alpha, V^\alpha) \tag{2.109}$$

$$I^\alpha = g^\alpha(\delta^\alpha, V^\alpha) \tag{2.110}$$

where δ^α is an $(n_\alpha \times 1)$ vector of machine angles, V_α is an $(2N_\alpha \times 1)$ vector of the real and imaginary part of load bus voltages, M^α is the area inertia matrix, f^α is a vector of acceleration torques, and g^α is the loadflow equation area α power network. The current injection I^α is nonzero at a given boundary bus and represents the connections to other areas, but need no calculation, since boundary injections will be canceled when reconnected for the formation of the whole system. Linearizing (2.110) around a solved loadflow we obtain the model:

$$M^\alpha \ddot{\delta^\alpha} = \frac{\partial f^\alpha(\delta^\alpha, V^\alpha)}{\partial \delta^\alpha}\Delta\delta^\alpha + \frac{\partial f^\alpha(\delta^\alpha, V^\alpha)}{\partial V^\alpha}\Delta V^\alpha = K_1^\alpha \Delta\delta^\alpha + K_2^\alpha \Delta V^\alpha \tag{2.111}$$

$$\Delta I^\alpha = \frac{\partial f^\alpha(\delta^\alpha, V^\alpha)}{\partial \delta^\alpha}\Delta\delta^\alpha + \frac{\partial f^\alpha(\delta^\alpha, V^\alpha)}{\partial V^\alpha}\Delta V^\alpha = K_3^\alpha \Delta\delta^\alpha + K_4^\alpha \Delta V^\alpha \tag{2.112}$$

All matrices are in regard to the generators and buses of area α, that is, they are bolcks of the system matrix, where K_j is computed as in Equation (2.90). Applying transformation (2.92), and separating slow and fast variables, and then solving for the slow variables the model obtained is:

$$m_a^\alpha \ddot{y}_\alpha = K_{11}^\alpha y_\alpha + K_{13}^\alpha \Delta V^\alpha \tag{2.113}$$

$$\Delta I^\alpha = K_{31}^\alpha y_\alpha + K_4^\alpha \Delta V^\alpha \tag{2.114}$$

The last aggregation step necessary is the elimination of internal bus voltages. The reduced order model of the $\alpha - th$ area would consist of the aggregate machine, the retained load buses and the boundary buses:

$$m_a^\alpha \ddot{y}_\alpha = \overline{K}_{11s}^\alpha y_\alpha + \overline{K}_{13s}^\alpha \Delta \overline{V}^\alpha \tag{2.115}$$

$$\Delta \overline{I}^\alpha = \overline{K}_{31s}^\alpha y_\alpha + \overline{K}_{4s}^\alpha \Delta \overline{V}^\alpha \tag{2.116}$$

Once each aggregate model is obtained, they are all reconnected, to form the aggregate system model:

$$M_a \ddot{y} = \overline{K}_{11s} y + \overline{K}_{13s} \Delta \overline{V} \tag{2.117}$$

$$0 = \overline{K}_{31s} y + \overline{K}_{4s} \Delta \overline{V} \tag{2.118}$$

It is shown in (DATE; CHOW, 1991) that (2.118) and (2.105) are the same dynamic model. **This invariance property is due to the fact that from a singular perturbation analysis, the first-order correction terms to the slow subsystem involve only the connections from the generator internal nodes to the terminal buses. For higher order correction terms, the per area aggregation concept is no longer applicable since the impedance corrections will depend on parameters in the other areas.**

The slow-coherency aggregation for two machines A and B is show in Figure 2.9. In the construction of (2.118), only the fast variable z is eliminated, while all the bus voltage variables are retained. This allows the reconstruction from the connection matrices K_{11s}, K_{13s}, K_{31s}, and K_{4s} of a power network consisting of impedances and phase shifters (Figure 8b). Although branch parameters can be reconstructed from the connection matrices, the recovered network, in general, would not have a balanced load flow. For tightly connected areas, the load flow mismatch would be small and loads can be added to the generation terminal buses to balance the load flow. The elimination of the fast variable z results in K_{4s} being a dense matrix. Thus in the reconstruction, all the generator terminal buses in the same area will be interconnected. **This interconnection is dependent only on the parameters within an coherent area, and represents the improvement to the inertial aggregate.** For practical reasons, such as implementing voltage regulator control, it is desirable to have the machine connected to only one terminal bus. Thus for each aggregate machine, we modify (2.118) by inserting two buses which are connected with reactances of x'_d and -x_d between the machine internal node and the remaining network (Figure 8c). The reactance x_d is an aggregate machine transient reactance, which can be computed as the MVA-weighted average of the individual machine transient reactances.

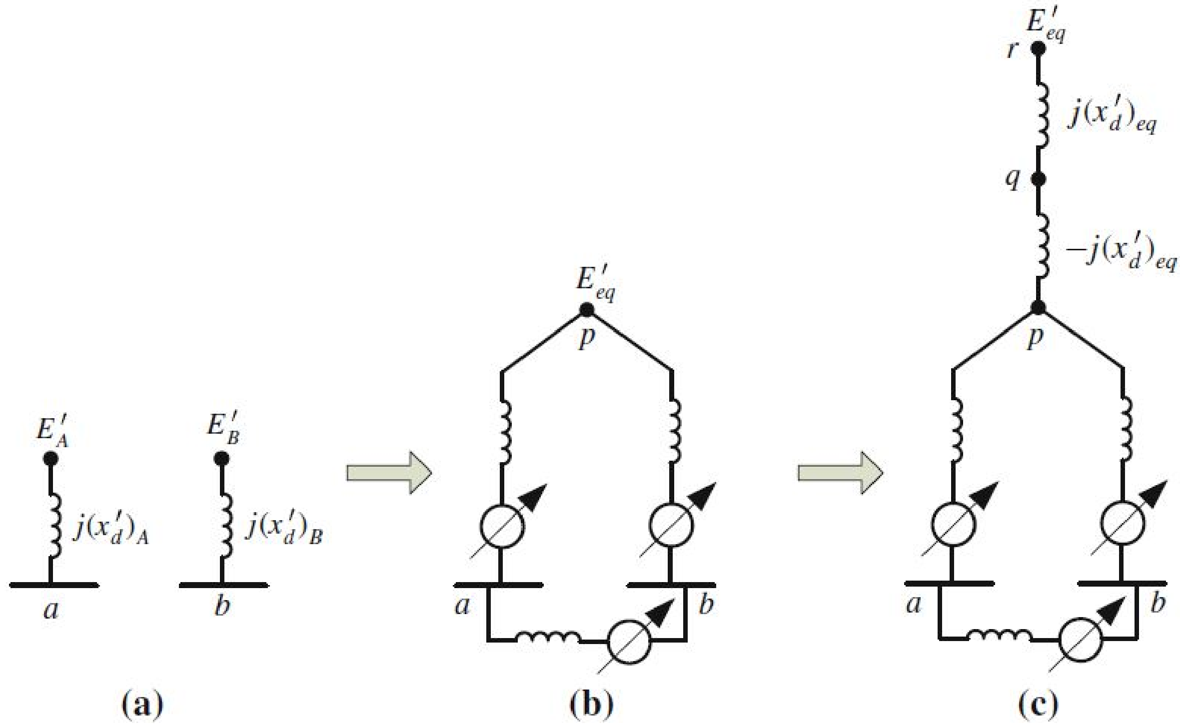

Figure 2.9 – Slow-coherency aggregation method

Finally, all the non-essential buses including the boundary buses can be eliminated from the model to form:

$$M_a\ddot{y} = \overline{K}_{11}y + \overline{K}_{12}\Delta\overline{V} \tag{2.119}$$

$$0 = \overline{K}_{21}y + \overline{K}_{22}\Delta\overline{V} \tag{2.120}$$

As the last step, the linear aggregate model (2.120) has to be converted into a physical power system model whose data can be used directly by conventional stability analysis and simulation programs. The parameters of interest are, for each transmission line, the line resistance, reactance, transformer ratio and phase shifter angle, and for each load bus, the active and reactive parts of the constant impedance, current and power type loads. The aggregate network needs to retain the dynamics represented by the aggregate sensitivity matrices $\overline{K}'s$, as well as preserve the network loadflow on the portions of the system retained in full detail.

Lets assume that the nonlinear representation of the network (2.120) is of the form:

$$M_a\ddot{y} = f_a(y, \overline{V})0 = g_a(y, \overline{V}) \tag{2.121}$$

where f_a and g_a are of the same form as (2.69), only the parameters are of the reduced model. The aggregate sensitivity matrices $\overline{K}'s$ must satisfy

$$\overline{K}_{i,j} = \hat{K}_{i,j} \qquad i, j = 1, 2 \tag{2.122}$$

where $\hat{K}_{i,j}$ are the linearizations of (2.120) at y_0 and $\overline{V}_0$, i.e., the first-order approximation of the reduced aggregate model without non-essential buses around the solved load-flow for that model.

Adding all aggregate generators terminal buses all matrix equalities will be met, except for the matrices regarding the admittance matrix:

$$\overline{K}_{22} = \hat{K}_{22} \tag{2.123}$$

So, in summary, the reconstruction of the aggregate network is the solution of (2.123), subject to a balanced load-flow solution, which in practical terms will not happen exactly. So, to reconstruct the network a two-step leas-squares optimization is applied: first the line parameters are optimized, subject to physical limits and the load-flow solution. Then, in the second-step, the load parameters are optimized, subject to the current balance of the load.

The optimization scheme would yield an aggregate power system model with physical machine, line, and load parameters. In addition to being a close approximate of the slow dynamics of the original system, the aggregate model also preserves the power flow as well as approximates the network flow sensitivities of the original system.

The slow-coherency aggregation algorithm is now summarized as follows.

Step 1: For coherent area $\alpha, \alpha = 1, 2, dots, r,$

1. Linearize the coherent area model (2.110) to obtain the model (2.112).

2. Apply the transformation (2.114) to (2.112) and eliminate the fast variables to obtain (2.116).

3. Eliminate the non-essential internal buses of (2.116) to form (2.118).

Step 2.

1. Reconnect the aggregate models of the coherent areas to form (2.118).

2. Introduce aggregate generator terminal buses as needed.

3. Eliminate all the non-essential buses to form (2.120).

Step 3.

1. For each line, solve the least-square optimization problem to obtain the line parameters.

2. For each load, solve the least-square optimization problem to obtain the load parameters.

To summarize, the slow-coherency aggregation method represents an improvement over the generator terminal bus aggregation technique by providing impedance corrections to the aggregate models and a more accurate load-flow sensitivity. An immediate consequence of the impedance corrections is the improved low frequency approximation by a slow-coherency aggregate network. The improved load-flow sensitivity is important in using the aggregate model for nonlinear simulations.

2.5.2 Next Chapters

Following Chapters will present the thesis methodology divided into two Chapters: the first will propose the region detection data-driven method that relies mostly on the theoretical concepts of Sections 2.3, 2.4 and 2.5. The second Chapter, will present the methodology of this research work that detects regional pilot-buses, sensible to load inertial response contribution, which is theoretically based on Sections 2.1 and 2.2.

A research of the literature most modern methods for data-driven methods is presented first in each Chapter, followed by the new theory of EDA applied to power systems, named TDA, with mathematical derivations. Next in each Chapter, each methodology is validated, using several power systems simulations and collected data, and Chapter 4 also presents the regional inertia estimation using the technique proposed in (LUGNANI et al., 2020; PINHEIRO et al., 2021). Each Chapter presents a final discussion of that particular piece of the thesis.

3 A meaningful area to estimate inertia

This Chapter will present the data-driven method for the detection of coherent areas of a power system, following a disturbance. First, a brief literature review of coherency clustering methods is presented, followed by a quick review of coherency observed in measured signal through distance metrics. Next we propose the TDA method for clustering, showing the statistical guarantee provided by the method and the advantages with respect to other clustering methods. Finally, the thesis shows the application of the TDA to a benchmark test system (IEEE 68 bus test system, here named S1) and a real system (United States Eastern Interconnection, here named S2) and close with a brief discussion reiterating the advantages of the method and showing ways to further develop this part of the work.

Besides the proposed approach of reducing model order, the coherency detection of power systems can be useful to understand power system dynamic behaviors and develop advanced applications such as controlled islanding (YOU et al., 2004; Wang et al., 2010; GOMEZ; RIOS, 2015; LIN et al., 2017a; SIDDIQUI et al., 2017; KAMALI et al., 2018), wide-area control and protection (DÖRFLER et al., 2014; WU et al., 2015; BABU; SARKAR, 2020; WANG et al., 2014; CHOW, 2013; TYURYUKANOV et al., 2020a; ABRAHAM et al., 2018; Henneaux et al., 2018; PAPIC et al., 2020).

However, in this Chapter the thesis focus on the development of method for regional inertia estimation, although other applications results are briefly presented in this Chapter.

3.1 State-of-the-art

The concept of coherency proposed in (PODMORE, 1978) develops the slow modes analysis (the ones concerning inter-area oscillations) of the linearized inertial aggregated model which groups generators by considering the equivalent machine angle, with machines internal nodes connected by infinite admittances. In (CHOW, 2013), the method in (PODMORE, 1978) is further advanced by adjusting the inertia aggregated model of a cluster, since this corrects the admittance connecting the internal nodes of machines by the fast modes of the model (local oscillating modes), improving the representation of the system. These Model-based approaches (MBA) have been extensively explored in the literature and their recent advances are reported in (TYURYUKANOV et al., 2020b). Despite these strong advances, MBA rely on the linearized model of a high-dimensional and complex nonlinear system, resulting that there are no guarantees for employing this concept in power system contingencies that may change the system structure and excite nonlinear dynamics. Thus, MBA may not be useful for online application in modern power systems (KHALIL; IRAVANI, 2018; NAGLIC et al., 2019).

Conversely, with the advent of WAMS, there is a clear need to explore the use of PMU measurements (voltage phase angle and frequency) to identify generator coherency. Where the new paradigm is not to rely on power system models (parameters and topology), but rather make use of the power system measured responses. These Data-driven methods (DDM) can be divided into three main approaches: temporal signal clustering (Alsafih; Dunn, 2010; ARIFF; PAL, 2012; KHALIL; IRAVANI, 2015; KHALIL; IRAVANI, 2018; AGHAMOHAMMADI; TABANDEH, 2016; ZNIDI et al., 2017; LIN et al., 2017b; LIN et al., 2017a; LIN et al., 2018; BANNA et al., 2019; NAGLIC et al., 2019), oscillatory mode detection (SUSUKI; MEZIC, 2014; Raak et al., 2016; CHAMORRO et al., 2016; THAKALLAPELLI et al., 2018; PATERNINA et al., 2018; FARROKHIFARD et al., 2019) and Machine learning (ML) techniques (KAMWA et al., 2007; Guo; Milanovic, 2016).

Regarding the temporal signal clustering approaches, an independent component analysis method using the rotor speed and angle of synchronous generators to determine their clusters, is proposed in (ARIFF; PAL, 2012). Meanwhile, the authors in (KHALIL; IRAVANI, 2015; KHALIL; IRAVANI, 2018) employ frequency deviation signals within a two step method that identifies clusters of generators by a cosine correlation index and aggregates the remaining buses into the coherent clusters. In (AGHAMOHAMMADI; TABANDEH, 2016), authors present an average correlation coefficient for clustering which is focused on an improvement of the Euclidean norm in combination with a threshold-defined heuristic algorithm. The Pearson product-moment correlation coefficient (PPCC) is introduced in (ZNIDI et al., 2017) by defining a distance metric among PMU voltage angles and applying a Hierarchical density-based spatial clustering of applications with noise (HDBSCAN) to select the clusters. Other investigations explore several distance metrics obtained from a special device to estimate rotor speeds and internal angles of generators; such metrics are ranked and processed by means of the Criteria importance through inter-criteria correlation (CRITIC) and the Kernel principal component analysis (KPCA) (LIN et al., 2017b; LIN et al., 2017a; LIN et al., 2018). These processed indexes are then clustered using AAgglomerative hierarchical clustering (AHC), spectral clustering and Affinity propagation (AP) methods. In (BANNA et al., 2019), the use of PMU measurements and Dynamic time warping (DTW) method form a strategy to identify coherency online from the rotor angles' information. Likewise, the work in (NAGLIC et al., 2019) tackles a new data-driven methodology for slow-coherency clustering of generators, hinged on heuristically determined composition of cosine dissimilarity and Minckowski distance among PMU measurements of frequencies at the generator terminal buses. The clustering process itself is performed using the affinity-propagation technique.

In the second approach, recent works propose the use of oscillatory mode extraction techniques, such as the Koopman method(SUSUKI; MEZIC, 2014; AL-MASRI; EHSANI, 2016), to identify the coherency of generators. In (Raak et al., 2016), a data-driven method that estimates the system's modes using angle measurements from all buses is proposed by performing a spectral analysis using the Koopman operator to identify the dominant modes and clustering with the K-means method. Also, the work in (CHAMORRO et al., 2016) extracts the modes of WAMS measurements applying the Koopman operator and then applies spectral analysis to identify coherent groups of generators with high penetration of non-synchronous generation. Meanwhile, the authors in (THAKALLAPELLI et al., 2018) employ a Linear quadratic regulator (LQR) and Kalman filtering applied to synchrophasor measurements to estimate space-state variables for determining oscillations among areas and apply to those clustered areas in controlled islanding schemes. Likewise, the authors from (PATERNINA et al., 2018) extract the modes using Taylor-Fourier Transform and cluster the generators using hierarchical agglomerative technique, with Elbow's method to improve the initial guess for the number of clusters. In (FARROKHIFARD et al., 2019), a Fast frequency domain decomposition (FFDD) modal analysis method is applied to real measurements of oscillation monitoring, from the Réseau de Transport d'Électricité (RTE) power system, and the clustering is processed by the Density-based spatial clustering of applications with noise (DBSCAN) method.

Finally, ML approaches rely on large data sets to train the classifiers. In (KAMWA et al., 2007), bus angle and frequency measurements from PMUs are used to determine a dissimilarity rms-coherency criterion index between buses, for each disturbance event, forming a matrix of dissimilarity indexes. Gathering matrices from several events, a probability of similarity among buses is constructed and applied to a Fuzzy medoids algorithm (FCMdd) to perform the clustering. In (Guo; Milanovic, 2016), the coherency detection is applied to unstable simulated transient events, which are first classified using binary labeling. Once, a relative large number of cases is simulated, hierarchical clustering is applied to group formation. Then, different classification techniques (decision tree, ensemble decision tree and multi-class support vector machine) are explored to identify the unstable responses (unstable groups).

Despite all advantages enclose in the three aforementioned approaches, there are some gaps to be fulfilled. The main limitations of the temporal signal clustering methods are usually associated with an empirical threshold that must be tuned, which may have to be re-tuned for anomalous events by expert users with a previous knowledge of the system dynamic behavior. Regarding the oscillatory mode extraction methods, the authors in (NAGLIC et al., 2019) claim that these techniques are often affected by the inaccuracies of the mode estimation and the high computational burden required to process long observation windows. Finally, the key requirement for the success of machine-learning approaches is to have a representative database used in the training process to prevent over-fitting problems. This accuracy crucially depends on the quantity and quality of the available data as well as the time consuming task of manually labeling a huge amount of events. The training process of machine-learning methods also involves a large computational burden and manual configuration of hyper-parameters that must be retrained after possible classification failures. Furthermore, the interpretability may also be a limitation for deep learning methods when they are applied to critical tasks.

3.2 Problem statement

Nowadays, the power system industry has been experiencing a major challenge since synchronous machines and controllers are replaced by IBR. The effects of the integration of a large amount of IBR, whose regulation and interaction with the rest of the system is still to be fully understood, may impact the identification of groups depending on the state of the system and location of the disturbance (CHAMORRO et al., 2016; LIN et al., 2017b; KHALIL; IRAVANI, 2018; NAGLIC et al., 2019; LIN et al., 2017b). To develop fully data-driven applications capable to process large amount of collected PMU data, it is helpful to understand the effects of IBR on coherency identification, islanding detection and model reduction of power systems. Table 3.1 shows a comparison of the required information/assumptions by the methods, this is marked by **X** and additional information that some of the methods can provide, besides machine clustering, such as islanding detection, marked by checkmark ✓, when compared with the method proposed here. It is important to point out that, to the authors' best understanding, some of the methods may be able to provide additional information, but they do not present any comment or results to that regard.

This thesis introduce the concept and explore the advantages of a non-parametric statistical method for coherency tracking. This method does not have the constraints that the parametric methods impose for their application, which requires a previous knowledge about the process and dataset (population). This clearly reduces the effort to apply and understand the proposed method, improving its use in real world applications.

Table 3.1 – Comparison of requirements for coherency methods

	# clusters	Center seeds	User const's.	Gen. parameters	Grid parameters
(CHAMORRO et al., 2016)	**X**		**X**	**X**	
(KHALIL; IRAVANI, 2015; KHALIL; IRAVANI, 2018)			**X**	**X**	
(PATERNINA et al., 2018)	**X**	**X**		**X**	**X**
(AGHAMOHAMMADI; TABANDEH, 2016)			**X**	**X**	
(Znidi et al., 2020)			**X**		
(KAMWA et al., 2007)	**X**	**X**	**X**	**X**	
(Raak et al., 2016)	**X**			**X**	**X**
(Guo; Milanovic, 2016)	**X**		**X**		
(LIN et al., 2017a; LIN et al., 2017b; LIN et al., 2018)			**X**	**X**	
(BANNA et al., 2019)	**X**	**X**	**X**		**X**
(THAKALLAPELLI et al., 2018)	**X**	**X**	**X**		
(NAGLIC et al., 2019)	**X**	**X**			
TDA					

	Alg. train	PMU meas.	Buses clustering	Robustness	Islanding detection
(CHAMORRO et al., 2016)		**X**		✓	
(KHALIL; IRAVANI, 2015; KHALIL; IRAVANI, 2018)		**X**	✓	✓	✓
(PATERNINA et al., 2018)		**X**			
(AGHAMOHAMMADI; TABANDEH, 2016)		**X**			
(Znidi et al., 2020)	**X**	**X**	✓	✓	✓
(KAMWA et al., 2007)	**X**	**X**	✓	✓	
(Raak et al., 2016)		**X**	✓		
(Guo; Milanovic, 2016)	**X**	**X**			✓
(LIN et al., 2017a; LIN et al., 2017b; LIN et al., 2018)		**X**			
(BANNA et al., 2019)		**X**			✓
(THAKALLAPELLI et al., 2018)		**X**		✓	
(NAGLIC et al., 2019)		**X**		✓	
TDA		**X**	✓	✓	✓

3.3 Contributions

The main contribution in this work is related to the extraction of statistical characteristics exclusively from the data, without any assumption of the distribution of the data. This idea establishes a new paradigm for data handling, as the number of clusters is automatically found from each data-set, regardless of parameter tuning like most data-driven methods. Further, the statistical information extracted from the data is supported mathematically. The method, typicality-based data analysis (TDA), is applied to distances between frequency dynamic responses by employing the methodology in (ANGELOV et al., 2017). It is also customized to be implemented along with synchrophasor measurements from dynamic transient responses for the detection of power system islands by performing a clustering process. The main contributions are stated as follows: (*i*) this is a fully data-driven method which means that there is no necessity to determine the optimal number of clusters or initial guesses of centroids to initialize the grouping algorithm; (*ii*) contrary to conventional parametric statistical methods that must rely on probability density functions (PDF), assuming a set of fixed parameters that determine a probability model, non-parametric methods do not require previous knowledge of the process and the dataset (population) being handled; (*iii*) there is no necessity to manually label all the huge amounts of training data to build a representative database to be used in a training process aiming to prevent over-fitting problems; (*iv*) the mathematical background of the proposed approach is clear, allowing understanding of the results; (*v*) the method is capable of detecting the islanding conditions of the system and is robust to noisy measurements; (*vi*) due to its low computational complexity, it is suitable for transitory period applications; and (*vii*) the method is tested and validated using real PMU measurements from a large power system.

3.4 Fundamentals

3.4.1 Coherency

Coherent trajectories are defined as machines with responses indistinguishable from each other, i.e., the difference between their angles (θ) or frequencies (f) , remains very small (CHOW, 2013):

$$\theta_k(t) - \theta_j(t) \leq \gamma \tag{3.1}$$

where k and j are generator buses, γ is an arbitrarily user-defined value for the maximum divergence between any two responses within an area. This method can be applied to either f or θ, since the first is a derivation of the second one, as stated by

$$\Delta f_i|_{t+\Delta t} = \frac{1}{\omega_0}\frac{\theta_i|_{t+\Delta t} - \theta_i|_t}{\Delta t} \tag{3.2}$$

where $\Delta f_i|_{t+\Delta t}$ stands for the frequency deviation (in Hz) of the i-th bus at the time step Δt, $\omega_0 = 2\pi f_0$, f_0 is the system nominal frequency in Hz, and θ_i is the i-th bus voltage angle. Since Δt and ω_0 are constant in (3.2), we can regroup them as a constant η and considering $\theta_i|_{t+\Delta t} - \theta_i|_t = \Delta\theta_i|_{t+\Delta t}$, such that Δf_i becomes:

$$\Delta f_i|_{t+\Delta t} = \eta\Delta\theta_i|_{t+\Delta t} \tag{3.3}$$

where $\eta = 1/(\omega_0 \Delta t)$.

3.4.2 The Euclidean norm

A norm maps vectors onto a scalar to represent the distance between two time-domain responses. The Euclidean norm is used since is considered stable, i.e., it is reliable to the adjustments of window lengths when it is compared with the absolute norm, which is considered more robust to outliers. Meanwhile, the outlier robustness can be readily overcome by filtering (JAMES et al., 2013). Given two points of measurement k and j for every time instant t, the distance $dd_{k,j}(t)$ between their frequencies is expressed by (BATISTA et al., 2014)

$$dd_{k,j}(t) = [f_k(t) - f_j(t)]^2 \tag{3.4}$$

where $dd_{k,j}(t)$ is squared since the value of $f_k(t) - f_j(t)$ may be negative. The Euclidean norm is a distance metric that satisfies all the following conditions (ANGELOV; GU, 2019): *i)* non-negativity: $dd_{k,j} \geq 0$; *ii)* identity of indiscernible: $dd_{k,j} = 0 \iff k = j$; *iii)* symmetry: $dd_{k,j} = dd_{j,k}$; and *iv)* triangle inequality: $dd_{k,h} + dd_{j,h} \geq dd_{k,j}$. Metrics such as the cosine similarity do not attain such conditions. This is important because, with the Euclidean norm, we are able to represent the distance among two responses by a scalar and retain the signal mathematical properties.

Additionally, the nominal frequency f_0 is removed, so that $dd_{k,j}(t)$ is calculated as

$$dd_{k,j}(t) = [(f_k(t) - f_0) - (f_j(t) - f_0)]^2 = [\Delta f_k(t) - \Delta f_j(t)]^2 \tag{3.5}$$

Next, the square root of the sum of all values for a time window T is computed, $T = t_0, \ldots, t_f$, where t_0 is the moment of the disturbance, and t_f corresponds to the time window ending. The square root of the sum of $dd_{k,j}(t)$ is calculated projecting it onto a matrix of scalar quantities $\nu(k,j)$, with each entry representing the distance between points of measurements k and j, expressed as (BATISTA et al., 2014)

$$\nu(k,j) = \sqrt{\sum_{t=t_0}^{t_f} [\Delta f_k(t) - \Delta f_j(t)]^2} \tag{3.6}$$

For every bus k, ν_k is a $1 \times N$ vector, corresponding to the distances between the dynamic response from bus k to the other buses, where N is the total number of buses with available measurement.

3.4.3 The distance metric: correlation

The vector of scalar quantities ν_k represents the norm of the distance from bus k to the other buses, making up a data point in the data-set to be used by the TDA method. The proposed method requires a measured quantity between the data points in the set, defined by the user (ANGELOV et al., 2017). Therefore, the correlation $\rho_{k,j}$ between two data points in the vector $\nu(k,j)$ is defined by

$$\rho_{k,j} = corr(\nu_k, \nu_j) = \frac{cov(\nu_k, \nu_j)}{\sigma_{\nu_k}\sigma_{\nu_j}} \tag{3.7}$$

where $corr(\nu_k, \nu_j)$ indicates the correlation between the distances of buses k and j, distributed in R^N, $cov(\nu_k, \nu_j)$ represents the covariance between the distances ν_k and ν_j, and σ is the standard deviation.

3.5 Typicality-Based Data Analysis

In this section, the fundamentals and definitions of a non-parametric statistical method (ANGELOV et al., 2017) applied to the coherency tracking are presented. This is a distribution free method that is exclusively based on ensemble statistical properties of the data derived entirely from the experimental discrete observations. These properties are defined as follows (ANGELOV et al., 2017).

3.5.1 Cumulative proximity

In graph (networks) theory, a measure of *centrality* is defined as the inverse of the so-called *farness* which is a sum of distances from one point to all other points (FREEMAN, 1978). From (ANGELOV et al., 2017), the cumulative proximity is defined as a squared form of the *farness*:

$$q_N(\nu_k) = \sum_{j=1}^{N} \rho_{k,j}; \qquad \nu_k \in \nu_N \tag{3.8}$$

Cumulative proximity is an important association measure that is empirically derived from the observed data without making any *prior* assumptions about their generation model, and plays a fundamental role in deriving other statistical properties for the TDA method (ANGELOV et al., 2017).

3.5.2 Standardized eccentricity

This quantity is defined within the TDA method as a normalized cumulative proximity by half of the average cumulative proximity:

$$\epsilon_N(\nu_k) = \frac{2q_N(\nu_k)}{\frac{1}{N}\sum_{j=1}^{N} q_N q_N(\nu_j)} \tag{3.9}$$

where the coefficient two is included to compensate distance duplication in the denominator. If ϵ is divided by the amount of data N, then the non-standard eccentricity ξ becomes $\xi_N(\nu_k) = \frac{1}{N}\epsilon_N(\nu_k)$, leading to the following bounds for the eccentricity value:

$$0 \leq \xi_N(\nu_k) < 1 \tag{3.10}$$

This property makes up a significant measure of the ensemble property related to the distribution tail and it is also empirically derived from the observed data. It plays an important role in anomaly detection, analysis of rare events, as well as for the estimation of the typicality (ANGELOV et al., 2017). By considering the *Chebyshev inequality* (SAW et al., 1984) that indicates the probability of data being outlier (a data sample ν is more than $n\sigma$, where σ denotes the standard deviation, distance away from the *mean* in a given distribution) and applying the standard eccentricity to it, the TDA version of the *Chebyshev inequality* becomes (ANGELOV et al., 2017):

$$P(\epsilon_N(\nu_k) \leq n^2 + 1) \geq 1 - \frac{1}{n^2} \tag{3.11}$$

By expressing the *Chebyshev inequality* by means of the standard eccentricity, this allows detecting anomalies in data. For instance, if the standardized eccentricity $\epsilon_N(\nu) > 10$, then ν exceeds the 3σ limitation, this event can be categorized as an anomaly. This information is significant for boundary data, since it minimizes the probability of data miss-location in wrong clusters.

3.5.3 Discrete local density

This property is defined as the inverse of the *standardized eccentricity* (ANGELOV et al., 2017), becoming

$$D_N(\nu_k) = \frac{\sum_{j=1}^{N} q_N(\nu_j)}{2Nq_N(\nu_k)}, \quad \text{with} \;\; i = 1, 2, \cdots, N. \tag{3.12}$$

3.5.4 Discrete typicality

This quantity is established as the normalized *density*. It quantifies how common, or typical, a value is within the data set under study. As comparison, the typicality can be seen as a probability equivalent of a given random variable that takes the value of the measured point. The typicality is obtained from the data set instead of being assigned by model fitting of a probability mass function (PMF), and it is given by (ANGELOV et al., 2017)

$$\tau_k(\nu_k) = \frac{D_N(\nu_k)}{\sum_{j=1}^{N} D_N(\nu_j)} = \frac{q_N^{-1}(\nu_k)}{\sum_{j=1}^{N} q_N^{-1}(\nu_j)} \tag{3.13}$$

The *discrete typicality* resembles the traditional unimodal PMF, being constructed from the data set and excluding the possibility of non-feasible values that may result in consequence of fitting to PMF (ANGELOV et al., 2017). In the following section, the proposed method is applied to frequency measurements.

3.5.5 Proof of the clustering concept of TDA

Let's assume a system with B buses and their respective frequency measurements that are converted into a scalar by (3.6), where $N_B = \nu_1, \ldots, \nu_n, \ldots, \nu_B$, $\nu_1 = \nu(1,1), \nu(1,2), \ldots, \nu(1,B)$. The distance metric of correlation among points given by $\rho_{1,2}$. Once the TDA is applied, the initial set points N_B is divided into clusters of points $(\alpha, \beta, \ldots, c)$, where c is the number of clusters found by the TDA method. Let α be a cluster of buses, whose Euclidean norms from N_B are denoted by

$$N_\alpha = \{\nu_i, \nu_k, \ldots, \nu_a\}$$

and their distances with respect to all buses are given by

$$P_\alpha = \{\rho_i, \rho_k, \ldots, \rho_a\}$$

Then, their eccentricities are expressed by

$$E_\alpha = \{\epsilon_i, \epsilon_k, \ldots, \epsilon_a\}$$

And their typicalities are symbolized by

$$T_\alpha = \{\tau_i, \tau_k, \ldots, \tau_a\}$$

where T_α and P_α are used to determine the closest points in the data-set distribution, as shown in **Algorithm 1**. Once, a cluster is found, the mean $\mu_\alpha(\nu)$ and standard deviation $\sigma_\alpha(\nu)$ are calculated for the cluster. ρ^*_α is the minimal correlation, i.e., maximum distance in cluster α.

The probability of the point ν^*_α of α being less than $3\sigma_\alpha$ distant from μ_α of cluster α, i.e., bus α^* belonging to cluster α, can be seen by its eccentricity ϵ^*_α, when we apply ϵ^*_α to (3.11), with respect to the cluster standard deviation

$$P\Big(\epsilon *_\alpha (\nu *_\alpha) \leq 3\sigma_\alpha^2 + 1\Big) \geq 1 - \frac{1}{3\sigma_\alpha^2} \tag{3.14}$$

If we assume a normalized standard deviation of $\sigma_\alpha = 1$, then we get

$$P\Big(\epsilon *_\alpha (\nu *_\alpha) \leq 10\Big) \geq \frac{8}{9} \tag{3.15}$$

which is a conservative estimate since the Chebyshev inequality does not assume any prior information about the distribution of the data. For instance, the usual assumption for normal distribution in our case, the probability of being under 3σ of the mean is 99.7%. As it will be shown in the next section, the construction of the algorithm allocates each point ν to the cluster whose highest typicality point ν_τ has the closest distance ρ to ν. This in turns means that ν^*_α has the highest probability of belonging to cluster α, of all clusters. This is further exemplified in Figure 3.1, where a visual representation of the statistical proof and algorithmic construction of the clusters is depicted. This will be also discussed in detail in the next section. Such construction and mathematical proof indicate the meaningfulness of the clustering produced by the TDA method.

3.6 TDA Application for Coherency Detection

This subsection will introduce a methodological implementation of the EDA properties proposed above to the coherency detection problem in power systems after events, using data collected by WAMS, including practical aspects relating to filtering and missing packets.

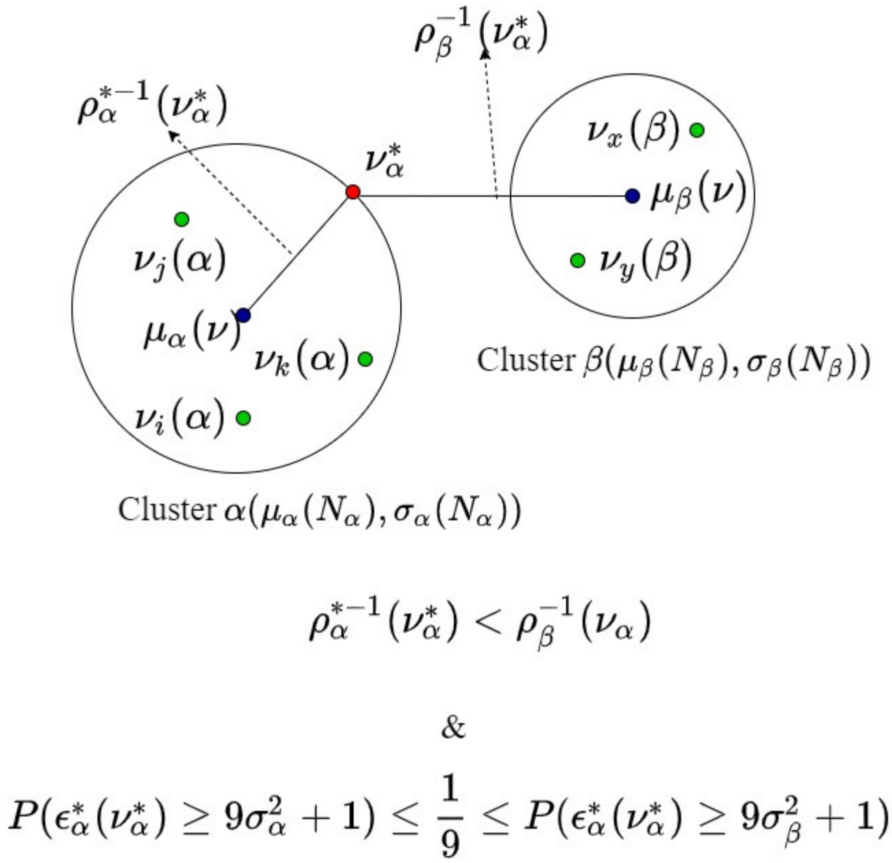

Figure 3.1 – Clustering validity example.

3.6.1 Stage I. Pre-processing

Due to non-electromechanical phenomena, the voltage angles may present spikes known as phase-shifts (SAUER et al., 2016), which are unrealistic for machines rotor dynamics and bus frequencies overall. For this reason, a *moving median* filter is the first step in the pre-processing stage. Additionally, any PMU that reports data quality issues per flags STAT (ASSOCIATION et al., 2011) (bits 6 to 15), is discarded. Errors in measurement that bring bias to the reported synchrophasors must be addressed by the state estimation and are out of the scope of this work. However, it is noteworthy to mention that a constant bias in the angle measurements would not impact the frequency since this is estimated regarding the angle variation. This stage comprises: (*i*) outlier removal with the *movmedian* Matlab function (this is applied using a 5-sample window); (*ii*) DC offset removal, i.e., difference from 60 Hz Δf is computed; the resulting signal is detrended with the dynamics separation algorithm (LACKNER et al., 2020), which is of great importance particularly in events such as generation trips, where the steady state component of the signal changes; (*iii*) computation of the Euclidean norm using (3.6), that is, $\nu(k,j) = \sqrt{\sum[dd_{k,j}^2]}$ (BATISTA et al., 2014). This norm maps vectors onto scalars in order to represent time-domain responses in a scalar space distribution (reducing the dimension of the data-set). At the end of the pre-processing stage, a data set is generated in R^N, that is, the dimensional space of the data set is equal to the number of measurement points (ideally, equal to the number of buses), with points $\nu_i = [\nu_{i,1}, \nu_{i,2}, ..., \nu_{i,K}]^T$, $i = 1, 2, ..., N$, where each value in vector ν_i is a norm of bus i to another bus, and ν_i denotes the coordinates of bus i in such space.

3.6.2 Stage II. Metric (correlation) computation

In this investigation, the correlation ρ is adopted as a distance metric, being implemented as exhibits lines 4 to 8 of **Algorithm 1**.

3.6.3 Stage III. Properties calculation

The TDA method clusters data using the typicality of each data point in the data set, using ρ as a metric. To reach the typicality value, the properties provided in the previous section are calculated for a given set of data points ν_k: the cumulative proximity $q_N(\nu_K)$ is computed using (3.8); the standardized eccentricity $\epsilon_N(\nu_k)$ is quantified using (3.9) (which is an important measure for data-handling correction, as $\epsilon_N(\nu_k)$ must be a value between 0 and 1); the discrete local density $D_N(\nu_k)$ is obtained from (3.12).

Finally, the typicality $\tau_k(\nu_k)$ of ν_k is calculated using (3.13) and taking into account the following properties: (i) the sum of the typicalities for all data points $\tau_k(\nu_k)$ is 1; (ii) all values of τ_k are between 0 and 1; and (iii) no prior assumptions of the data model are gathered. This is indicated through lines 10 to 12 of **Algorithm 1**.

3.6.4 Stage IV. Typicality ranking

Once all τ_k are computed, the one with the maximum value is tagged as the global typicality τ_N^{D*} and placed in the first element of the vector $ranked_\tau$. A ranking of typicalities is accomplished as follows: the data point ν^2, where the superscript 2 indicates the position in the ranking of typicalities with the highest metric ρ to the data point of the global typicality τ_N^{D*}, and its τ_k^2 is assigned next in the vector $ranked_\tau$. Then, the data point ν^3 with the highest metric ρ to the data point ν^2 of the typicality τ_N^2, and its τ_k^3 arrayed next in the vector $ranked_\tau$. This is recursively performed until all typicalities are ranked, as pointed out in lines 15 to 19 of **Algorithm 1**.

3.6.5 Stage V. Cluster formation and filtering

The typicalities' peaks are found locating the points ν_k^* as initial cloud centers. This is carried out employing lines 20-26 of **Algorithm 1**. Once all cloud centers are located, the remaining data points ν_k are assigned to the center's cluster, in which it has the highest correlation ρ. This is conveyed in **Algorithm 1** from lines 28 to 30. For all clusters, the mean ($Cluster_\mu$) and deviation ($Cluster_\sigma$) of data points are computed by lines 34 to 37 in **Algorithm 1**. Finally, the clusters are filtered by clustering all clouds that are close together and recalculating their statistical properties. This is performed by lines 39 to 42 of **Algorithm 1** until the number of clusters remains unchanged. The final clusters correspond to the areas found using the TDA method. Here, it is important to point out that, by using the Euclidean distance among the measured frequency deviations, the TDA method implicitly takes into account the inertia of the generation units in the system as the typicality property of the method. All the process performed by **Algorithm 1** takes place in a single step manner, unlike the approach in (KHALIL; IRAVANI, 2015), where the constant of neighborhood defined by the user must be changed for non-generator buses and supposes uniform inertia distribution. Other methods assume that the center of the inertia frequency deviation vector considers equal weights to all generators, unlike the TDA method that implicitly regards the inertia of each generator, since the Euclidean distance of frequencies is greatly influenced by the inertia of the areas.

3.7 Performance of the Typicality-Based Data Analysis

The TDA method is now applied to the New England 68-bus and 16-machine test system (S1) (PAL; CHAUDHURI, 2006) and to real measurements from FNET/GridEye WAMS (ZHANG et al., 2010) for the Eastern Interconnection (S2).

The nonlinear simulations that provide the input data for the TDA method obtained from the power system toolbox (PST) (CHOW; CHEUNG, 1992; CHOW, 2020), assuming the availability of voltage angle/frequency responses at all buses. All simulations are carried out for 20 s with a time-step of $1ms$. The time window considered for calculation of ν_k in all cases is of $10s$ after disturbance takes place, as in (KHALIL; IRAVANI, 2015). The responses are decimated to 120 Hz, complying with the IEEE synchrophasor standard (ASSOCIATION et al., 2011), to the simulated system *S1*. The transitory period of the response is useful for the detection of islanding condition; meanwhile, the transient period allows the correct slow-coherency detection. Additionally, the method was explored in *S1* for measurements with rates of 60 and 30 Hz, displaying similar results. The measurements from *S2* are by default 10 Hz.

Algorithm 1 TDA implementation for PMU dynamic response

Input: Let ν_k, $k = 1, \dots N$ (data points) vector of scalar Euclidean norms between frequencies responses, with N being the number of PMUs.
Output: A set of coherent areas with generators and non-generator buses (**Clusters**).
Initialization: $\mathbf{t}_0$, $\mathbf{t}_f$, set of correlation metrics $\rho_{k,j}$
for k=1,k++ **do**
  for j=1,j++ **do**
    $\rho_{k,j} \leftarrow \frac{cov(\nu_k,\nu_j)}{\sigma_k \sigma_j} \quad \nu_k, \nu_j \in \nu_N$
  end for
end for
TDA properties computation
Cumulative proximity: $q_N(\nu_k) \leftarrow \sum_{j=1}^{N} \rho_{k,j}$;
Discrete local density: $D_N(\nu_k) \leftarrow \frac{\sum_{j=1}^{N} q_N(\nu_j)}{2N q_N(\nu_k)}$
Discrete typicality: $\tau_k(\nu_k) \leftarrow \frac{D_N(\nu_k)}{\sum_{j=1}^{N} D_N(\nu_j)}$
Global typicality: $\tau_N^{D*} \leftarrow max(\tau_i^D) \quad i = 1, \dots, N$
Starting from data point ($\nu(\tau_N^{D*})$), rank of typicalities (τ_k^D) for all data points (ν_k) based on the correlation metric ($\rho_{k,j}$):
for k=2, k++ **do**
  for j=1, j++ **do**
    $ranked_\tau(k) \leftarrow \tau_j(max(\rho_{\nu_{k-1},j}))$
  end for
end for
Finding data centers and data clouds: Find peaks of $ranked_\tau(k)$:
for k=1, k++ **do**
  if $[\tau^D(\nu(k-1)) < \tau^D(\nu(k))]$ & $[\tau^D(\nu(k)) > \tau^D(\nu(k+1))]$ **then**
    ν_k is a local maximum
    $\nu_k* \leftarrow \nu_k$ cloud center vector
  end if
end for
Forming data clouds around ν_k*, considering ρ:
for k=1, k++, $k \neq \nu_k*$ **do**
  $Cluster(k) \leftarrow argmax_k(\rho(\nu*, \nu_k))$
end for
Filtering data clouds:
while $size(Cluster)$ is unchangeable **do**
  Computing statistical of clouds:
  for k=1, k++ **do**
    $Cluster_\mu(k) \leftarrow \mu(\rho_{\nu,\nu*})$
    $Cluster_\sigma(k) \leftarrow \sigma(\rho_{\nu,\nu*})$
  end for
  Filtering the data clouds using $Cluster_\mu$ and $Cluster_\sigma$ and τ:
  if $[||\mu_N^i - \mu_N^j|| \leq 2\sigma_N^i]$& $[\tau_N^D(\mu_N^i) < \tau_N^D(\mu_N^j)]$ **then**
    $Cluster(j) \leftarrow [Cluster(j); Cluster(i)]$
  end if
end while
return Clusters

3.7.1 68-bus System (*S1*) - Comparison to DCD

The 68-bus and 16-machine system *S1* is a reduced order equivalent of the interconnected New England transmission system (NETS) and New York power system (NYPS). All generators are represented by a sixth order model equipped with automatic voltage regulators (AVRs), and all loads are assumed as constant impedance (CANIZARES et al., 2017). *Cases S1.C1* and *S1.C2* intend to compare the areas found with those ones in (KHALIL; IRAVANI, 2015), and illustrate the advantages against MBA, since it detects islands and areas not connected, which is of great interest for wide-area control purposes. The noise tolerance is assessed including tests with noisy signals up to 30dB of signal-to-noise ratio (SNR) for *Cases S1.C1* and *S1.C2*, but they are not displayed for the sake of brevity, since the TDA method is able to find the same areas.

3.7.1.1 Application on Case S1.C1

the first case is a three-phase fault at bus 27 in Fig. 3.4, at $t = 0.5s$, lasting 5 cycles.

The result of Stage I is a data set of the Euclidean norms ν_k in R^{68}, with number of points $N = 68$. In Stage II, each point ν_k have its correlation metric ρ_k to every other point ν_j, forming a metric vector with the same dimension. The correlations among the norms of all signals from *S1.C1* are projected onto the heat map in Fig. 3.2, where the strong correlations are represented in brown color. The main challenge now is to compute how the groups of high correlation buses can be formed into clusters.

In the proposed method, the clusters are obtained without any arbitrary cutoff constant using the TDA properties. The main result is the vector of typicalities for every point ν_k, which is depicted in Fig. 3.3(a) (before ranking). The high values of typicalities indicate that these buses consist of representative frequency responses. Otherwise, these buses are the ones with minor deviations when compared to the other ones in the same data set. It is also a clear indication that these buses have a strong connection within the measured buses. For example, Buses 10-13,30,31,36,48,49,53 and 61, with high typicality values, are part of the meshed area (NYPS area).

Next, in Stage IV, these typicalities values must be ranked starting from the global typicality τ_N^{D*} (maximum typicality value) according to the correlation illustrated in the Fig.3.3(b). Where the peaks are the initial centers for each cluster that must be processed using **Algorithm 1 (line 24)**. In Fig. 3.3(b), the $x-axis$ refers to the position of τ in the ranked vector $ranked_\tau(k)$. At Stage V, the TDA algorithm detects the peaks in the ranked vector to form the initial clusters around those peaks. A filtering process is carried out regarding the mean and standard deviation from the clusters around the peaks. This filtering process takes place until the numbers of clusters does not change. In this case, the algorithm found the solution in three iterations. The final clusters of typicalities are depicted in Fig. 3.3(c), where the $x - axis$ still displays the buses ranked by the correlation metric.

The resulting seven clusters (areas) are presented in Table 3.2 and illustrated in Fig. 3.4. For comparison purposes with both DDMs and MBA, Table 3.2 summarizes the areas found by (KHALIL; IRAVANI, 2015), (CHOW, 2013), **and applying the AP algorithm (FREY; DUECK, 2007) for the same correlation metric,** ρ. The results from (CHOW, 2013) are the same for all case, since it does not consider events, so it will be shown only in Table 3.2.

Figure 3.3(c) illustrates the ranked typicalities, demonstrating that the TDA method exhibits a fine definition of clusters, separating Area 1 from (KHALIL; IRAVANI, 2015) into Areas 5, 6 and 7, shown in Figure 3.4. This shows a stronger effect of local modes in the NETS system, which can only be captured if the window length considers the initial transitory period of the frequency response. This effect is not captured by traditional slow-coherency methods. The TDA approach also includes tie-line buses from NETS to NYPS into Area 4, which has the generators electrically closer to NYPS, whereas in (KHALIL; IRAVANI, 2015) those buses get separated into Areas 1 and 5.

However, looking at the closeness in the responses of buses from Areas 6 and 7 in Figure 3.5, we can see that TDA is sensitive to very small variations.

This additional information may be used for islanding control schemes purposes, as Area 6 is only comprised of load buses. Such information would not be achievable with MBA since they construct areas with the consideration that every area has at least one generator. Also, DCD method from (KHALIL; IRAVANI, 2015) would also not be able to detect such an area as it starts its construction of areas by the generators.

It is very interesting to remark that the TDA eccentricity ϵ is calculated using only the data and a distance metric, in this case, the correlation ρ. However, with this value (ϵ) and the first two moments, $\mu(\nu)$ and $\sigma(\nu)$, calculated once TDA clusters the buses, we can address how likely a point in the data-set is of belonging to the cluster, using the proof in Section III.E. In other words, we can attest that the selection of points, i.e., the area, by the TDA method from the data-set distribution is valid, using only the data information and the data distribution information, without the definition of any constant or limit.

To explore the meaning of the areas (clusters) provided by TDA, we show in Table 3.3 a summary of the distribution and distance metrics where the mean is adopted as the center of the cluster, and the typicality $\tau^D(\mu)$ of the center of the area calculated

Table 3.2 – Areas identified by the TDA method for *Case S1.C1.*

Area - TDA	**Coherent Generators**	**Associated Non-Generator Buses**
1	10,11,12,13	17,30-36,38-40,43-51,53,61
2	14,15,16	18,41,42
3	9	28,29
4	1,8	25-27,54-57,59,60
5	2,3	37,52,58,62-67
6	–	21,24,68
7	4,5,6,7	19,20,22,23
Area - DCD (KHALIL; IRAVANI, 2015)	**Coherent Generators**	**Associated Non-Generator Buses**
1	2,3,4,5,6,7	19-24,37,52,56-60,62-68
2	1,8	25-27,55
3	9	28,29
4	12,13	17,34-36,39,43-45
5	10,11	30-33,38,40,46-49,51,53,54,61
6	15,16	18,42,50
7	14	41
Area - SlowCoh. (CHOW, 2013)	**Coherent Generators**	**Associated Non-Generator Buses**
1	1,2,3,4,5,6,7	19-29,37,52,55-60,62-68
2	10,11,12,13	17,30-36,38,39,43-51,53,54,61
3	14	41
4	15	42
5	16	18
Area - AP (FREY; DUECK, 2007)	**Coherent Generators**	**Associated Non-Generator Buses**
1	4,5,6,7	19-24,67,68
2	9	26,28,29
3	10,11,12,13	17,30-36,38-40,43-51,53,61
4	14,15,16	18,41,42
5	1,2,3,8	25,27,37,52,54-60,62-66

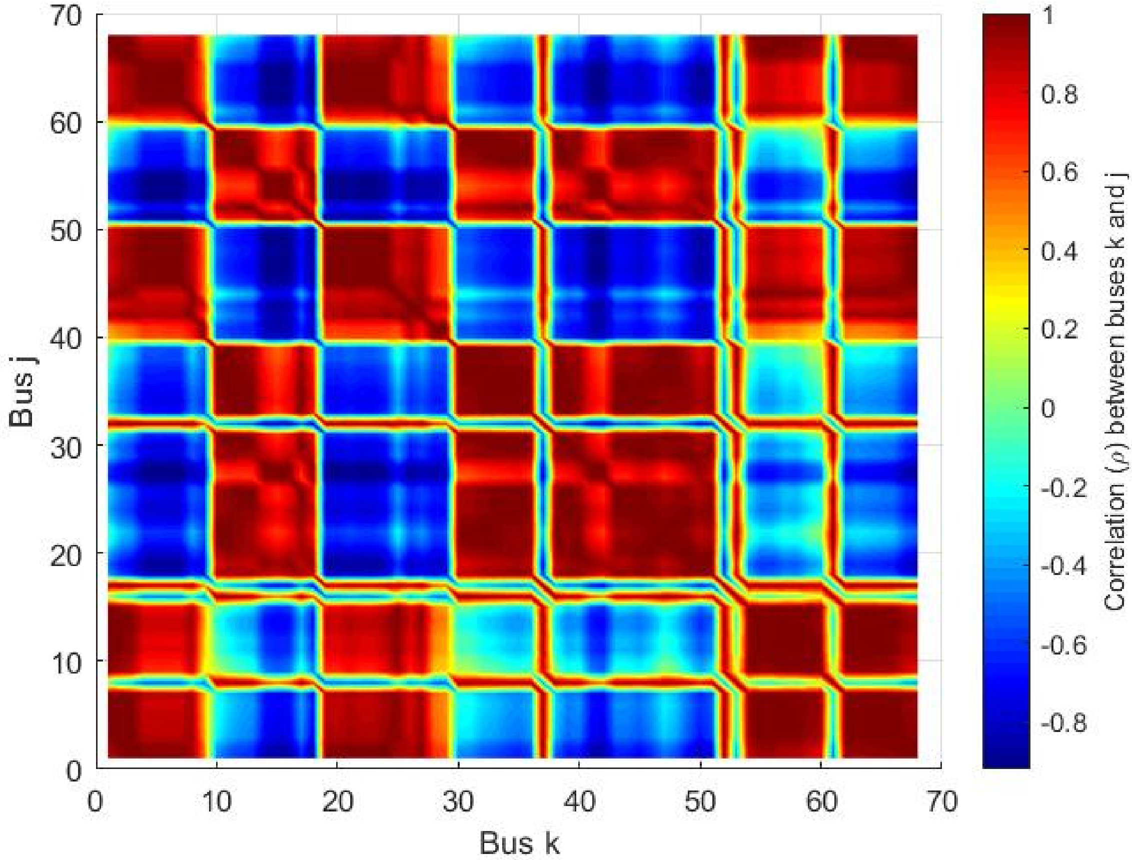

Figure 3.2 – Correlation map for *Case S1.C1*, for **TDA - Stage II**.

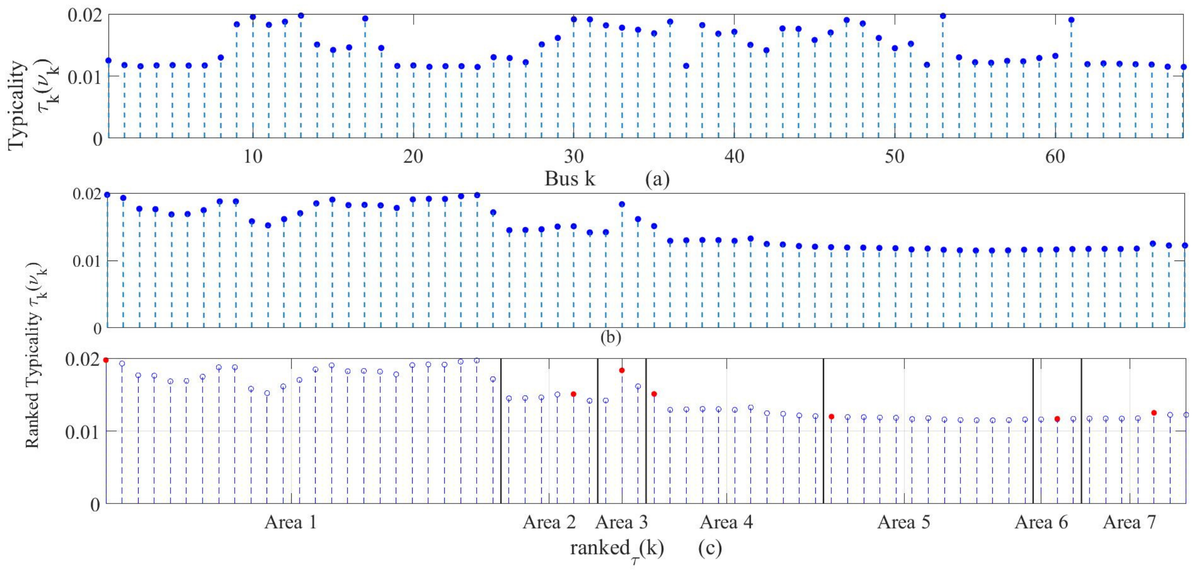

Figure 3.3 – *Case S1.C1*: Stages III and IV of the **TDA Algorithm 1**.

using (3.13), where Area 2 and Area 7 exhibit the lower and higher peak of the local distributions. Notice that these values, i.e., μ and $\tau^D(\mu)$, are equivalent to the mean of a PDF distribution and its peak. Notice that this is extracted exclusively from the data and the distance metric, without any a priori assumption of the PDF. The cluster

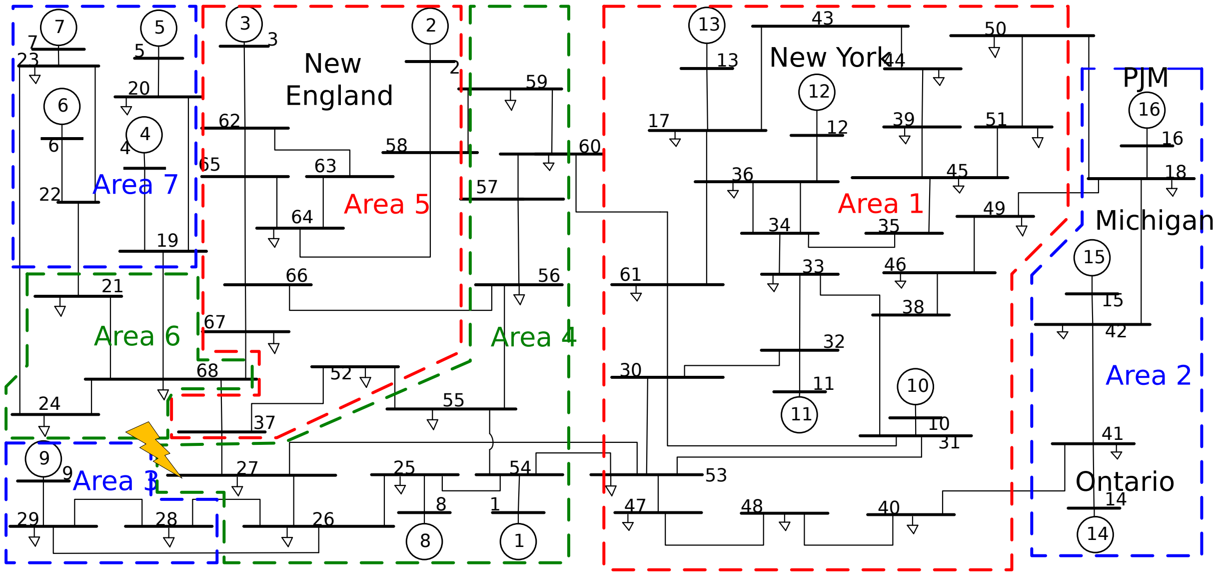

Figure 3.4 – Areas by the TDA method for *Case S1.C1*.

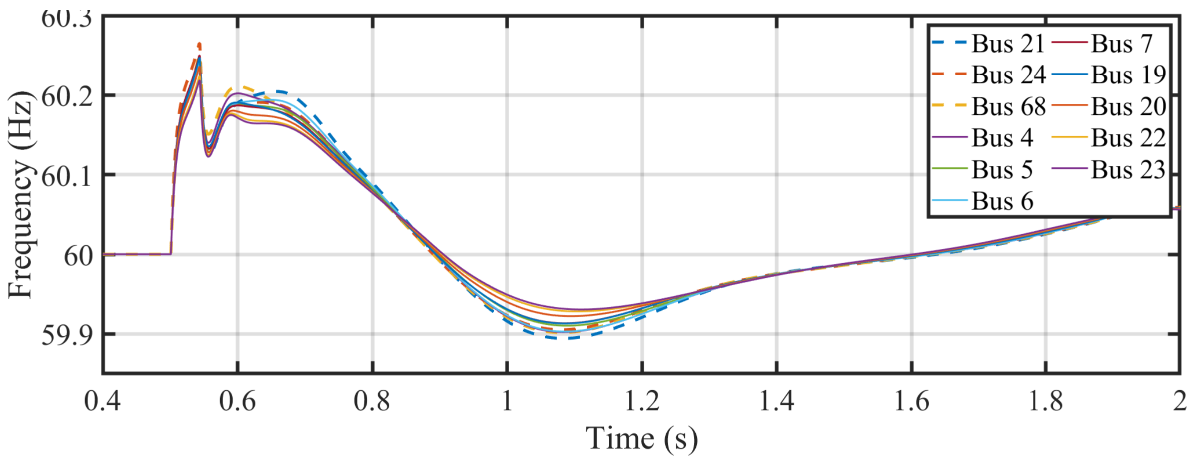

Figure 3.5 – Frequency signals of Areas 6 and 7 during transitory period.

average $\rho(\nu)$ shows that Area 7 is the most tightly coherent group, since it has the highest correlation average between buses. The largest value of the maximum deviation $\Delta\rho_{max}$ is found in Area 1 and the smallest one is located in Area 7, showing that these are respectively the least and most coherent areas, in accordance with $\rho(\nu)$. The bus associated with the maximum deviation is displayed in column 6. To prove the correct grouping, the eccentricity ϵ and standard deviation $\sigma(\nu)$, measures are calculated in columns 7 and 8, resulting in the ratio between eccentricity and standard deviation, which shows the conservative probability of the least coherent buses being inside the clusters, due to this ratio being less than $3\sigma(\nu) + 1$. This probability is higher, in reality. The overall average correlation ρ_{all} indicates that Areas 1 and 2 are the least coherent with the system. Summarizing the results in Table 3.3, these statistical measures represent a proper clustering pattern, confirming that the clusters provided by the method are correct.

Table 3.3 – Correlation statistics for Case 1 (*S1.C1*)

Area	$\mu(\nu)$	$\tau^D(\mu)$	Avg. $\rho(\nu)$	$\Delta\rho_{max}$	Bus($\Delta\rho_{max}$)	$\epsilon(\nu(\Delta\rho_{max}))$	$\sigma(\nu)$	$\epsilon\backslash\sigma$ ratio	Avg. ρ_{all}
1	1.7946	0.2585	0.9324	0.1118	50	1.2138	0.7689	1.5786	-0.1716
2	2.7639	0.0899	0.9522	0.0152	18	2.1766	7.4491	0.2922	-0.2684
3	1.9645	0.1669	0.9952	0.0022	29	2.4451	2.1275	1.1493	0.1176
4	2.3639	0.1399	0.9552	0.0639	26	2.2177	1.3381	1.6573	0.2587
5	1.9669	0.2141	0.9883	0.0114	67	1.6388	2.1445	0.7642	0.2167
6	1.7422	0.1010	0.9986	0.0006	24	2.1875	1.4153	1.5456	0.2222
7	3.1269	0.3828	0.9990	0.0005	5	2.3993	1.3876	1.7290	0.1087

3.7.1.2 Application on Case S1.C2

In this case, a three-phase fault is applied at bus 33 at $t = 0.5s$ and cleared after 5 cycles. The TDA method finds 7 areas which are displayed in Table 3.5 and illustrated in Figure 3.6. Table 3.5 also shows the areas for this case using the DCD method from (KHALIL; IRAVANI, 2015) for comparison. We can see that TDA is able to find additional important local oscillations when the compared method fails to do so.

It is noteworthy to remark that the severity of the fault caused the isolation of the closest generator, i.e., Generator 11, and its closest load bus, bus 33, showing the method captures local modes whereas slow-coherency methods would not, as can be seen in Table 3.5 areas provided by TDA, slow-coherency, DCD from (KHALIL; IRAVANI, 2015) **and the AP algorithm from (FREY; DUECK, 2007) for the correlation metrics** ρ. This separation can also be seen in Figure 3.7, in the frequency response of generators 11, 12 and 13, which are traditionally clustered together. Figure 3.7 shows that the TDA method makes the appropriate separation, where Generator 11 gets isolated. This fact points out a great advantage of the proposal when compared with MBA, since these methods would not be able to detect the isolation of this generator.

With this information, operators are able to detect islands in the system that can be intentionally produced aiming to prevent cascading events leading up to blackouts. From Tables 3.2 and 3.5 and Figs. 3.4 and 3.6, we can see the potential of the method for detecting islanding conditions, despite no lines are tripped in those simulations. This information is very valuable for the operator since it can be useful for determining possible parts of the system that can get isolated, without generation (like Area 6 in *Case 1* and part of Area 3 in *Case 2*). It can also be used as an indication of suitable intentional islanding schemes, where Areas 3 and 7 in *Case 1*, and Areas 5 and 7 in *Case 2* could become self-sustained in case of islanding, which can be required for preventing cascading events.

Since the islanding and protection phenomena require responses in faster times,

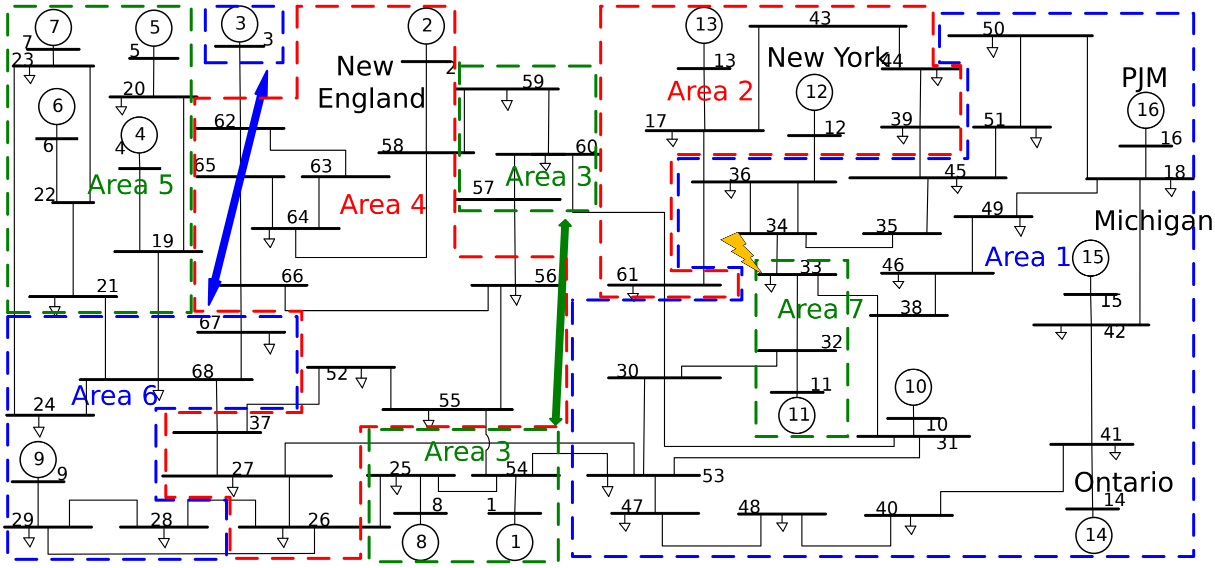

Figure 3.6 – Areas by the TDA method for *Case S1.C2*.

the TDA method is also examined with smaller time windows. It is important to emphasize that a minimal window of 10 cycles must be observed considering the length of the fault (5 cycles) and initial transients. The method is able to detect the isolation of Generator 11 with only 15 cycles, with an average processing time of 24.6ms, providing the detection of separation in less than a second after the fault. For the base window length of 10s, we note that Areas 3 and 6 in Fig. 3.6 are not consecutive, which is also valuable information for deciding islanding control schemes.

Table 3.4 depicts that the method is able to address the same areas for window lengths starting at 3s, for *Case 2*. For smaller time windows, since the response is dominated by faster modes and more damped modes, the number of areas is greater, indicating mostly local phenomena, such as islanding. It is important to note that for longer windows, the more important fast modes still show in the Areas, such as the isolation of Generator 11. Table 3.4 also shows that the TDA method finds the same results to the three considered sampling rates, which is the case for all simulations, despite of the window length.

Table 3.4 – Clustering results with different time windows

Sampling rate	0.25s	1s	2s	3s	5s	10s
120 Hz	**X**	**X**	**X**	✓	✓	✓
60 Hz	**X**	**X**	**X**	✓	✓	✓
30 Hz	**X**	**X**	**X**	✓	✓	✓

Table 3.5 – Areas identified by the TDA method, *Case S1.C2*.

Area - TDA	**Coherent Generators**	**Associated Non-Generator Buses**
1	10,14,15,16	18,30,31,34,35,38,40-42,45-51,53
2	12,13	17,36,39,43,44,61
3	1,8	25,54,57,59,60
4	2	26,27,37,52,55,56,58,62,66
5	4,5,6,7	19-23
6	3,9	24,28,29,67,68
7	11	32,33
Area - DCD (KHALIL; IRAVANI, 2015)	**Coherent Generators**	**Associated Non-Generator Buses**
1	9	28,29
2	10	–
3	11	32,33
4	14	41
5	15	42
6	16	18,50
7	1-8,12,13	Remaining Buses
Area - AP (FREY; DUECK, 2007)	**Coherent Generators**	**Associated Non-Generator Buses**
1	11	–
2	3,4,5,6,7,9	19-24,29,67,68
3	–	32
4	–	33
5	14,15,16	18,41,42
6	12,13	17,36,39,43,44
7	10	30,31,34,35,38,40,45-51,53,61
8	1,2,8	25-28,37,52,54-60,62-66

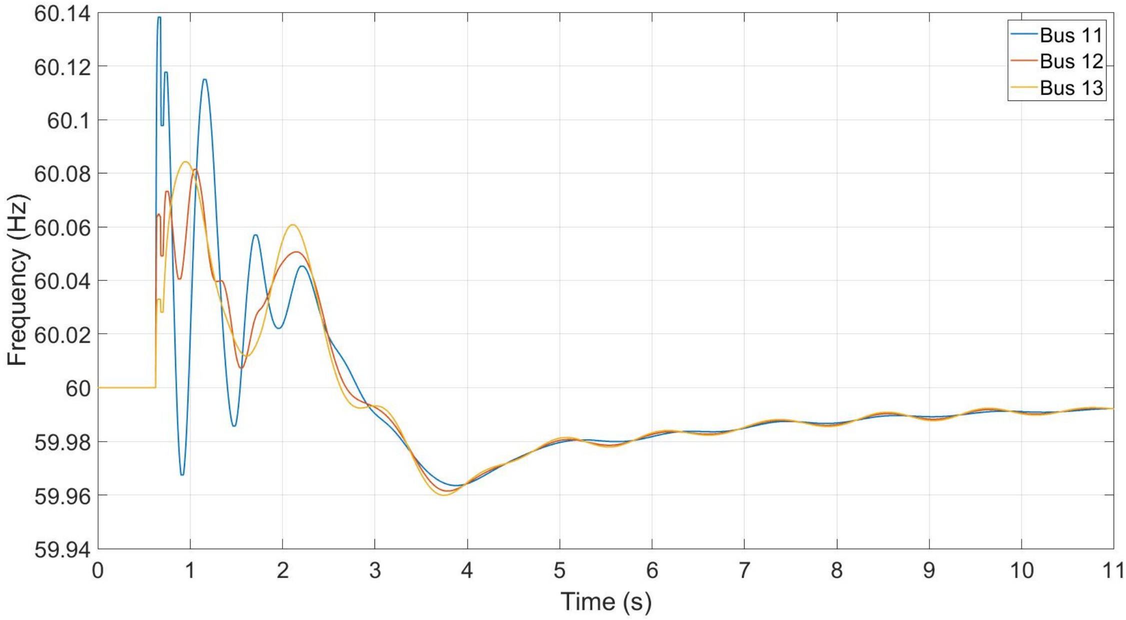

Figure 3.7 – Areas 2 and 7 generators responses for *Case S1.C2.*

3.7.2 Application on Case S1.C1, with presence of wind generation (S1.C3w)

The fault in *Case S1.C1* is now applied to a wind generation scenario (*S1.C3w*), enabling the investigation of how non-synchronous generation affects the coherence of the system and the TDA method. Thus, the total load is increased by 20%, homogeneously at all load buses as in (KHALIL; IRAVANI, 2018). A 13.3% of the additional load is supplied by wind power plants (WPPs), located in four new buses, shown in Table 3.6. An additional 6.7% generation is distributed by the synchronous generators, from New England system. The choice for installation of the WPPs takes into consideration the concentration of generators (for WPP at bus 121), load buses (for the WPPs at buses 127 and 144), and tie-lines in the case of the third WPP, at bus 153. The new generators are comprised of doubly-fed induction generators (Type-3 wind generators) equivalent models, with 30% of power output injected via inverters with voltage regulation and unitary power factor. The 10% additional generation is equally shared by all four WPPs.

Table 3.6 – WPPs for *S1.C3w*

New Bus	Connection	P_{gen}[MW]
121	121-21	630
127	127-27	630
144	144-44	630
153	153-53	630

It is noteworthy to remark that, while the increase in load is met by the non-synchronous generation, the transmission system remains unchanged, with the exception of the lines connecting the WPPs to the system. This alters the stability of the system,

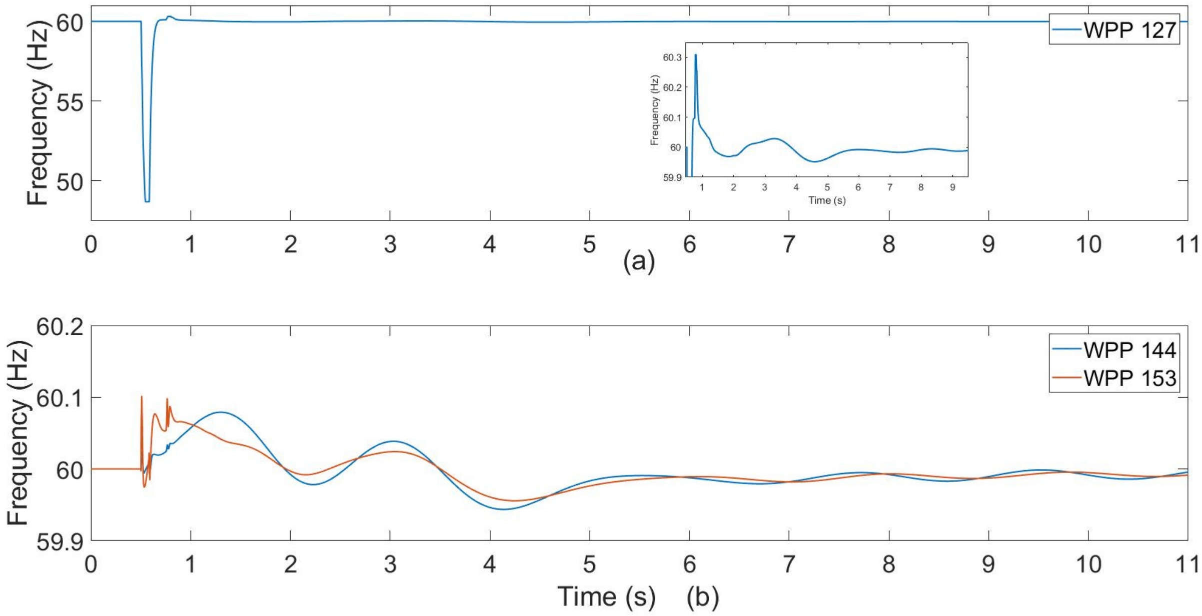

Figure 3.8 – WPPs frequency responses to fault at bus 27.

as the transmission lines may become overloaded, i.e., the poles of the system can come closer to the $j\omega$-axis in the s plane.

Once the initial condition is calculated for the new configuration of the system, the same three-phase fault is applied at bus 27. The frequency responses of the four WPPs is shown in Fig. 3.8a), for WPP 127 with zoom after the initial frequency dip for better observation of oscillations, and 3.8b) for the three remaining WPPs.

Note that the response from the WPP closer to the fault has a severe frequency dip at the moment of disturbance, due to its closeness to the fault. This behavior is also observed in WPP 121. Also note that the main difference between the responses of WPP 144 and 153 is in the transitory period, which appears in the resulting areas shown next.

The TDA method is applied following the same configurations, i.e., window length, sampling frequency, etc. The areas found by the method are displayed in Table 3.7, where the areas for the base case are reproduced for better visualization.

As mentioned before, the addition of non-synchronous generation influences the coherency of areas. 12 areas are found, that is, five additional areas, where it can be seen that Area 1 from *Case S1.C1* is split into Areas 2 and 3 in *Case S1.C3w*. Each of these areas has the addition of a WPP, i.e., the WPPs contribute to the coherency of these groups. Additionally, Area 7 from *Case S1.C1* is also split into Areas 8 and 9 for *Case S1.C3w*. The last area from *Case S1.C1* that was split was Area 2, which got separated into Areas 10, 11 and 12, each with a single equivalent generator. The impact of the presence of WPPs can clearly be seen in Fig. 3.9, where the frequency responses

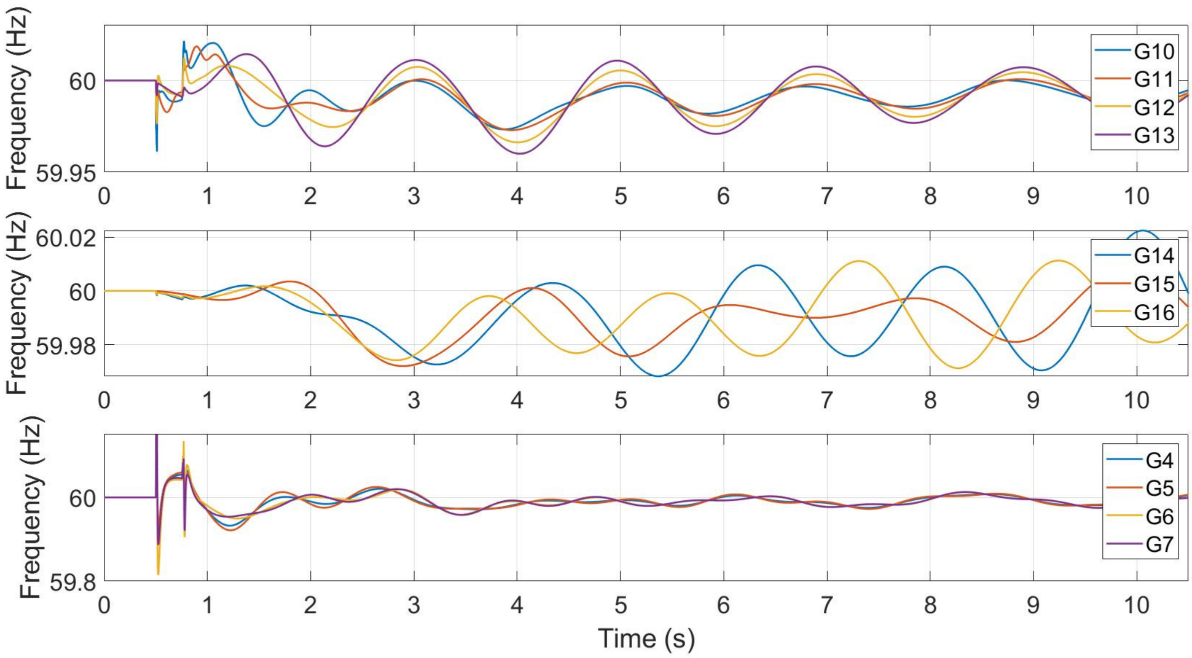

Figure 3.9 – Generators from Areas 1, 2 and 7 of *Case S1C1* in *Case S1.C3w.*

of the generators from Areas 1, 2 and 7 in *Case S1.C1* are plotted as if being grouped in the original case. It is clear that these generators no longer oscillate together, in the new configuration of the system, where WPPs are introduced.

The final additional area, however, is composed only of the new WPP at bus 127. This is reasonable since the non-synchronous generator is close to the fault, and has a degree of isolation from the system through its inverter. The area from Generator 9 gained one bus (the fault bus 27), due to its interaction with the WPP. Also, Area 6 from *Case S1.C1*, which did not possess any generator, gained two new buses (37 and 67) and WPP 121, all being close to the fault. Particularly, these two last effects, i.e., the isolation of WPP 127 and enlargement of the Area 6 show the effect of WPP in the power system, and also, the ability of the proposed method in capturing such events.

We can observe that, as seen in (LIN et al., 2017b; KHALIL; IRAVANI, 2018), the addition of renewable generation to the system may reduce the damping of oscillations in the system, separating further the areas. This separation is also a consequence of the faster modes added by these plants, which cannot be observed if the transitory response is omitted. However, our estimation of the areas is done without user defined threshold constant γ for clustering as in (KHALIL; IRAVANI, 2018), or complex algorithms like in (LIN et al., 2017b).

Table 3.7 – Areas identified by the TDA method, *Case S1.C3w.*

Area - TDA - *S1.C3w*	**Coherent Generators**	**Associated Non-Generator Buses**
1	12,13,144	17,36,39,40,43-45,50,51
2	10,11,153	30-35,38,46-49,53,61
3	9	26-29
4	1,8	25,54,57-60
5	127	—
6	2,3	52,55,56,62-66
7	121	21,24,37,67,68
8	5,4	19,20
9	6,7	22,23
10	14	41
11	15	42
12	16	18
Area - TDA - *S1.C1*	**Coherent Generators**	**Associated Non-Generator Buses**
1	10,11,12,13	17,30-36,38-40,43-51,53,61
2	14,15,16	18,41,42
3	9	28,29
4	1,8	25-27,54-57,59,60
5	2,3	37,52,58,62-67
6	–	21,24,68
7	4,5,6,7	19,20,22,23

3.7.3 Application on Case S1.C4i - Islanding detection

To emphasize the capability of the method in detecting islanding conditions, an additional test is made. *Case S1.C1* is run again, with the lines between buses 28 and 26 and between buses 29 and 26 open, $100ms$ after the fault is cleared. This effectively islands Area 3, as those are the only connections of this area to the rest of the system.

In the pre-fault condition of the system, Generator 9 is injecting 800 MW in the system, and the loads at buses 28 and 29 are consuming 206 and 284 MW, respectively. Thus, the lines 28-26 and 29-26 are exporting the remaining 310 MW, minus losses. Due to such pre-fault condition, when the lines are opened Generator 9 would accelerate indefinitely, as it does not contain a speed regulator. A speed regulator is added to Generator 9, as can be seen in Fig. 3.10(a) and the oscillations in that area cease since there is only one Generator supporting the loads.

The disturbance in generation at Bus 9 and loads at Buses 28 and 29 is shown in Fig. 3.10(b), and the interruption of power transfer from Area 3 to the rest of the system is shown in Fig. 3.10(c). The TDA method is run again for the PMU data-set of all buses in this case, without the knowledge of separation of those buses. The TDA method properly finds the same areas as the ones showed in Table 3.2, that is, all the coherency detection features, with additional evaluation of Area 3 islanding.

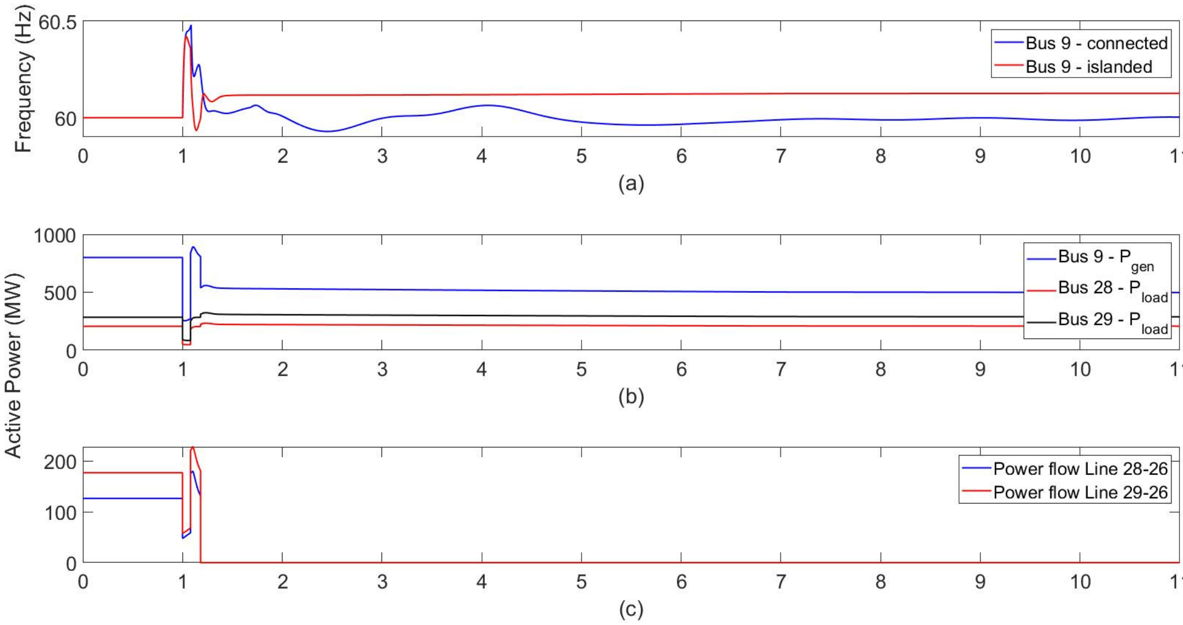

Figure 3.10 – Generator 9 frequency response: connected and islanded with speed regulator.

3.7.4 Eastern Interconnection (S2)

Next, the TDA is applied to 10 real events recorded in the Eastern Interconnection (EI) by the FNET/GridEye project (a low-voltage WAMS synchronized via GPS (ZHANG et al., 2010)). It is noteworthy to remark that the EI system has non-synchronous generators connected and operating (BLOOM et al., 2016) which is expected to be handled by the TDA method. All events consisting of generation trips that taken place during the summer season in 2020, from July until September, are considered in this investigation. The number of frequency measurements per event varies from 92 up to 102. For instance, a generator trip occurring on September 12 (the sixth case) is depicted after the filtering process in the first plot in Fig. 3.12. The filter reduces the noise interference demonstrating the TDA robustness to the minimal remaining noise.

After clustering all above-mentioned events employing the **Algorithm 1**, an average of 7 groups per event are found, with a minimum of 2 and a maximum of 15 groups.

For the sixth case, the detrended frequency responses of the PMUs are displayed in Fig.3.12, exhibiting the concept of coherency from (3.1) in the buses grouping (groups 1 to 11); i.e., the frequency measurements for buses in the same electrical region behave similarly. It is important to point out that the clustering process carried out by the TDA does not impose any user-defined parameter as γ in (3.1). All buses are clustered using the typicalities and correlation metrics, as shown in Fig. 3.11. Note that the first group is shaped by a single bus located at the edge of the EI (Bus 3001 in the Sasketchwan Province).

Considering all 10 events, the size of groups varies from 46 buses to single bus; particularly, some buses located at the edge of the EI. The most commonly clustered together buses are depicted in their geographical distribution in Fig. 3.13, where the proximity of the groups indicates that the method can successfully identify coherent groups. As most of the events consisted of generator trips on the eastern side of the EI, the coherent groups closer to the Atlantic coast are smaller in geographic extent, as such disturbances excited more modes in these areas.

3.7.5 Processing time

Since the method was not implemented on a specific purpose hardware which impacts the time duration. Each case was simulated 10 times to acquire the average time of CPU processing. The TDA method is implemented with MATLAB R2018a on an Intel Core i7-8850U 2.00 GHz processor with 8 GB of memory, resulting in the average times presented in Table 3.8, confirming the computational efficiency of the method to deal

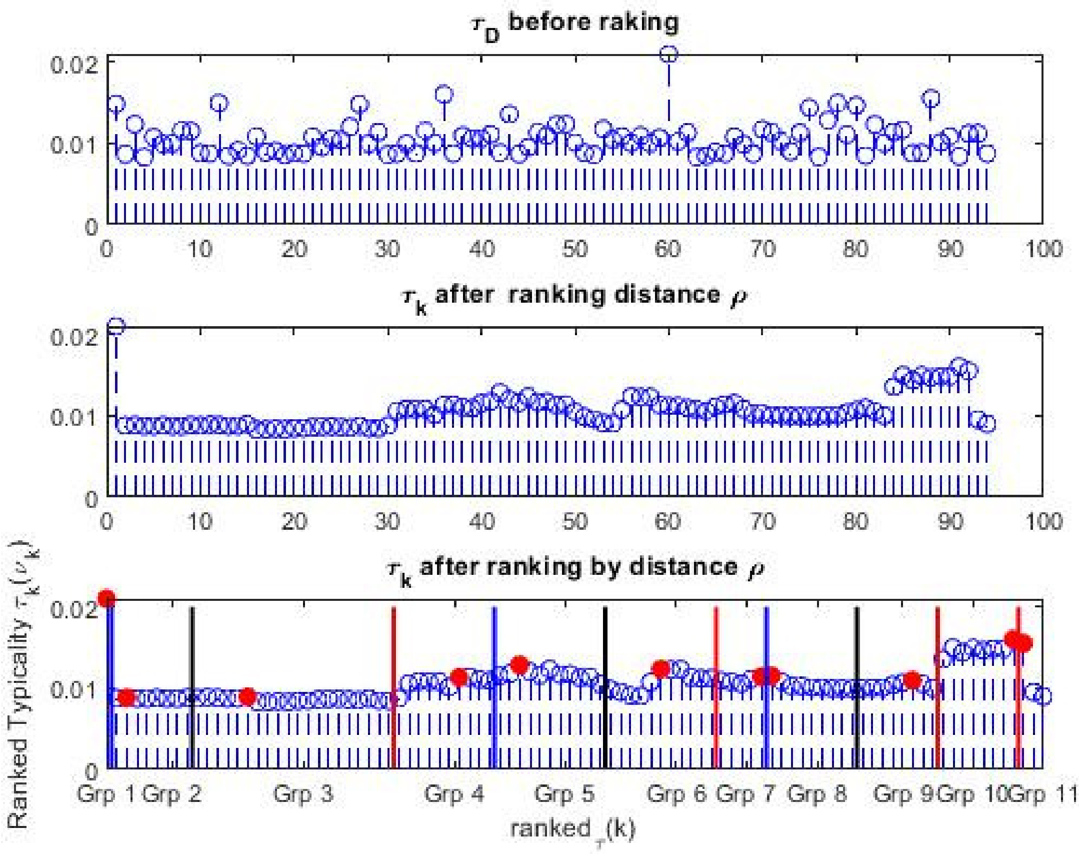

Figure 3.11 – Stages III and IV of the TDA for the sixth case in the EI system.

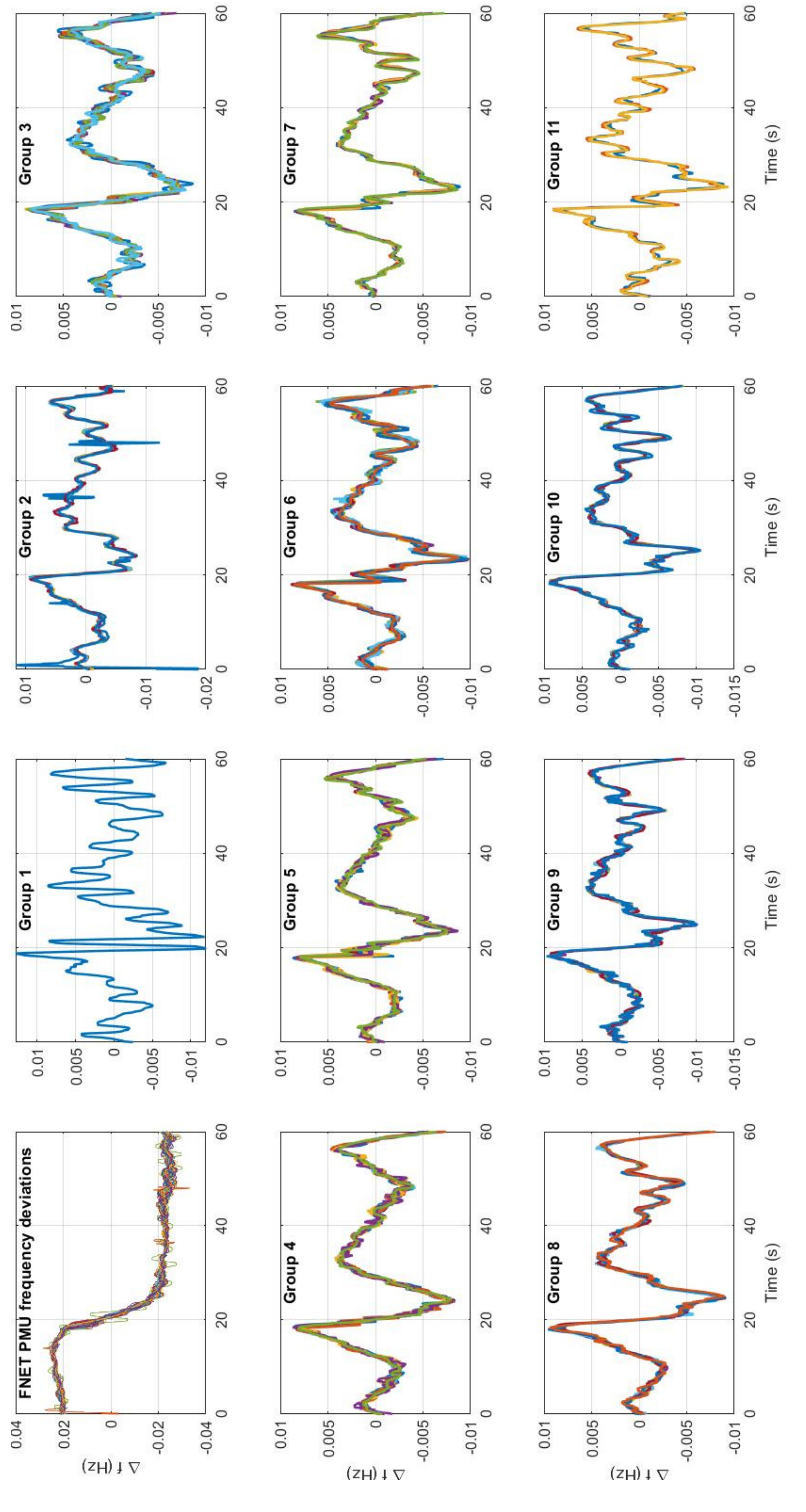

Figure 3.12 – FNET/GridEye groups for the sixth event.

with hundredth of measurements in less than $82ms$. For comparison purposes, the work in (KHALIL; IRAVANI, 2015) presents an average of $72.3ms$ for 68 measurements. It can be seen that the TDA method is a faster method than DCD and slow-coherency, without requiring load flow results, the number of clusters like slow-coherency, and cutoff coherency constant in both methods, except for frequency measurements. It must also be pointed out that the TDA's execution time also includes the pre-processing stage time.

3.7.6 Discussion

For all three cases, the number of iterations, until the final number of clusters is reached, is maximum of 3. It is interesting to note that the correlation metric inherently takes into account the electrical proximity of buses. This is specially important for the

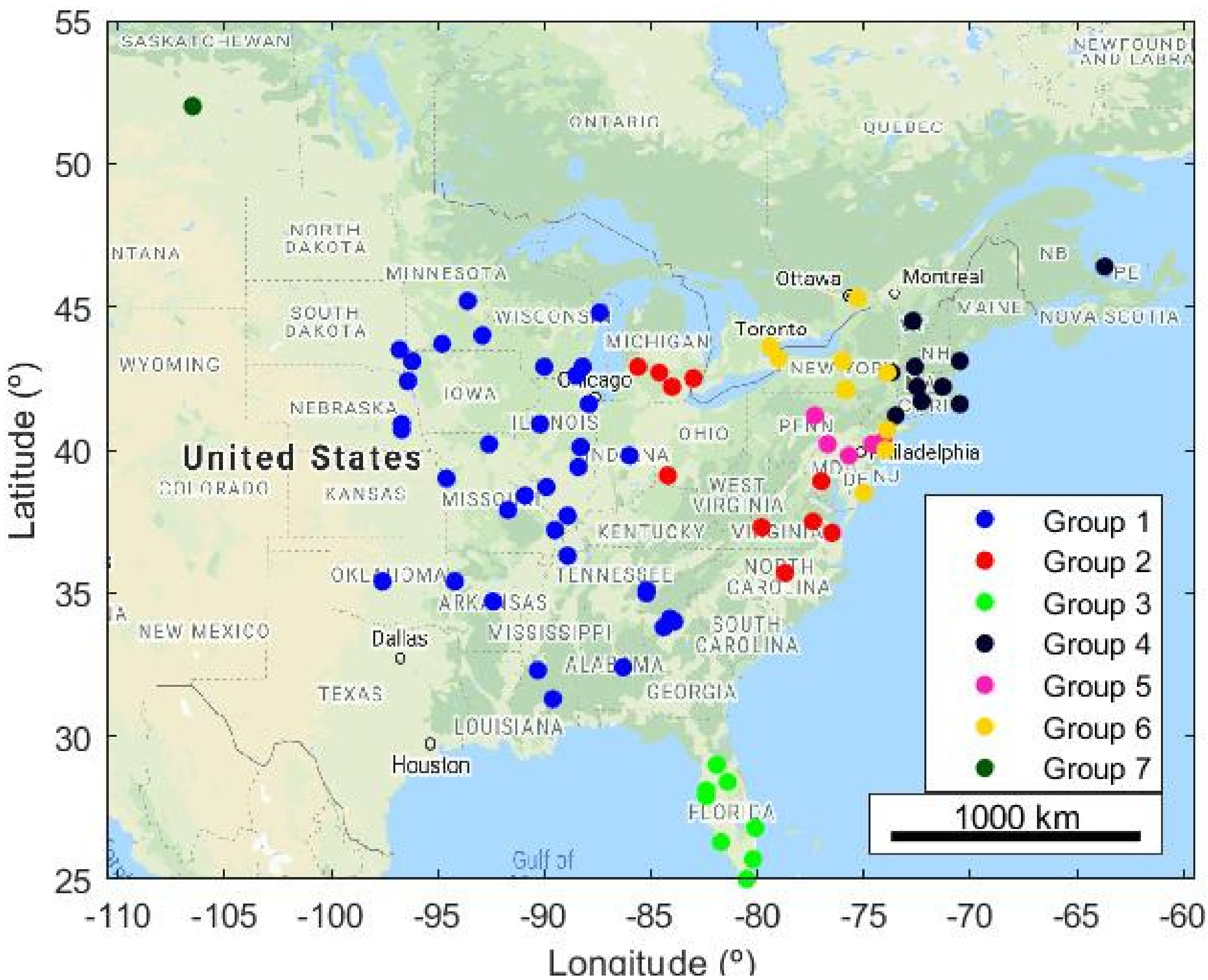

Figure 3.13 – Geographical distribution of groups in the EI.

Table 3.8 – Execution time for *Cases S1.C1, S1.C2, and S2* and comparison methods.

	S1.C1	S1.C2	S2	DCD avg.	Slow-coh.
Run Time (s)	0.04568	0.04213	0.08143	0.0723	0.0692

clustering process to prevent miss-clustering. The number of areas with the TDA method partially depends on the initial behavior of bus responses, suggesting the importance of local characteristics like weak connections that indicate electrical islands.

The islanding condition is evidenced in both cases for the NETS-NYPS grid, where *Case 1* exhibits Area 6 only composed of non-generator buses and *Case 2* has an exclusive area defined by Generator 11 and its closest load bus (bus 33). This result is also confirmed for *Case 2* in Fig. 3.7. This information, along with additional PMU coordinates, may support operators for islanding detection and define better islanding schemes.

3.8 TDA validation

It is worth noting that DDMs find areas for the event under study, whereas MBA find areas for all small-disturbance around the equilibrium point (CHOW, 2013). Thus, by comparing the reduced model from the TDA method with MBA, we quantify how efficient the method is in producing a reduced order model while showing possible islands in the system, for controlled islanding and WAMS monitoring purposes.

Besides the dynamic simulations accomplished for the system *S1* and the TDA application, the PST is also used for its model reduction and linearization, being both applied to the areas found by the TDA and slow-coherency methods, and the ones provided in (KHALIL; IRAVANI, 2015). The comparison is done by using the slow-coherency (CHOW, 2013) aggregation method whose implementation is available in the PST function *s_coh*3 (CHOW, 2020). This function uses as inputs: the areas found by the clustering method, the number of areas, the data of the system. The areas provided by the three clustering methods (TDA, slow-coherency and DCD) are used as input by the PST slow-coherency aggregation algorithm.

After gaining all three reduced models, their modes are compared with the ones of the complete model for *Case S1.C1*, using the *svm_mgen* function from PST to linearize the reduced models and extract the modes. This validation is achieved by contrasting the modal information derived with the TDA method against the one resulting from the DCD and slow-coherency techniques. For the sake of brevity, we only show *Case S1.C1*, however the same comparison is accomplished for *Case S1.C2* and the third case in (KHALIL; IRAVANI, 2015). There is a consistency in the error of the modes throughout the cases and adherence to the real value of the modes. This is of great importance for the validation of the method as a clustering method.

Table 3.9 – Slow modes Comparison - S1.C1.

S1.C1 Slow-coherency aggregation (Hz)						
Reference	**TDA**	**Error** (%)	**Slow-coh.**	**Error** (%)	**DCD (KHALIL; IRAVANI, 2015)**	**Error** (%)
0.3976	0.4050	1.86	0.3809	4.2	0.3566	10.31
0.6888	0.6365	7.59	0.6790	1.42	0.7861	14.12
1.0433	0.9754	6.50	0.7784	25.39	1.0143	2.77
Avg. Error		**4.39**		10.33		9.07

3.8.1 Validation against existing methods for Case S1.C1

Table 3.9 depicts the slowest modes obtained from the reduced model provided by the TDA areas compared with the full model and the areas from the slow-coherency and DCD techniques for *Case S1.C1*. The TDA clustering attains the best modes approximation. As mentioned in the previous section, the method performs without arbitrary tuning of coherency parameter γ as required by the compared methods. The proposed method also suggests the islands' detection and it is able to achieve all this within transitory speed conditions.

3.9 Discussion

In this work, a new data-driven method was proposed to track changes of coherent measurements belonging to generator and non-generator buses in large-scale interconnected power systems. This is a non-parametric statistical method that does not require any previous knowledge of the power system dynamics or collected data. As a result, it is not necessary to use any parameter of the system, to specify and tune empirical thresholds or to check if statistical premises necessary to build a formal probability density functions for the data are met. The TDA method was first applied to an equivalent 68-bus test system and the results were compared against slow-coherency (model-based) and DCD (data-driven) methods, exhibiting improvements in terms of modal frequency approximation of reduced order models provided by each method using (PODMORE, 1978) and(KHALIL; IRAVANI, 2015), respectively. Additionally, test results and validation were carried out using real measurement collected (FNET/GridEye project) from a large interconnected power system (Noth-America Eeastern Interconnection). The application of the method in a real system shown that the approach is robust to real noise and outliers, being capable to present high accuracy and consistent results. From the practical perspective, the method is also capable to detect local areas for islanding and accurate develop reduced order models with low computational burden.

3.10 Conclusion

Here we have showed a method to cluster generators and other buses exclusively based on data, which relies minimally on any expert knowledge and thus ease the work load for control rooms. This closes the first objective of this thesis.

Next we will show an also data-driven way to estimate the pilot-bus of the COI of each region, which also relies on TDA. This method is presented and tested and then, with the identified pilot-bus of each area, a regional inertia estimation is performed using the ARMAX methodology proposed in (LUGNANI et al., 2020), closing the contributions of the thesis, as proposed in Objective 1.1.1.

4 Where in the area to measure the inertia?

This Chapter will present the data-driven method for the detection of pilot-buses of regions of a power system, following a disturbance. Besides the proposed approach, the regional inertia estimation is also performed for the disturbances, using also a data-driven method. First, a brief literature review of coherency clustering methods is presented, followed by a quick review of the frequency response model and the aggregation of the inertial response through the COI. Next, the TDA application to extract means of distributions is proposed to retrieve the pilot-bus of a region. The method is applied to the IEEE 68 bus test system for validation of both the pilot-bus detection and inertial response estimation of the method. The Chapter closes with a brief discussion of the advantages of this portion of the proposed work and possible future contribution related to this research.

4.1 Literature Review

Several works in the literature deal with the estimation of inertia of synchronous generators at their point of interconnection using synchrophasors (WALL; TERZIJA, 2014; GORBUNOV et al., 2019; LUGNANI et al., 2020). However, the assessment of the total system inertia or regional inertia imposes additional challenges. For instance, in (WALL; TERZIJA, 2014) an inertia estimation is conducted using WAMS without considering the COI displacement. Other approaches address the COI's estimation (CEPEDA et al., 2014; MILANO, 2017; ZHAO et al., 2018; YOU et al., 2020; AZIZI et al., 2020; GORBUNOV et al., 2022), without discussing the regional inertia estimation. Likewise, some works tackle the regional inertia estimation to some extent classifying them by their distinct characteristics into the following categories: (*i*) disturbance methods (ASHTON et al., 2015; WILSON et al., 2019; ZOGRAFOS et al., 2017; ALSHAHRESTANI et al., 2018; SCHIFFER et al., 2019; PHURAILATPAM et al., 2019; YANG et al., 2020a; MAKOLO et al., 2021; KERDPHOL et al., 2021); (*ii*) probing signal methods (ZHANG; XU, 2017; TAMRAKAR et al., 2020); and (*iii*) ambient-signal methods (TUTTELBERG et al., 2018; CAI et al., 2019; YANG et al., 2020b; WANG et al., 2022; CUI et al., 2020; ALLELLA et al., 2020; ZENG et al., 2020; BARUZZI et al., 2021). While disturbance methods require occurrence of events that are atypical, these methods produce more accurate estimates, as the frequency of the constant of interest is better excited (CEPEDA et al., 2014). Furthermore, this thesis is interested in regional inertia estimation, which entails larger systems, the occurrence of severe events is fairly greater than for a single machine, for instance, providing a reasonable amount of opportunities for estimation. It is also important to point out that severe disturbance methods provide reference values of estimation for the development of other two types of method, that is, probing and ambient signal methods. Hence, the choice of a disturbance method is advocated and the thesis focus its investigation on disturbance methods reported in the literature.

In (ASHTON et al., 2015), the authors rely on extensive WAMS measurements and event detection and selection using detrended fluctuation analysis (DFA) to monitor clusters of generators in the Great Britain (GB) system. Frequency signals stemming from PMU are filtered using a low-pass filter, and the power deviation of generators is estimated. Then, the ratio between a known power deviation and its estimate multiplied by the total inertia of synchronous generators produces the estimate of total system inertia, considering load contribution. The authors in (WILSON et al., 2019) perform a report on the effective inertia of the GB and Icelandic system, taking into account load contribution and using the swing equation. In (ZOGRAFOS et al., 2017), the total inertia estimation is computed using WAMS measurements, Particle swarm optimization (PSO), and load contributions that are conceived into an optimal formulation, where loads are modeled as voltage-dependent To represent load contribution, a Constant Impedance, constant current, constant power load model (ZIP) aggregated load is considered, with voltage used to calculate the power parcel of the model approximated by generator bus voltages and the PSO algorithm is applied to the estimation of the constant impedance and constant current portions of the ZIP load model, the power loss in the system and the total system inertia and The method is validated at the Nordic57 test system. In (ALSHAHRESTANI et al., 2018), authors use frequency and active power measurements along with the knowledge of generators inertia to fit the frequency response of a disturbance using polynomial techniques. This method is tested in the IEEE 68-bus test system. In (SCHIFFER et al., 2019), the assessment of the equivalent inertia is done using a first-order nonlinear aggregated power system model in combination with the recently proposed Dynamic regressor and mixing (DREM). Where the equivalent machine inertia is estimated approximating the active power deviation through the power deviation caused by primary frequency control and the COI frequency response by a simple average of all generators frequency responses. In (PHURAILATPAM et al., 2019), a polynomial fitting is performed over the swing equation and frequency measurements, demonstrating robustness to topology and location of disturbance. The method proposed in (YANG et al., 2020a) uses dynamic mode decomposition (DMD) to extract the eigenvalues and eigenvectors, from which inertia is derived. This method does not require the COI knowledge, since it is based on inter-area electromechanical oscillations. However, the accuracy may be influenced by topology changes that shift the modes' frequencies. In (MAKOLO et al., 2021), the equivalent inertia of a power system is estimated using the Recursive least-squares (RLS) by fitting oscillation data, where an initial model is estimated with a non-recursive system identification method. The authors in (KERDPHOL et al., 2021) estimate the inertia of areas from the 60Hz Japan system using frequency and rate of change of frequency measurements applying a frequency spectrum and performing mode shape analysis. Here, they find that PMU further away from the COI of the system provide imprecise estimations due to the effect of inter-area oscillation.

PROBING SIGNAL: In (ZHANG; XU, 2017), the authors propose a closed-loop Microperturbation method (MPM), which is used in an online manner to estimate the equivalent inertia of the system assuming that the connection bus of a machine electrically close to the center of the system can represent the inertial response of the system to the probing signal. A method of system inertia estimation envisioned for Electrical storage systems (ESS) frequency response algorithms is proposed in (TAMRAKAR et al., 2020), where small periodic load step signals are applied and the model of the equivalent system model is estimated using least square estimation applied to the frequency measured at the ESS connection bus. Once the model is estimated, the inertia is extracted from the impulse response of the model.

AMBIENT MEASUREMENT: The authors in (TUTTELBERG et al., 2018) use WAMS signals from tie-line active power deviations and frequency measurements from generators to estimate the center of inertia frequency of the region as input and output of an ARMAX parametric identification method with variable order for estimation of the regional inertia. The method is applied to real measurements from the Icelandic power system. The regional inertia estimation is performed in (CAI et al., 2019) and (YANG et al., 2020b; WANG et al., 2022) deriving relations between electromechanical oscillations (frequency, damping and mode shape) and the regions inertias extracted from ambient data. The first method is validated with the IEEE 39bus test system and laboratory experiments and the latter method is tested both in the IEEE 68bus NETS/NYPS system and real data from the northern China system. The method developed in (CUI et al., 2020) extracts features from ambient synchrophasor measurements for machine-learning-based inertia estimation using Multivariate random forest regression (MRFR) algorithm. The method also uses weather and load data providade by the FNET/GridEye WAMS for further precision of inertia estimation and the method is test in the Western Electricity Coordinating Council (WECC) system. The authors in (ALLELLA et al., 2020) propose an Autoregressive (AR) model capable of predicting the evolution of inertia of a region, where the inertia is composed of a periodic component and a non-Gaussian distribution stochastic process noise. The method identifies the inverse correlation between inertia and renewable generation penetration and propose a linear model for this correlation. The intercept term is the periodic component whose frequencies are extracted through spectral analysis (with frequencies relating to 24, 12, 6 and 4 hours) using Goertzel technique, the noisy is modeled as an additive term with Logistic distribution and the angular coefficient is estimated by the AR model. While this method can be applied online, it requires large central knowledge of dispatched generators and overall measurement of online CCGs. In (ZENG et al., 2020) the inertial of an area or a system is estimated using PMU active power and frequency measurements at generators connection buses, where the power deviation is the summation of their power deviations and the area or system COI is the average of generators connection buses frequencies weighted by the inverse of the generators frequency variances. The estimation uses N4SID algorithm, where the state space input is the active power deviation and the output is the center of inertia frequency. The inertia estimation is updated with a sliding window with exponential smoothing method. An extension of this method is proposed in (BARUZZI et al., 2021) where the estimation considers the presence of CCGs with synthetic inertia and thus considers the simple average of frequencies to approximate the center of inertia frequency.

It is evident in the literature that regional inertia estimation methods do not consider the proper estimation of the COI frequency (KERDPHOL et al., 2021; GUO et al., 2022) and the load contribution to the effective inertia, making simple assumptions. The assumption that loads contribute to the inertia response is well established in (Khan et al., 2015), but overall ignored until recent years with the high penetration of CCG in modern systems. As these generators have small inertia constants and are isolated from the system by the converter interface, but are displacing synchronous generation, it becomes useful for system operators to acknowledge and estimate the load inertial contribution as an important resource for frequency stability.

4.2 Contribution

This investigation proposes a disturbance based and data-driven method for the detection of regional COI pilot-bus, using a compound of the *cosine* and *correlation* distance metrics of frequency and active power signals at buses. This compound distance is processed by the TDA's features (CHOW, 2013) to approximate the probability distribution of the regional inertial responses and find the highest *typicality* value, corresponding to the mean of the distribution, that is, the COI.

Our proposal also estimates the effective regional inertia through a swing equation equivalent machine representation for each Region, where the Region tie-lines active power is used as input, whereas the pilot-bus frequency response as output, using ARMAX model identification. The estimations of the regional equivalent machine inertia are validated comparing with the actual inertia of the IEEE 68-bus simulated power system, in two scenarios: with or without load contributions. Where aggregated induction motors are added to the load buses of the system model.

Thus, the primary contributions of this research are enclosed in the following: *i)* a fully data-driven detection of the COI pilot-bus is achieved using only disturbance synchrophasor measurements; *ii)* the sensibility to the load inertia impact in the detection of the COI pilot-bus is investigated; *iii)* a fully data-driven regional equivalent inertia estimation H_{est} is conducted using disturbance measurements and a variable order ARMAX-based identification model.

The remainder of the paper describes the representation of the COI per Region through an estimated pilot-bus and the effects of the load in the inertial response in Section 4.3. Section 4.4 discloses the methodology for inertial estimation using pilot-bus frequency and tie-line active power signals and ARMAX-based identification. Section 4.6 presents the validation of the methodology using the IEEE 68-bus NETS/NYPS test system and its modified version considering dynamical load representation. Finally, Section 4.7 summarizes the presented contributions regarding our proposed methodology and points out the future works related to the inertial response estimation in power systems.

4.3 Fundamentals

This Section will present the COI concept which will be exploited for single representation of the frequency response of a region, as well as some basic concepts of TDA which will be used to extract the COI closest bus, that is, the pilot-bus. A brief review of inertia estimation is also presented to close the fundamental concepts necessary to introduce in the next Section the pilot-bus detection and ARMAX estimation method proposed ahead.

4.3.1 Pilot-bus detection using TDA

The assumption that the Region is coherent, it is important for regional inertia estimation because the frequency response of buses within a single Region will present the same trend, that is, it will be unimodal. In this sense, note that (4.9) is a weighted average, that is:

$$f_{coi}(t) = \frac{\sum_{n=1}^{N_g} f_n(t)H_n + \sum_{m=1}^{N_m} f_m(t)H_m}{\sum_{n=1}^{N_g} H_n + \sum_{m=1}^{N_m} H_m} = \frac{\sum_{i=1}^{N} x_i w_i}{\sum_{i=1}^{N} w_i} \tag{4.1}$$

where N_g is the number of generators plus synchronous condensers in the Region, N_m is the number of load buses with motors connected to them. $f_n(t)$ and H_n are respectively the frequency and inertia of each generator and synchronous condenser, $f_m(t)$ is the frequency of the transmission load bus to which a considerable amount of motors, i.e. a industrial district, is connected via a distribution system, and H_m is the equivalent inertia of the motors connected at that load bus. On the right-hand side, x_i denotes frequency measurements of every generator or motor bus, meanwhile w_i symbolizes its respective inertia. Since $f_{coi}(t)$ is essentially virtual, it may not necessarily correspond to the frequency of any particular bus of the Region. Note also that, for non-generator and non-motor load buses its frequency ($f_k(t)$) is a function g of the Region inertias and the admittance matrix (Y_R) of the Region (MILANO; ORTEGA, 2016):

$$f_k(t) \sim g(H_{[n,m]}, Y_R) \tag{4.2}$$

Since $f_{coi}(t)$ is a virtual quantity, it may be arbitrarily close to any frequency in the Region. For example, a generator with inertia orders of magnitude that are higher than any others in the Region, or a bus which corresponds to the center of a symmetrical Region:

$$f_{coi}(t) \approx f_i(t), \forall i \in N = \{n, m, i\} \tag{4.3}$$

where N is the set of all buses in the Region. We can represent the distance of the frequency response of each bus to the virtual f_{coi} by a probability density function (pdf) of any type (e.g. Gaussian, colored, Weibull, etc). However, we do not have information regarding the type of distribution, nor precise knowledge of the weights (inertias) to calculate the mean of the distribution, but only synchrophasor measurements. Using TDA (CHOW, 2013) we are able to approximate the pdf of the Region, where we find the bus whose frequency $f_i(t)$ is closest to the COI frequency $f_{coi}(t)$, the mean of the Region's pdf (ANGELOV; GU, 2019).

To find the bus closest to the COI, we assume that the inertial response of each bus $f(t)$ is the first 2 seconds (t_f) of after disturbance (t_0), where no speed governor has had time to act. Additionally, $f(t)$ can be represented by the Euclidean norm β of its frequency deviation ($\Delta f(t)$) with respect to the nominal frequency (f_0). To determine the closest bus to the mean ($f_{coi}(t)$), we calculate the norm between the frequency deviations of every pair of buses k and j $\beta(k, j)$ to indicate the closeness to the mean of the pdf. Then, the inertial response for bus k with respect to bus j can be represented by:

$$\beta(k,j) = \sqrt{\sum_{t=t_0}^{t_f} [\Delta f_k(t) - \Delta f_j(t)]^2} \tag{4.4}$$

To find the pilot-bus that embodies the inertial response of the Region, the electrical power response deviation of every bus $\pi(k,j)$ with respect to every other bus j is expressed in (4.5). It is important to consider the relative norm between buses k and j for electrical power as a weighting factor, since generator and motor buses will present higher power deviations than other buses (transmission buses). This is due to their inertial content, which may deviate the mean of the distribution. For transmission buses, total power equals zero, so we convention that the power injected by the bus at the grid is considered, as in the generators case. Hence, for any bus k with respect to any other bus j, the electrical power norm $\pi(k,j)$ will be:

$$\pi(k,j) = \sqrt{\sum_{t=t_0}^{t_f} [\Delta Pe_k(t) - \Delta Pe_j(t)]^2} \tag{4.5}$$

where the power deviation $\Delta Pe_k(t)$ is calculated with respect to the value of the electrical power at $t = t_0$.

For every bus k in the Region R with N buses, the inertial response of k can be represented by a vector $2 \times N$, forming a point $\alpha(k)$ in the distribution space. For the TDA application, a distance metric in this space must be defined for the computation of the properties that will produce the approximation of the distribution's pdf. The choice of the metric for TDA must consider the physical aspects such as space and phenomena in question. Also, the metric may be compounded to consider relevant aspects that may be secluded to one given metric. For such purpose, a compound distance metric which takes into account the angle delay between buses (cosine metric - d_{cos}) and the linear coefficient of their distribution (correlation metric - d_{corr}) is used. Hence, the compound distance metric δ is given by:

$$\delta(k,j) = d_{cos} + d_{corr} = \frac{\alpha(k) \cdot \alpha(j)}{\alpha(k) \times \alpha(j)} + \frac{cov(\alpha(k), \alpha(j))}{\sigma_{\alpha(k)}\sigma_{\alpha(j)}} \tag{4.6}$$

where $cov(\alpha(k), \alpha(j))$ stands for the covariance between points $\alpha(k)$ and $\alpha(j)$, and $\sigma_{\alpha(k)}$ represents the standard deviation of $\alpha(k)$ and likewise for $\alpha(j)$.

Now, we can define the TDA properties as proposed in (LUGNANI et al., 2022d), where the aim is to produce *typicality* values $\tau_N(\alpha(k))$, for each point k indicating the distribution of the inertial response, according to algorithm 2.

Algorithm 2 TDA implementation for COI pilot-bus detection.

Input: Let α_k, $k = 1, \dots N$ (data points) vector of scalar Euclidean norms between active power responses $\pi(\mathbf{k},\mathbf{j})$ and frequencies responses $\beta(\mathbf{k},\mathbf{j})$, with N being the number of PMUs in Region R.
Output: Pilot-bus that represents the COI of the Region R with maximal typicality τ_N^*.
Initialization: $\mathbf{t}_0$, $\mathbf{t}_f$, set of correlation metrics $\delta_{k,j}$
for k=1,k++ **do**
  for j=1,j++ **do**
    $\delta_{k,j} \leftarrow \frac{\alpha(k).\alpha(j)}{\alpha(k)\times\alpha(j)} + \frac{cov(\alpha_k,\alpha_j)}{\sigma_k\sigma_j} \quad \alpha_k, \alpha_j \in \alpha_N$
  end for
end for
TDA properties computation
Cumulative proximity: $q_N(\alpha_k) \leftarrow \sum_{j=1}^{N} \delta_{k,j}^2$;
Discrete local density: $D_N(\alpha_k) \leftarrow \frac{\sum_{j=1}^{N} q_N(\alpha_j)}{2Nq_N(\alpha_k)}$
Discrete typicality: $\tau_k(\alpha_k) \leftarrow \frac{D_N(\alpha_k)}{\sum_{j=1}^{N} D_N(\alpha_j)}$
Global typicality: $\tau_N^{D*} \leftarrow max(\tau_i^D) \quad i = 1, \dots, N$
return $\tau_N^* \rightarrow \alpha(\tau_N^*)$

The *typicality* property is exclusively computed by using data and has the following common properties in commonality with pdf: *i)* $0 \leq \tau_N(\alpha(k)) < 1$; *ii)* $\sum_{j=1}^{N} \tau_N(\alpha(k)) = 1$. Since it is constructed from the data unlike traditional pdf, then it will not generate values of τ_N for infeasible virtual data points (like over-frequency norms for a generation trip disturbance). The distribution of typicalities will be exact, unlike traditional pdf. As pdf, the higher the value of $\tau_N(\alpha(k))$, this is analogous to the probability of the realization in pdf, the closer it is to the mean of the distribution. In our case, this means that the bus with the highest $\tau_N(\alpha(k))$ is termed $\tau^*(k = pb)$ and is the closest to the COI, that is, its frequency $f_k(t)$ is the closest to $f_{coi}(t)$, and thus, is the pilot-bus of the Region.

4.3.2 Regional Inertia Estimation

The inertial frequency response for a single synchronous machine is characterized by the classical swing equation, as follows (SAUER et al., 2016):

$$\frac{d\omega(t)}{dt} = \frac{1}{2H}(P_m(t) - P_e(t) - D\Delta f(t)) \tag{4.7}$$

where H is the inertia constant of the generator, which represents the machines rotor kinetic energy in seconds at the machines rated power, $P_m(t)$ is the machine mechanical power provided by the primary energy source, $P_e(t)$ is the machine electrical power output injected at the grid, D is the load damping coefficient and $\frac{d\omega(t)}{dt}$ is the generator rotor speed derivative after disturbance. Assuming that the electrical frequency $f(t)$ at the machine point of connection is approximately equal to the rotor speed and there is no reasonable time for the machine speed governor to take action during the period of the inertial response, (4.7) can be rewritten as:

$$\frac{df}{dt} = \frac{-(\Delta P_e(t) + D\Delta f(t))}{2H} \tag{4.8}$$

where $\Delta P_e(t)$ is the amount of electrical power deviation caused by a given disturbance at the generator. If the Region is strongly connected, this representation can be extended to a whole Region. Then, an equivalent frequency of the Region ($f_{coi}(t)$) can be determined, being the COI frequency. In turn, it is an weighted average of the frequency of generators, synchronous condensers and motors by their respective inertias:

$$f_{coi}(t) = \frac{\sum_{n=1}^{N_g} f_n(t)H_n + \sum_{m=1}^{N_m} f_m(t)H_m}{\sum_{n=1}^{N_g} H_n + \sum_{m=1}^{N_m} H_m} \tag{4.9}$$

Then, for any given disturbance in the system, like generation trip or transmission line disconnection, the equivalent inertial response of the Region can be given by the COI frequency response as follows

$$\frac{df_{coi}(t)}{dt} = \frac{-(\sum_{n=1}^{N_g} \Delta P_e^n(t) + \sum_{m=1}^{N_m} \Delta P_e^m(t) + D\Delta f_{coi}(t))}{2H_{Req}} \tag{4.10}$$

Now, $\Delta P_e^n(t)$ is the electrical power deviation of each generator and synchronous condenser connected in the Region R and $\Delta P_e^m(t)$ is the electrical power deviation at the transmission bus connected to a relevant portion of motors.

The definition of the Region R, where the inertia estimation is carried out, depends on several factors such as location of the disturbance, size of the disturbance, topology of the system and exchanges at tie-lines (CHOW, 2013). It is usually performed using coherency analysis of electromechanical modes as in (LUGNANI et al., 2022d). However, due to a power system is usually very well connected within itself with weaker links to other systems, and the inertial response excites slower electromechanical loads, it is reasonable to assume that this system is a coherent Region for inertial response purposes.

In the next section, we present the methodology to estimate the regional inertial response using only synchrophasor signals from the pilot-bus. To this end, a parametric approach is adopted to identify an equivalent machine that encompasses the dynamics of the Region.

4.4 Methodology: ARMAX-based regional inertia estimation

The purpose of defining a pilot-bus for a Region of interest is estimating the inertia of that Region with minimal data, particularly without any model parametric information. In this section, we present the steps in the pre-processing stage for signal filtering of the data, the pilot-bus detection stage and the steps for estimation using Auto-Regressive Moving Average eXogenous input (ARMAX) model identification technique (LUGNANI et al., 2020; PINHEIRO et al., 2021). It is important to indicate that the filtered signals $f_{filt}(t)$ and $Pe_{filt}(t)$ are first used for pilot-bus detection, and then the filtered frequency signals of the pilot-bus f_{filtPB} and the active power of the Region interconnections signal Pe_{filtTL} are used by ARMAX for identifying the equivalent machine model for regional inertia estimation. Figure 4.1 presents the overall pathway of the proposed methodology for regional inertia estimation.

4.4.1 Signals pre-processing

These are acquired by PMUs and must be filtered due to presence of non-electromechanical phenomena in the voltage phase angles that are used for frequency estimation. These phenomena come from the voltage regulation action that has no relationship to disturbances associated with frequency stability. To deal with noisy signals (and any other high-frequency noises contained in the signals), a low-pass frequency *moving median* filter is applied using Matlab function *movmedian* with a 5-sample window.

4.4.2 Pilot-bus detection

Once the signals are filtered, the TDA strategy is applied according to Algorithm 2 from 4.3.1. The filtered signals of active power and frequency and output the detected pilot-bus are the TDA inputs. It is important to emphasize some points regarding the application of TDA for pilot-bus detection: (i) each bus k will represent a point $\alpha(k)$ in the data distribution with an active power ($Pe_k(t)$) and a frequency ($f_k(t)$) component; (ii) both power and frequency signals will be represented by the Euclidean norm respective to every other bus j (as in (4.4) and (4.5)), which is calculated for a typical inertial response interval of two seconds; and (iii) the compound distance metric δ calculated between every two points has equal weight for both metrics (Line 6 of Algorithm 2).

With the distances, the TDA properties are calculated according to Algorithm 2. Where the final property, typicality $\tau_N(\alpha(k))$ (Line 12 of Algorithm 2), of each data point is calculated representing a data-driven pdf of the inertial response. The distribution of inertial responses has as mean $f_{coi}(t)$ in most cases virtual. In our case, the TDA renders a vector of $\tau_N(\alpha(k))$ values of equal dimension as the number of PMUs, where

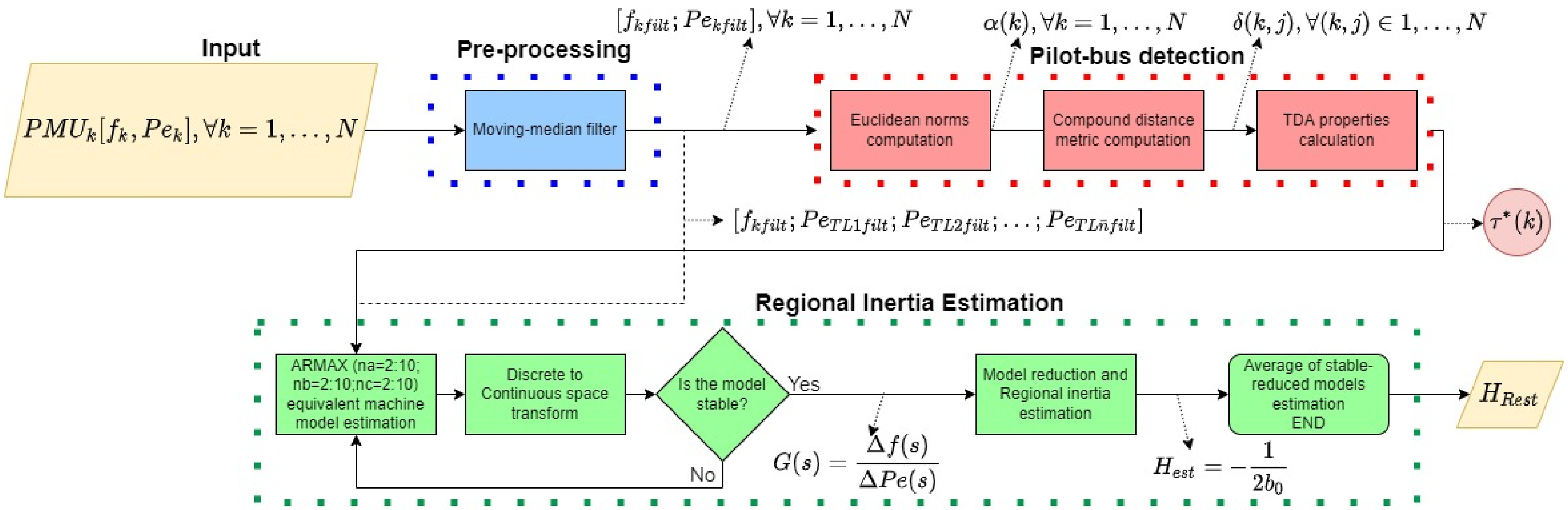

Figure 4.1 – Pilot-bus detection and regional inertia estimation.

each value of τ_N represents the probability of a realization assuming that particular value of $\alpha(k)$. Hence, the highest value of τ_N, that is τ_N^*, is the most probable realization, which is the closest to the mean of distribution. Thereby, once all typicalities are calculated, we can detect the pilot-bus (Pb) as the bus corresponding to τ_N^* (Line 13 of Algorithm 2).

It is also important to reiterate that data-driven methods are usually event specific, so the detected pilot-bus will be valid for the particular event. However, as availability of data from WAMS is abundant, the method can be readily applied to every new event and a statistics analysis can be performed on the behavior of the pilot-bus movement according to disturbance location, size, operation point of the system and season effects on renewable generation. With the detected pilot-bus and the measurements of active power of the $\bar{n}$ interconnections of the Region ($Pe_{TL\bar{n}-filt}$), the regional equivalent inertia can be estimated using ARMAX model identification method presented in the following.

4.4.3 Regional inertia estimation

Once the pilot-bus is detected, the COI is also identified. Then, the regional inertial response in (4.10) can be represented in p.u., since the active power deviation in generators and motors is approximately proportional to the active power deviation at interconnection buses among regions (TUTTELBERG et al., 2018). Additionally, since the frequency response of the pilot-bus (f_{pb}) is approximately the frequency response of the COI ($f_{pb} \approx f_{coi}$), thus (4.10) can be rewritten as:

$$\frac{df_{pb}(t)}{dt} = \frac{-(\sum_{k=1}^{\bar{n}} \Delta Pe_{TLk-filt}(t) + D\Delta f_{pb}(t))}{2H_{Req}} \tag{4.11}$$

where the boundary deviation is defined as $\Delta Pe_B(t) = \sum_{k=1}^{\bar{n}} \Delta Pe_{TLk-filt}(t)$. By taking the Laplace transform of (4.11), the frequency-domain inertial response can be defined by a first order transfer function, where active power deviation is an input and frequency deviation is an output, such that:

$$G(s) = \frac{\Delta f_{pb}(s)}{\Delta Pe_B(s)} = \frac{-1/2H_{Req}}{s + D/2H_{Req}} \tag{4.12}$$

Thus, the inertial response of the selected Region is represented by the transfer function in (4.12), but only using pilot-bus frequency measurements and interconnection buses active power deviations. To perform such assessment, an ARMAX approach is advocated (LUGNANI et al., 2020).

To prevent outliers and gross errors, the ARMAX model estimation is performed for different orders of polynomials such as: $A, n_a = [2, \ldots, 10]$, $B, n_b = [2, \ldots, 10]$;

and $C, n_b = [2, \ldots, 10]$. This is carried out in a two-step manner: (*i*) stability of $G_e(s)$, where all of transfer function poles are analyzed; and (*ii*) quality of prediction, where the normalized root squared error (NRSE) given by (4.13) is determined.

$$NRSE = \left(1 - \frac{||f_{pb}(t) - f_{est}(t)||}{||f_{pb}(t) - mean(f_{pb}(t))||}\right) \times 100[\%] \tag{4.13}$$

Stable models are reduced to first-order transfer functions using MATLAB function *balred*. For the assessment of the inertial response, the estimated transfer function $G_e(s)$ in (4.14) is inspected.

$$G_e(s) = \frac{b_0}{s + a_0} \tag{4.14}$$

Then, (4.12) is compared to infer the regional inertia as:

$$H_{Req} = \frac{-1}{2b_0} \tag{4.15}$$

Finally, the last step is the average of the adequate estimates of H_{Req}, i.e. the estimations whose $G_e(s)$ transfer functions are stable and whose NRSE prediction error is under 5%, rendering the final estimation of the regional inertia by this exclusively data-driven method.

4.5 IEEE Test Benchmark System

The well-known IEEE 68-bus system (PAL; CHAUDHURI, 2006) is a reduced order equivalent of the inter-connected New England test system (NETS) and New York power system (NYPS). It is composed of 16-machines represented by a sixth order model equipped with AVRs, PSSs (PSS1a simplified with three lead-lag steps), and a generic model of governor with one operating mode representing steam turbine generator (DYNAMIC. . . , 2013). The load model is represented by constant impedance.

The contribution of induction motors to power system inertial response is considered in this work. To this end, a 10 % of the load at each bus is represented by a dynamic load corresponding to a set of aggregated motors with an equivalent inertia of $H_m = 5s$ (100 MVA) (RAHIM; LALDIN, 1987; DATTARAY et al., 2017). Table 4.1 summarizes this modification for each Region, showing the number of load buses, the total contribution of aggregated inertia, and the ratio ρ of H_m/H_g.

Table 4.1 – Dynamic load for of NETS/NYPS system.

Region	# buses	Region Load inertia [s]	ρ
NETS	17	85	0.3014
NYPS	15	75	0.1157

4.6 Performance of the COI and Regional Inertia Estimation with Load Contribution

To assess the performance of the fully data-driven methodology in finding the COI and estimating the regional inertia, nonlinear time-domain simulations are performed using the ANATEM simulation software (DEPARTMENT, 2017) with a total time of 20 s. Since our methodology adopts the disturbance approach according to (ASHTON et al., 2015; WILSON et al., 2019; ZOGRAFOS et al., 2017; ALSHAHRESTANI et al., 2018; SCHIFFER et al., 2019; PHURAILATPAM et al., 2019; YANG et al., 2020a; MAKOLO et al., 2021; KERDPHOL et al., 2021), all simulations include disturbances provoked by load steps occurring at 0.6s at the higher load buses. Active power and frequency measurements are collected using 60 phasors per second in fulfillment with the synchrophasor standard (IEEE. . . , 2011).

4.6.1 Application of the TDA method for pilot-bus detection

4.6.1.1 S1.w - Detection of pilot-bus per Region without motor contributions

The application of the TDA method, described in (CHOW, 2013), for the identification of coherent regions for the selected disturbance is illustrated in Figure 4.2. Table 4.2 shows in detail the limits of each Region, given the disturbance at bus 17.

Table 4.2 – Regions and their respective buses for Figure 4.2.

Region	Buses
1	14-16;18;41-42
2	10;31;38;40;46-49;53
3	11;30;32-35;45;50-51;61
4	12-13;17;36;39;43-44
5	4-7;9;19-24;26-29;68
6	1-3;8;25;37;52;54-60;62-67

For each Region a pilot-bus (Pb) is detected and the results are summarized in Table 4.3 along with the normalized root mean square error (NRMSE) (%) in reference to the true calculated COI frequency response, given by:

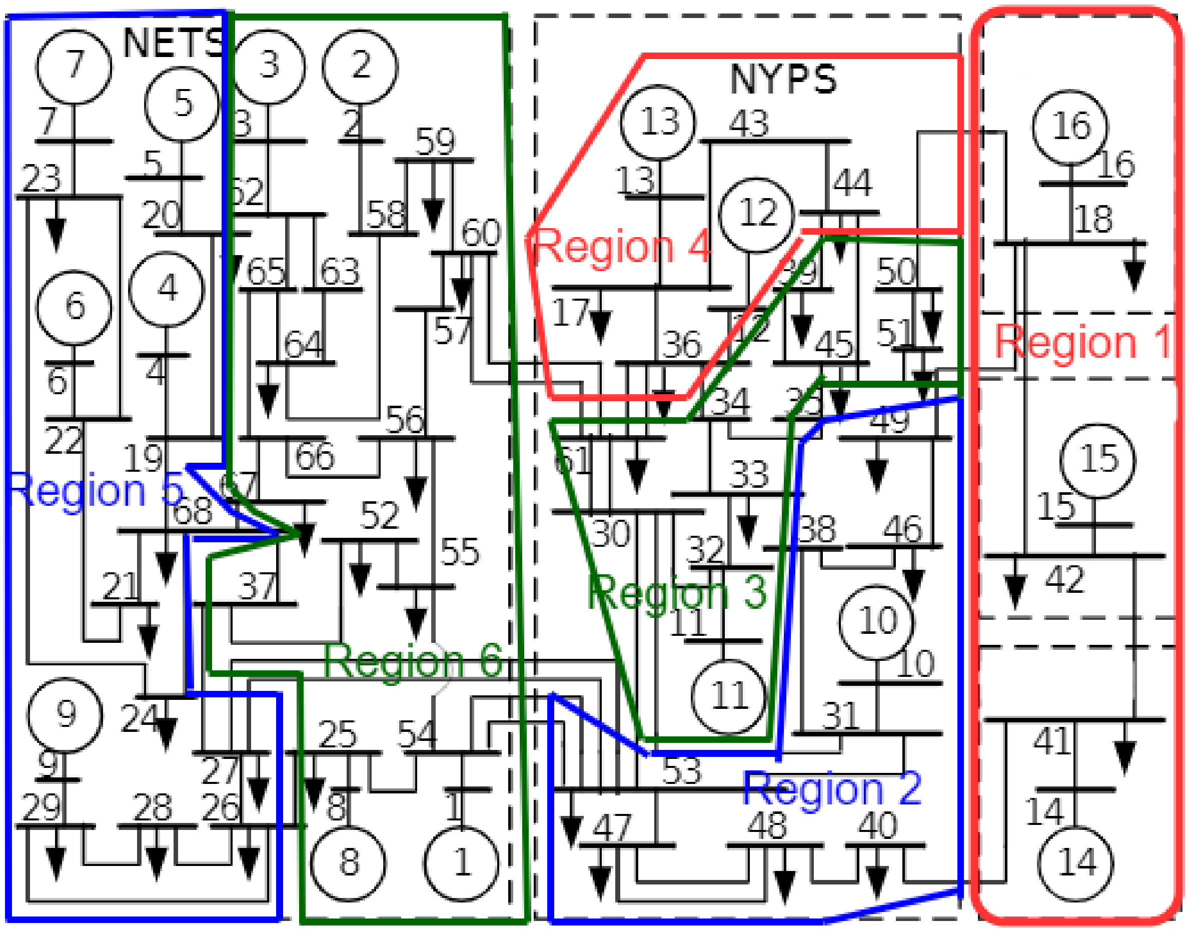

Figure 4.2 – IEEE 68-Bus with 6 areas determined by the TDA method.

$$NRMSE = \frac{\sqrt{\frac{\sum_{t=t_0}^{t_f}(f_{pb}(t)-f_{coi}(t))^2}{T}}}{\bar{f}_{coi}} \tag{4.16}$$

where t_0 is the moment of disturbance, t_f is the two seconds assumed for the inertial response, f_{pb} and f_{coi} are the detected pilot-bus frequency response and the COI calculated frequency response using knowledge of the model, respectively, T is the number of samples of the window, and $\bar{f}_{coi}$ is the mean of the frequency response of the COI. Besides the NRMSE calulated to the pilot-bus frequency response (f_{pb}), Table 4.3 also shows the NRMSE calculated for the average of the generators frequency response (f_g), and the average frequency response for all buses (f_b), all in reference to f_{coi}. Table 4.3 also provides the NRMSE threshold of first quartile ($1^{st} - q$) of the frequency response of all buses in the Region.

For regions 2 and 3 (NYPS, except Region of disturbance), the attained results are within the $1^{st} - q$ of the distribution, without surpassing the average response of the generators frequency response f_g and the average frequency response of all buses in the Region f_b. This is because regions 2 and 3 are each composed of one generator, thereby the frequency response of the generator is equivalent to the COI frequency response

Table 4.3 – Regions, detected pilot-buses and NRMSE of frequency responses, with respect to f_{coi} for S1.w.

Region	Pb	f_{pb}	f_g	f_b	$1^{st}-q$
1	41	2.12	0.62	0.61	2.11
2	48	0	0	2.13	0.88
3	35	2.62	0	1.96	1.18
4	13	6.95	2.06	3.97	2.48
5	22	0.50	0.05	0.69	0.71
6	37	0.70	0.14	0.97	1.08

($f_g = f_{coi}$). Also, these regions are closer to the disturbance and with a smaller sample of buses, impoverishing the detection. For Region 4, the results were impaired due to Region having only two generators with high inertias each, that is, the inertia of generator 12 $H_{g12} = 92.3s$ and generator 13 $H_{g13} = 496s$. The TDA method detected that generator 13 had a higher influence in the Region COI frequency response by pointing its connection bus as the pilot-bus. However, since generator 12 corresponds to 15.7% of the inertia of the Region, the error is increased. We can note that for regions with better evenly distributed inertia, the results of the pilot-bus become more precise. For regions 5 and 6 (NETS), the detected pilot-buses also present results within the the first quartile $1^{st}-q$, but this time, the TDA pilot-bus frequency response (f_{pb}) is better than the average of the inertial response of all buses in the Region. Nevertheless, the inertia values of generators in the NETS vary only slightly, thus the weights of their inertias are similar to every generator, hence the generators frequency response (f_g) is closer to the COI frequency response (f_{coi}) than (f_{pb}).

Additional tests were carried out introducing step changes of 10% in the 5 largest loads of both NYPS and NETS systems, showing similar results, confirming the validity of the TDA methodology. However, a more realistic scenario includes the contribution of the load inertial response, which is particularly relevant in today's power systems with high penetration of CCG and lowering generator inertia contribution. With this more realistic scenario we show that considering only the mean of the inertial responses of synchronous generators may be a poorer choice of representation of the f_{coi}.

4.6.1.2 S1.m - Detection of pilot-bus per Region including motors

The load's inertia is relevant and must not be ignored for pilot-bus detection; however, this configuration essentially displaces the COI's position. Thus, the use of generators mean frequency response f_g as pilot-bus becomes inaccurate. Therefor, this scenario includes the same load step (10%) over the dynamical loads added to the system. The TDA method is applied to the previously identified regions for the detection of the pilot-bus. As an example, Fig. 4.3 shows the calculated similarities for Region 5.

Notice that the values in Fig. 4.3 range in an arbitrary interval, containing positive and negative values. The first steps in the TDA method, i.e. the computation of the cumulative proximity $q_N(\alpha(k))$ and the standardized eccentricity $\epsilon_N(\alpha(k))$, deal with the normalization of the data, like other methods. But in our proposal, the normalization process does not assume any model of distribution for the collected data, but rather uses the data exclusively. This generates only feasible values in the normalized range, i.e. no compound distance produced by unrealistic frequency deviation or active power deviation values would be part of the range. Fig. 4.4 displays the calculated proximities for the same Region.

The detected pilot-bus with the corresponding NRMSE is presented in Tab. 4.4, showing the displacement of the COI when load inertial response is added to the system, as the results from the TDA pilot-bus frequency response f_{pb} become equivalent or more precise, i.e. with a lower RMSE, than the generators mean frequency response f_g. The typicality distribution of each Region is presented in Fig. 4.6, showing that even though the representation of generators is significant, the load buses dislocate the mean of the distribution, having themselves more participation in the inertial frequency response.

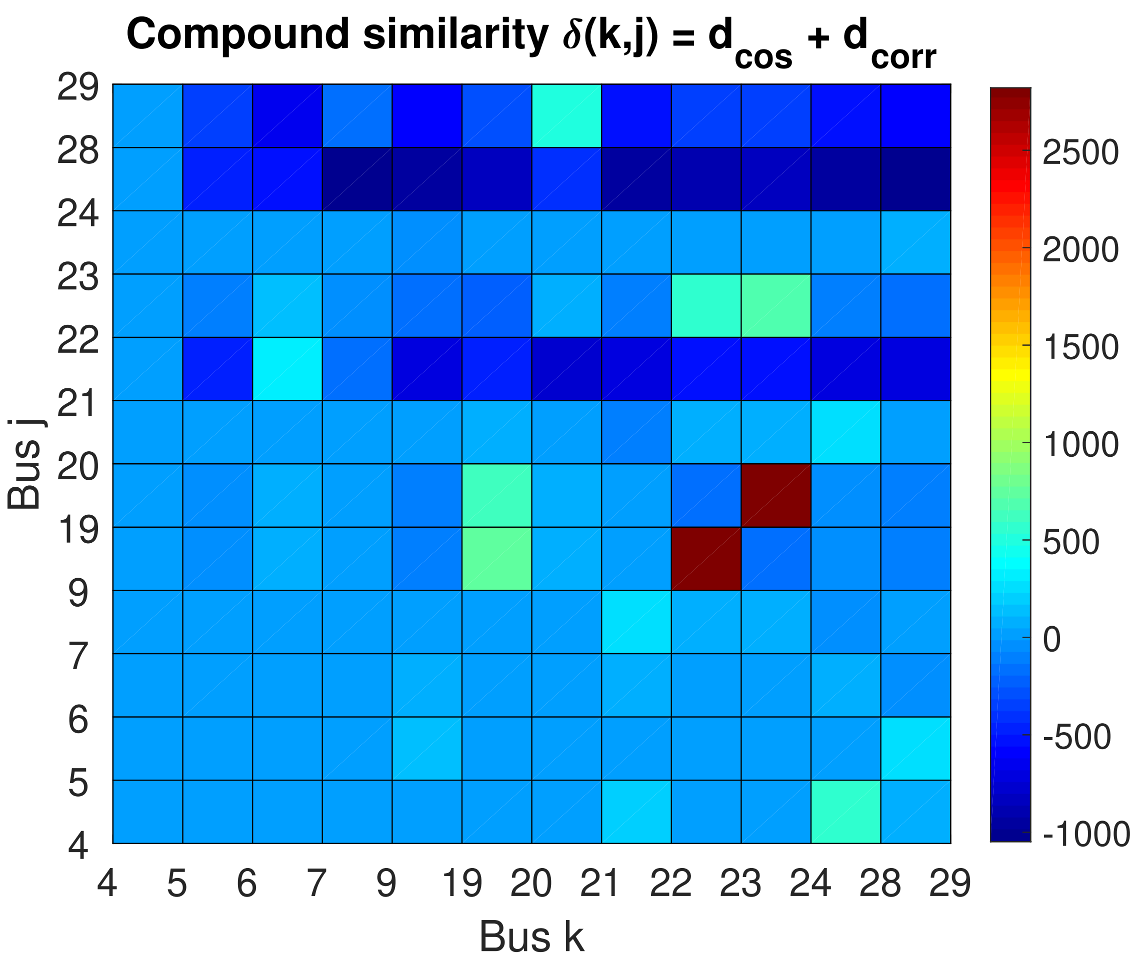

Figure 4.3 – Metrics Region 5.

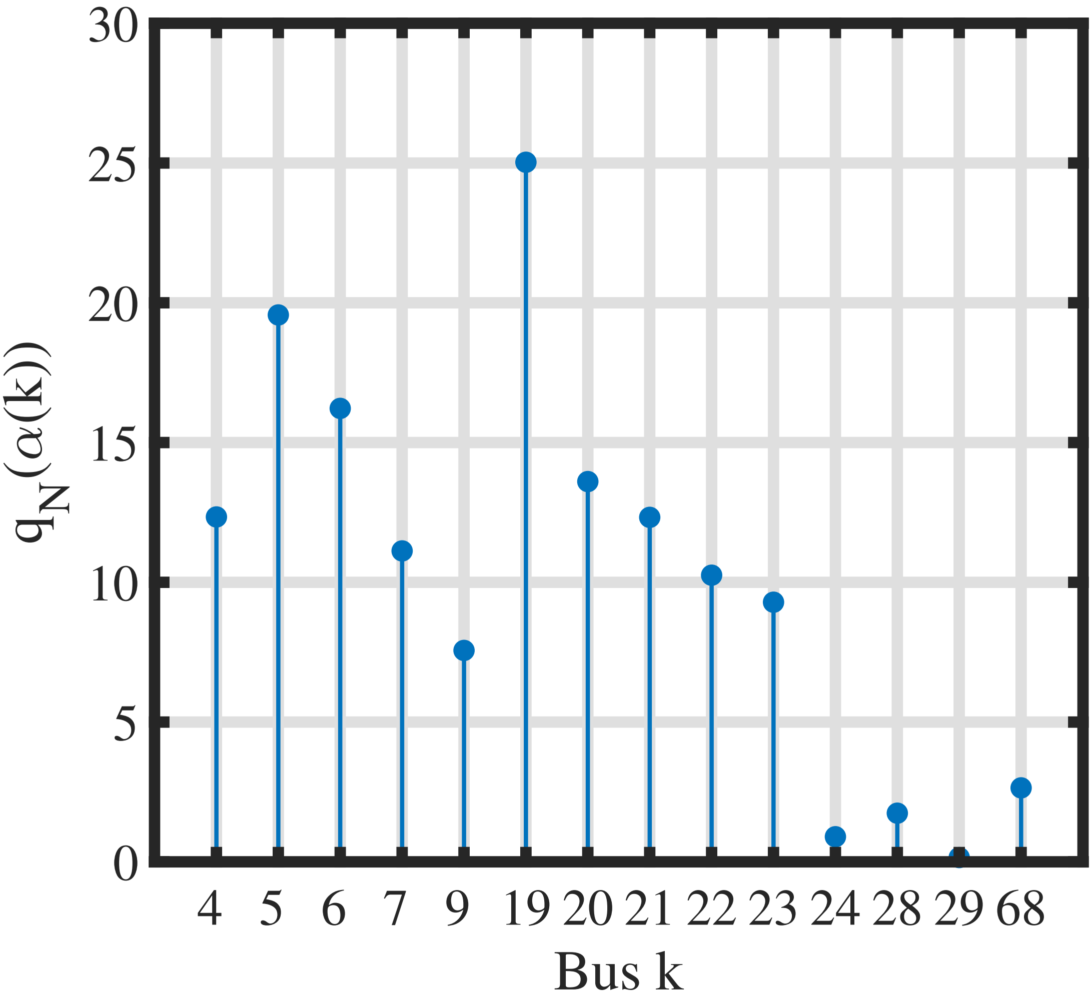

Figure 4.4 – Cumulative proximities Region 5.

Table 4.4 – Regions, detected pilot-buses and NRMSE of frequency responses, with respect to f_{coi} for S1.m.

Region	Pb	f_{pb}	f_g	f_b	$1^{st} - q$
1	41	1.27	0.21	0.22	1.22
2	31	0	0.17	1.64	1.79
3	35	1.44	1.44	3.29	1.96
4	13	3.42	3.14	4.57	3.58
5	29	0.22	0.31	0.49	0.49
6	59	0.19	0.25	0.19	0.28

As expected from Tab. 4.4, it is noteworthy to validate that: the presumption that f_g is the best approximation of the COI is erroneous, since the load is not represented by constant impedances. Then, the TDA matches the result from f_g for regions 2 and 3 due to the f_{pb} frequency response surpassing the inertial response of the single generation in Region 2, as the TDA pilot-bus detection takes into account load contribution. For Region 3, the RMSE of the bus detected by the TDA method coincides with the error of the Region f_g.

For Region 4, the result of the pilot-bus detected by the TDA method approximates f_g as the contribution of load inertia is small in this Region, compared with the generator's inertia. For regions 5 and 6, the RMSE of f_{pb} is smaller than f_g, as these regions have a high number of load buses and as we assume equal distribution of dynamical loads among load buses, the value of f_{coi} displaces more from the weighted mean of the generators.

It is also noteworthy to remark that the pilot-bus detected by the TDA method in all five regions is within the first quartile, indicating a consistency in approximating the distribution of data with the proposed method. For instance, selecting the pilot-bus and the mean of generators and every bus for Region 5, Fig. 4.5 illustrates the comparison of the frequency responses of the COI. Where it is noticed that the pilot-bus frequency response f_{pb} properly tracks the trajectory of the COI frequency response f_{coi}, even though no model information is provided for the TDA method. Additionally, the displacement of the COI is evident, as the frequency response of the generators f_g becomes more distant from the COI.

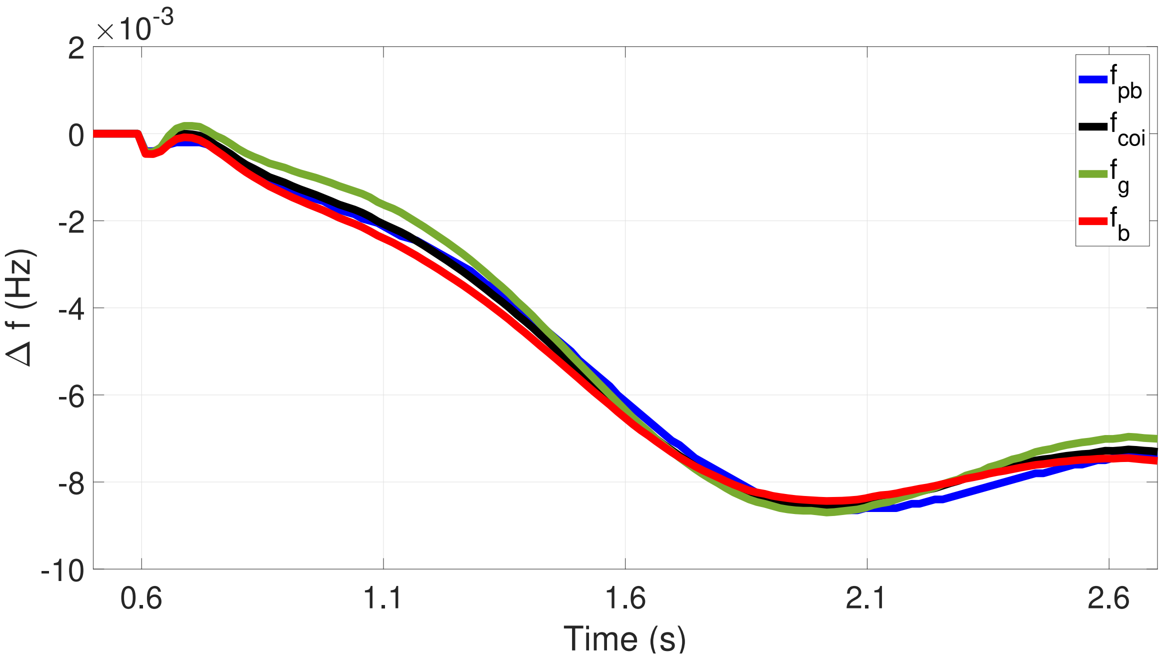

Figure 4.5 – Frequency response comparison of f_{coi}, f_{pb}, f_g and f_b for Region 5.

Next, we will apply the equivalent inertia's estimation method per Region for the above cases.

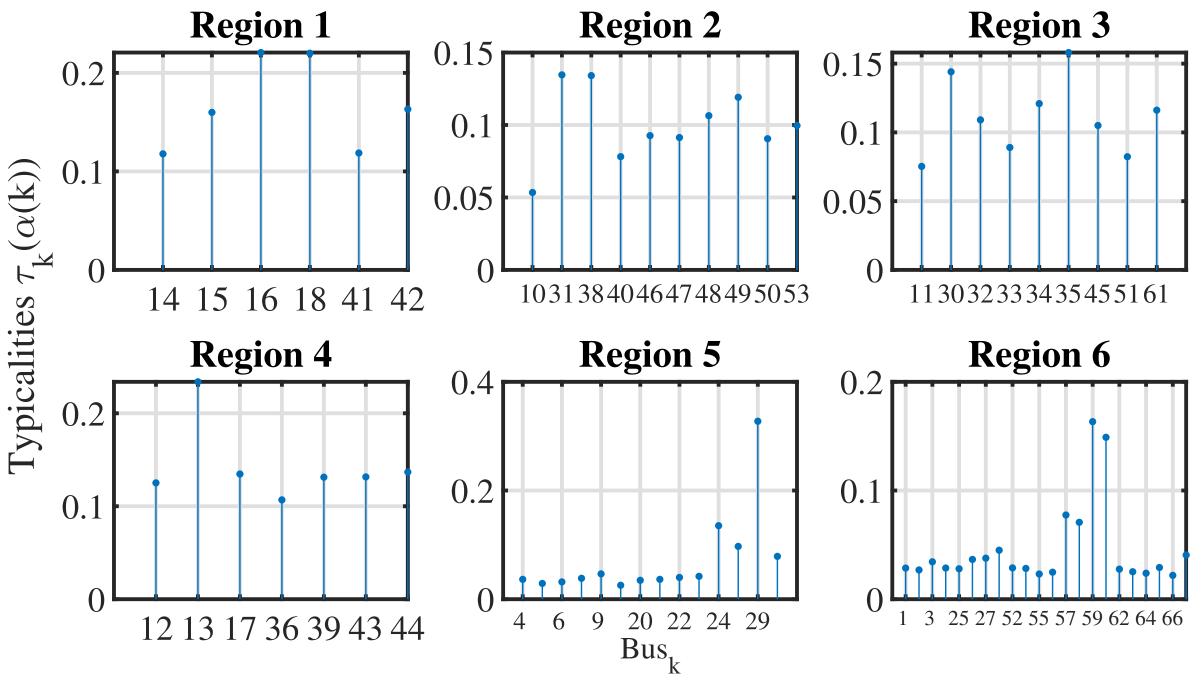

Figure 4.6 – Typicalities for S1.m.

4.6.2 Regional inertia estimation using the detected pilot-bus

In this section, the methodology schematized in Fig. 4.1 is followed taking advantage of the right detection of the pilot-bus provided by the TDA features, according to Section 4.4.2, to estimate the regional inertia seen from the COI or pilot-bus. This assessment is accomplished thanks to an ARMAX-based identification approach that seeks representing the total inertia per area as the inertia of an equivalent machine, such that this machine encompasses the regional dynamic. Finally, the application is carried out employing the cases described above, i.e. without and with motor inertial contributions.

4.6.2.1 ARMAX Regional inertia estimation for case 4.6.1.1

Once, the ARMAX-based methodology is applied according to Section 4.4.3, the assessment of the regional inertia is achieved and compared with the reference values used for simulations. Where H_{ref} in Table 4.5 represents the sum of the total inertia per Region, H_est denotes the estimate by our proposal, and RE is the relative error in percentage. To produce the regional inertia estimation, the interconnections' active power deviation of each Region are used as input signals, that is $u(t) = \Delta Pe_B(t) = \sum \Delta Pe_{TL(t)}$; meanwhile the pilot-bus frequency signal deviation is employed as output signal $y(t)$. Then, all steps contained in the green dotted box in Fig. 4.1 are applied to these signals. The ARMAX model is estimated for equal orders of $[n_a, n_b, n_c] = [2, \ldots, 10]$, and the final inertia estimation is considered as the average of all accepted estimates.

From Table 4.5, it is noteworthy to remark that the assessment of the COI together with the regional inertia results in errors in line with those found in the literature for regional estimation, even for pilot-buses with greater error to the true COI frequency response than the average of generators frequencies.

Table 4.5 – Regional Inertia Estimates for Case 4.6.1.1

Region	H_{ref}	H_{est}	RE [%]
1	1050	1777.4	2.61
2	31	30.4	1.94
3	28.2	28.9	2.48
4	588.3	568.9	3.29
5	115.9	119.4	3.02
6	106.7	110.3	3.37

4.6.2.2 ARMAX Regional inertia estimation for case 4.6.1.2

Here, all areas (except Area 1) have been added with the inertia provided by motors, resulting in the estimated regional inertias summarized in Table 4.6. Note that the additional inertia provided by the motors is also considered as reference in H_{ref}. This is an important aspect of regional inertia that is not usually considered in most methods found in literature (ASHTON et al., 2015; ALSHAHRESTANI et al., 2018) and applied to real systems, i.e. the ability of estimation methods in capturing load inertial contribution. This proposal provides a reference estimation of regional inertia with load contribution (H_{est}) with reasonable errors (RE), so applications to real systems can quantify the contributions of their respective loads. Our proposed approach does not require any model information, neither simplifies the COI inertial response f_{coi} by the average of generators, disregarding other sources of inertial response. Figure 4.7 shows the input and output signals for this case, which are used by the ARMAX estimation methodology.

Table 4.6 – Regional Inertia Estimates for Case 4.6.1.2

Region	H_{ref}	H_{est}	RE [%]
1	1050	970.49	7.57
2	61	63.3	3.77
3	58.2	54.3	6.7
4	603.3	592.1	1.86
5	190.3	183.4	3.63
6	148	144.5	2.36

From the numerical results, the ARMAX-based methodology is able to estimate the regional inertia using the pilot-bus provided by the TDA method with errors similar to those ones found in literature (WILSON et al., 2019; ALSHAHRESTANI et al., 2018), despite there are scarce resources to estimate the load contribution.

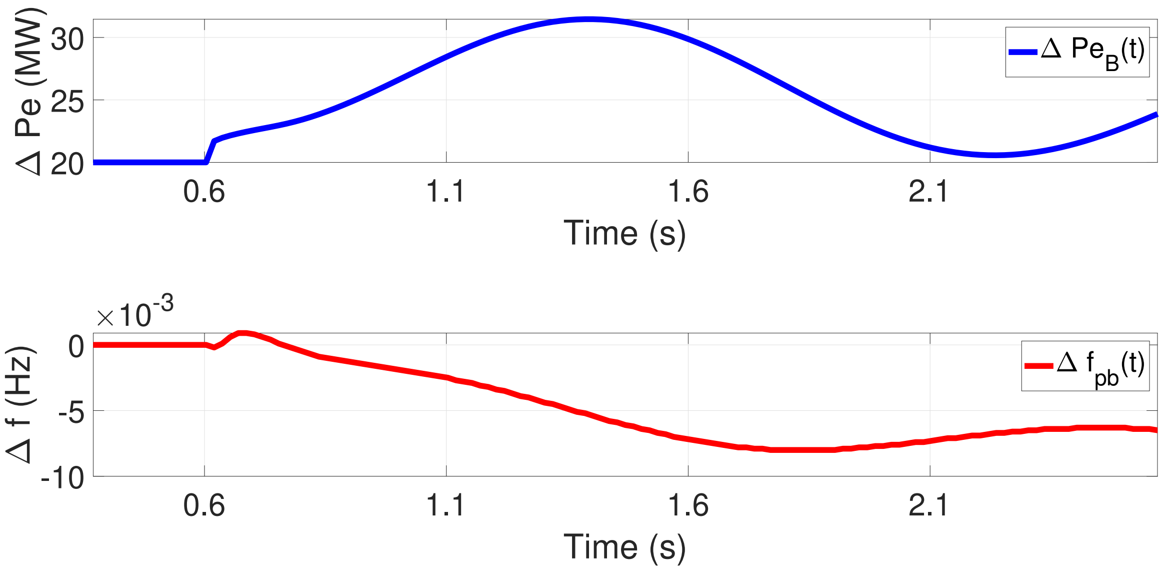

Figure 4.7 – Input signal - active power of Region 5 tie-lines. Output signal - pilot-bus frequency deviation of Region 5

4.7 Discussion

This work proposes an overall fully data-driven methodology for the COI and regional inertia estimation. The proposed method identifies a candidate pilot-bus, as the Center of Inertia, belonging to a Region. It estimates the inertia using only available PMU measurements such as frequency data from that bus and active power signals from interconnections of the Region after disturbances. The method is tested for the NETS/NYPS benchmark system and its modified version with dynamic load representation of aggregated induction motors to represent the inertial contribution of the load. Finally, the regional inertia is estimated providing satisfactory results.

Conclusion

This thesis aimed to provide a procedural sequence of methods for the data-drive analysis of the regional inertial response of power systems following disturbances. In that sense, to the author knowledge, it has been the first to describe methodologies that detect areas, pilot-buses with the specific purpose of regional inertia.

The methods rely mostly in the first-time application of statistical clustering (TDA) for the modal decomposition of signals distribution, for identification of clusters (electrical areas) and its means (pilot-buses). It has further relied on the parametric identification structure ARMAX for the inertial estimation of the regional equivalent machine, which is sensible to load inertial response contribution.

From the research work performed in this thesis some interesting ideas can be gathered, based on the assumptions taken in the process and presented in this manuscript. From the coherent analysis study we can enunciate the following:

- **Data-driven methods for coherency clustering maturity**: the abundance of data-driven methods found in the literature corroborates the development of the field. While there are different advantages between the methods, we can say that they are able to perform the clustering techniques at least with the same accuracy of model-based methods. The author would argue that the application of coherency in control rooms could be efficiently substituted (or merged with model-based methods) providing the control room with less model dependency;
- **Power system areas are becoming more dynamic**: as more IBR generation is added to the system, which must be installed where primary source is advantageous and are intermittent by nature, the topology of the system is modified and switched more frequently. This phenomena in turn mutate the areas of the system at a more fast pace and with more diversity than before. This in turn makes the application of model-based methods harder, as the changes in topology must be taken into account for clustering of the models of the linear model of the system;
- **Electrical islanding phenomena is (at least) more common than previously observed:** this affirmation is both with the respect of limited observabilitty available by model-based models, which are restrained to the neighborhood of the operating condition, and the changes in the generation fleet, where IBR are able to ridethrough disturbances isolated from the system;

- **Operator discretion is still advised in borderline cases:** although the method presented here provides statistical guarantees for the resulting clusters provided, some very specific cases where some specific condition of operation may be interested to maintain some machine into some area for other purposes that go beyond the frequency stability analysis. Additionally, data-driven methods are somewhat event-specific, or at least, event-like-specific. In that sense, the knowledge of the operator of the frequency of occurrence of such events in the system is advised, as it is hard to generalize the results found with data-driven method. It is rather more interesting for these methods to provide the operator with situational awareness of the current disturbance.

Furthermore, for the second portion of this doctorate work, some additional concepts were also observed and should be pointed out for the conclusion of the thesis.

- **Inertial response is not restricted to transmission level machines:** although we look at the transmission system in an isolated manner, disregarding lower level voltage buses, the rapid transition we face today in power systems has forced a change in perspective in that sense, considering some aspects of the distribution level system. One of these aspects, found in the second part of this system is that the contribution of load to the inertia response is relevant, specially as inertia of generators connected at the transmission level becomes scarce. This is interesting to consider as estimations done considering only transmission level inertia can be assumed to always underestimate inertia of the system. This is not to say however that the distribution of contribution of inertia is homogeneous, on the contrary, it may vary from almost none to places where heavy industrialized locations will contribute with high portions of the inertia response through its motors. Nonetheless, the method proposed here is able to estimate the inertia of a region with the presence of load contribution considered.

- **COI displacement by load:** not only load contributes to inertia response, it also interferes with the location of the COI of the system. Although we will discuss next the compactness nature of the frequency response may result in such displacement of the COI beign negligible, some extreme cases, ignoring the load contribution fro pilot-bus detection may result in very poor estimations;

- **COI response is predominant:** although the proper detection of the closest bus to the COI is ideal for estimation, it has been observed that a region of buses around the COI is very compact in terms of inertial response at least. This in turn leads to similar results for the estimation of the regional inertia. Further studies are suggested to quantify such compactness and determine when it isn't sufficient and may even predict in region separation;

- **Regions come in all shapes and sizes:** one of the main motivations of these work is that model-based methods may generalize responses up to a certain level, but never to a totality. Data-driven method proposed here may not prevent the same level of abstraction, but performs equally efficiently for case not considered in model-based cases. In that sense, it must be reiterated that some particular conditions may form regions with such low inertia that not even load contribution is sufficient and even smaller disturbances than the loss of the biggest generator may trip frequency protection schemes. This is to say that, while $N-1$ criteria is widely used as it covers most scenarios, modern power systems need to consider such data-driven methods inputs for control and protection of some particular conditions. These conditions may not lead to blackout, but merging data-driven information can increase the robustness of the system, in a *self-healing* philosophy approach, where adjustments can be made if such scenarios present themselves and the method is able to predict them being harmful;

- **Location of disturbance is more relevant than size:** the application of several disturbances during both parts of this research, but particularly the second, has shown that closeness to disturbance is a more impacting aspect than the size of said disturbance, this is of course not considering the extreme cases. Such information could be relevant for operation room procedures, where limited computational effort is available and a more directed effort could be made, like applying data-driven methods for reduction of farther regions to the disturbance and equivalent machine representation, while the area of disturbance is maintained in its entirety.

The thesis has been tested with some real data and provided some promising results in order to enrich decision-making in the control room, Among theoretical results, some concepts can be listed.

Contributions of the main papers of this doctorate thesis include:

- Regarding coherency studies:
  - Data driven method for regional detection after a disturbance;
  - User independent clustering technique for power system purposes;
  - Able to provide islanding detection;
  - Statistical guarantee of clustering;

- Regarding center of inertia studies:
  - Data driven method for regional pilot-bus selection after a disturbance;
  - Data driven method for regional inertia estimation
  - Quantitative study of load contribution to inertia response;

Thesis publications

Although the amount and quality of an academic work cannot be completely quantified, specially a long work such as a doctorate thesis, there are some measures that can indicate the depth of the research performed and its contribution to academia and industry.

This thesis produced and is supported by the publication of 1 national conference paper, 3 international conference papers, 4 research presentations, 3 international journal papers. Additionally, 1 national conference paper and two international journal papers related to the thesis are presently under the reviewing process. Papers published during the doctorate research period:

- Journal papers:
  1. LUGNANI, L.; JONES, M.; ALBERTO, L. F.; PEET, M.; DOTTA, D. Combining Trajectory Data with Analytical Lyapunov Functions for Improved Region of Attraction Estimation v. 7, p.271-276, 2023. IEEE Control System Letters, 2022. (LUGNANI et al., 2022c);
  2. ORTIZ-BEJAR, J.; PATERNINA, M. R. A.; ZAMORA-MENDEZ, A.; LUGNANI, L.; TELLEZ, E. Power system coherency assessment by the affinity propagation algorithm and distance correlation. Sustainable Energy, Grids and Networks, Elsevier, v. 30, p. 100658, 2022. (ORTIZ-BEJAR et al., 2022);
  3. LUGNANI, L.; PATERNINA, M.; DOTTA, D.; CHOW, J.; LIU, Y. Power system coherency detection from wide-area measurements by typicality-based data analysis. IEEE Transactions on Power Systems, v. 37, n. 1, p. 388–401, 2022. (LUGNANI et al., 2022d);
  4. LUGNANI, L.; DOTTA, D.; LACKNER, C.; CHOW, J. Armax-based method for inertial constant estimation of generation units using synchrophasors. Electric Power Systems Research, Elsevier, v. 180, p. 106097, 2020. (LUGNANI et al., 2020).
- Conference papers:

1. LUGNANI, L.; JONES, M.; ALBERTO, L. F.; PEET, M.; DOTTA, D. Combining trajectory data with energy functions for improved region of attraction estimation. IEEE Control Systems Society Conference, 2022 (LUGNANI et al., 2022b)
2. PINHEIRO, B.; LUGNANI, L.; DOTTA, D. Estimação da inércia regional utilizando dados ringdown e ambiente (under review). In: Congresso Brasileiro de Automática, CBA. [S.l.: s.n.], 2022. p. 1–7. (PINHEIRO et al., 2022);
3. LUGNANI, L.; DOTTA, D.; PATERNINA, M. R.; CHOW, J. Real-time coherency identification using a window-size-based recursive typicality data analysis. In: 2022 IEEE International Conference on Smart Grid Synchronized Measurements and Analytics. [S.l.: s.n.], 2022. (LUGNANI et al., 2022a);
4. PINHEIRO, B.; LUGNANI, L.; DOTTA, D. A procedure for the estimation of frequency response using a data-driven method. In: 2021 IEEE Power Energy Society General Meeting (PESGM). [S.l.: s.n.], 2021. p. 01–05. (PINHEIRO et al., 2021)Pinheiro, B.;
5. LUGNANI, L.; DOTTA, D. *Monitoramento da constante inercial de see utilizando sincrofasores*(In Portuguese). In: Seminário Nacional de Produção e Transmissão de Energia Elétrica (XXV SNPTEE). [S.l.: s.n.], 2019. p. 1–9.(LUGNANI; DOTTA, 2019);
6. ARGÜELLO, A.; LUGNANI, L.; DOTTA, D. Dfig model considering turbine mechanical limitations for frequency response control studies. In: IEEE. 2019 IEEE PES Innovative Smart Grid Technologies Conference-Latin America (ISGT Latin America). [S.l.], 2019. p. 1–6. (ARGÜELLO et al., 2019).

- Papers submitted during the doctorate research period:

  1. RODALES, D.; ZAMORA-MENDEZ, A.; SERNA, J. A. de la O.; RAMIREZ, J. M.; PATERNINA, M. R. A.; LUGNANI, L.; MEJIA-RUIZ, G. E.; DOTTA, D. Model-free inertia estimation in bulk power grids (under review). Elsevier Electic Power Systems Research, 2022. (RODALES et al., 2022);
  2. LUGNANI, L.; PATERNINA, M. A. R.; DOTTA, D. Center of inertia and equivalent inertia estimation: A fully data-driven method and load contribution (under review). XXXX JOURNAL, 2022. (LUGNANI et al., 2022e).

- The following presentations were made during the doctorate period:

  1. LUGNANI, L.; DOTTA, D. ; PATERNINA, MARIO R. ARRIETA ; CHOW, J. . Real-time Coherency Identification using a Window-Size-Based Recursive Typicality Data Analysis. May, 2022;

2. LUGNANI, L.; DOTTA, D. . *Monitoramento da Constante Inercial de SEE utilizando Sincrofasores*(In Portuguese). October, 2019;
3. FERNANDES, L. L.; DOTTA, D. . Frequency Response Estimation Following Large Disturbances using synchrophasors. August, 2018.

- Public available cumputer program: ORTIZ, J.; LUGNANI, L.; PATERNINA, M.; ZAMORA, A.; RAMIREZ, J.; REYES, R.; DOTTA, D.; TOLEDO, C.; ZARATE, J.; ZELAYA, F. Clustering Analytics for Power Systems Dynamics (CAPS-D). 2021. Eletronically. Avaiable at: <http://148.216.38.78/cict/app/clusters/.> (ORTIZ et al., 2021)

Some of the most relevant publications that are not directly part of the thesis, but are important peripheral contributions can be found at Appendix A.

Future Works

On Part 1, where areas are detected after disturbances, future work efforts will be to improve potential use of the TDA method for:

- **Fault location:** as mentioned above regarding the behavior of areas, it has been observed an inverse relation between the distance to the disturbance location and the number of the areas. A further study of the TDA provided areas fragmentation may deliver valuable information to detect disturbances location at early stages;
- **Designing advanced special protection schemes:** areas provided by TDA may be used for the designation of schemes that address at least a reference machine per area, so individual machines don't disconnect due to loss of synchronism. Such study may be readly implemented with TDA provided areas and available information of synchronous machines online;
- **Coherent area detection using ambient measurements:** ideally the identification of areas is done at every SCADA period. The goal here is to identify a characteristic of the coherency behavior in power systems that can be observed in nominal operation, such as power oscillations and angle swings, so TDA may define distance between buses at every, say, 15 minutes and the operator is provided with updated areas, or probable areas if a separation occurs;

On Part 2, where the Center of Inertia pilot-bus of each Area is detected after disturbances, future works include:

- **Assessment of the COI and regional inertia using an ambient data approach:** such as in the previous part, it is valuable to identify of areas in nominal conditions using TDA, if their detection is possible. Ideally the same metrics as the ones proposed for coherency with ambient data could be used for estimation of the pilot-buses, and power swing values used to update the ARMAX model inertia parameter within time periods that could provide operator with awareness of possibly inertia deficient areas;

- **Estimation of the load damping coefficient:** the frequency model presented in Section 2.1 considers also the frequency dependent portion of the load that varies with the frequency. Although the theory aspect for the estimation of this portion differs, where more constant excitation signal are necessary, it is possible and desirable to estimate this parameter, so the operator is provided with better information for control and protection tuning;

- **Estimation of the equivalent droop of the Region:** the same logic of the previous item apply here. It is possible to estimate an equivalent droop response of region, using ARMAX and the correct excitation signals. This research path would also provide the operator with valuable data, both for performance evaluation of the system, but also generators frequency control loop calibration.

Additionally, regarding TDA methodology, it can be further explored in:

- **Regional inertia distribution:** with a well established WAMS and the abbuandance of data it provides, starting from a reference value for each bus, the author argues that it is possible to use TDA **pdf!** (**pdf!**) approxiamtion to identify inertia variation within areas. This work would require very fine signal processing, to filter variations in power and frequency signals in ambient conditions from noise, but this would in term provide the control room with knowledge of changes in the system that could be used for dispatch of synthetic inertia, for instance;

- **Planning: scenario reduction:** as TDA is a clustering technique, and the increase in the number of possible cases due to the uncertainty of wind and solar generation, the evolving need to identify extreme cases within the thousands of cases generated during planning became even more pressing. Arguably, TDA can be applied to achieve such reduction;

- **IBR behavior clustering:** as the penetration of IBR increases, new behaviors are set to take place in the system, as each maker sets its control philosophies. In that context TDA can be used to observe the converging response of such generators so outliers are detected and investigated;

- **Applicability of TDA to voltage and angular and other fields of power system stability:** here, the goal is to investigate clustering needs within other stability fields that are not attended by traditional methods.

Other research paths that arise from the overall doctorate period are:

- **Load response modeling:** as power systems are becoming more iterative, as shown in this thesis, like the inertial contribution of load, it is of interest to better represent the load than the traditional ZIP model, such that simulations remain accurate for these responsive loads and stability and optimization problems may take advantage of load better description;

- **Identification studies for model parameter calibration issues using ARMAX and other techniques:** the objective here is to explore identification techniques and WAMS data to develop techniques for detection of uncalibrated parameters of generators control loops;

- **Study of Region of Attraction (ROA) estimation techniques study with inner approximation and scalabilty for large systems:** parallel work performed by the author regarding rotor angle stability has investigated methods for estimation of the Region of Attraction of the generators angle, using PMU data and inner approximation method. The objective here is to further investigate methods able to provide such inner approximation, using trajectory data, but with better computational performance and able to generalize to other operation conditions, that is, extrapolate the ROA to other equilibrium points.

Bibliography

ABRAHAM, E. E.; MARZOOGHI, H.; YU, J.; TERZIJA, V. A novel adaptive supervisory controller for optimized voltage controlled demand response. IEEE Transactions on Smart Grid, IEEE, v. 10, n. 4, p. 4201–4210, 2018. Citado na página 62.

AGHAMOHAMMADI, M.; TABANDEH, S. A new approach for online coherency identification in power systems based on correlation characteristics of generators rotor oscillations. International Journal of Electrical Power & Energy Systems, Elsevier, v. 83, p. 470–484, 2016. Citado 2 vezes nas páginas 63 and 66.

AL-MASRI, H. M.; EHSANI, M. Impact of wind turbine modeling on a hybrid renewable energy system. In: IEEE. Industry Applications Society Annual Meeting, 2016 IEEE. [S.l.], 2016. Citado na página 64.

ALLELLA, F.; CHIODO, E.; GIANNUZZI, G. M.; LAURIA, D.; MOTTOLA, F. On-line estimation assessment of power systems inertia with high penetration of renewable generation. IEEE Access, IEEE, v. 8, p. 62689–62697, 2020. Citado 2 vezes nas páginas 96 and 98.

Alsafih, H. A.; Dunn, R. Determination of coherent clusters in a multi-machine power system based on wide-area signal measurements. In: IEEE PES General Meeting. [S.l.: s.n.], 2010. p. 1–8. Citado na página 63.

ALSHAHRESTANI, A.; GOLSHAN, M.; ALHELOU, H. H. Wams based online estimation of total inertia constant and damping coefficient for future smart grid systems. In: IEEE. 2018 Smart Grid Conference (SGC). [S.l.], 2018. p. 1–5. Citado 4 vezes nas páginas 96, 97, 109, and 116.

ANGELOV, P. P.; GU, X. Empirical approach to machine learning. [S.l.]: Springer, 2019. Citado 3 vezes nas páginas 68, 101, and 138.

ANGELOV, P. P.; GU, X.; PRÍNCIPE, J. C. A generalized methodology for data analysis. IEEE transactions on cybernetics, IEEE, v. 48, n. 10, p. 2981–2993, 2017. Citado 5 vezes nas páginas 67, 69, 70, 71, and 137.

ARGÜELLO, A.; LUGNANI, L.; DOTTA, D. Dfig model considering turbine mechanical limitations for frequency response control studies. In: IEEE. 2019 IEEE PES Innovative Smart Grid Technologies Conference-Latin America (ISGT Latin America). [S.l.], 2019. p. 1–6. Citado na página 122.

ARIFF, M.; PAL, B. C. Coherency identification in interconnected power system - an independent component analysis approach. IEEE Transactions on Power Systems, IEEE, v. 28, n. 2, p. 1747–1755, 2012. Citado na página 63.

ASHTON, P. M.; SAUNDERS, C. S.; TAYLOR, G. A.; CARTER, A. M.; BRADLEY, M. E. Inertia estimation of the GB power system using synchrophasor measurements. IEEE Transactions on Power Systems, IEEE, v. 30, n. 2, 2015. Citado 4 vezes nas páginas 96, 97, 109, and 116.

ASSOCIATION, I. S. et al. C37. 118.1-2011 IEEE Standard for Synchrophasor Measurements for Power Systems. [S.l.], 2011. Citado 2 vezes nas páginas 73 and 75.

AZIZI, S.; SUN, M.; LIU, G.; TERZIJA, V. Local frequency-based estimation of the rate of change of frequency of the center of inertia. IEEE Transactions on Power Systems, IEEE, v. 35, n. 6, p. 4948–4951, 2020. Citado na página 96.

BABU, G. Y.; SARKAR, V. Transient instability mitigation via repetitive corrective actions based upon the real-time macrocoherency evaluation. IEEE Systems Journal, IEEE, v. 14, n. 4, p. 5084–5095, 2020. Citado na página 62.

BANNA, H. U.; YU, Z.; SHI, D.; WANG, Z.; SU, D.; XU, C.; SOLANKI, S. K.; SOLANKI, J. M. Online coherence identification using dynamic time warping for controlled islanding. Journal of Modern Power Systems and Clean Energy, Springer, v. 7, n. 1, p. 38–54, 2019. Citado 2 vezes nas páginas 63 and 66.

BARUZZI, V.; LODI, M.; OLIVERI, A.; STORACE, M. Analysis and improvement of an algorithm for the online inertia estimation in power grids with res. In: IEEE. 2021 IEEE International Symposium on Circuits and Systems (ISCAS). [S.l.], 2021. p. 1–5. Citado 2 vezes nas páginas 96 and 99.

BATISTA, G. E.; KEOGH, E. J.; TATAW, O. M.; SOUZA, V. M. D. Cid: an efficient complexity-invariant distance for time series. Data Mining and Knowledge Discovery, Springer, v. 28, n. 3, p. 634–669, 2014. Citado 3 vezes nas páginas 68, 69, and 74.

BLOOM, A.; TOWNSEND, A.; PALCHAK, D.; NOVACHECK, J.; KING, J.; BARROWS, C.; IBANEZ, E.; O'CONNELL, M.; JORDAN, G.; ROBERTS, B. et al. Eastern renewable generation integration study. [S.l.], 2016. Citado na página 89.

CAI, G.; WANG, B.; YANG, D.; SUN, Z.; WANG, L. Inertia estimation based on observed electromechanical oscillation response for power systems. IEEE Transactions on Power Systems, v. 34, n. 6, p. 4291–4299, 2019. Citado 2 vezes nas páginas 96 and 98.

CAI, J. Y.; HUANG, Z.; HAUER, J.; MARTIN, K. Current status and experience of wams implementation in north america. In: IEEE. 2005 IEEE/PES Transmission & Distribution Conference & Exposition: Asia and Pacific. [S.l.], 2005. p. 1–7. Citado na página 21.

CANIZARES, C.; FERNANDES, T.; GERALDI, E.; GERIN-LAJOIE, L.; GIBBARD, M.; HISKENS, I.; KERSULIS, J.; KUIAVA, R.; LIMA, L.; DEMARCO, F. et al. Benchmark models for the analysis and control of small-signal oscillatory dynamics in power systems. IEEE Transactions on Power Systems, IEEE, v. 32, n. 1, 2017. Citado na página 77.

CEPEDA, J. C.; RUEDA, J. L.; COLOMÉ, D. G.; ECHEVERRÍA, D. E. Real-time transient stability assessment based on centre-of-inertia estimation from phasor measurement unit records. IET Generation, Transmission & Distribution, IET, v. 8, n. 8, p. 1363–1376, 2014. Citado na página 96.

CHAMORRO, H. R.; GHANDHARI, M.; ERIKSSON, R. Coherent groups identification under high penetration of non-synchronous generation. In: IEEE. 2016 IEEE Power and Energy Society General Meeting (PESGM). [S.l.], 2016. p. 1–5. Citado 4 vezes nas páginas 63, 64, 65, and 66.

CHOW, J. Power System Toolbox. 2020. Disponível em: <https://www.ecse.rpi.edu/~chowj/PST_2020_Aug_10.zip>. Citado 2 vezes nas páginas 75 and 93.

CHOW, J.; SANCHEZ-GASCA, J. J. Power System Modeling, Computation, and Control. [S.l.]: JohnWiley & Sons Ltd, 2020. Citado 4 vezes nas páginas 8, 28, 33, and 144.

CHOW, J. H. Power system coherency and model reduction. [S.l.]: Springer, 2013. Citado 16 vezes nas páginas 18, 45, 46, 47, 53, 55, 62, 67, 78, 79, 93, 99, 101, 104, 109, and 136.

CHOW, J. H.; CHEUNG, K. W. A toolbox for power system dynamics and control engineering education and research. IEEE transactions on Power Systems, IEEE, v. 7, n. 4, p. 1559–1564, 1992. Citado na página 75.

CUI, Y.; YOU, S.; LIU, Y. Ambient synchrophasor measurement based system inertia estimation. In: IEEE. 2020 IEEE Power & Energy Society General Meeting (PESGM). [S.l.], 2020. p. 1–5. Citado 2 vezes nas páginas 96 and 98.

DATE, R. A.; CHOW, J. H. Aggregation properties of linearized two-time-scale power networks. IEEE Transactions on Circuits and Systems, IEEE, v. 38, n. 7, p. 720–730, 1991. Citado na página 58.

DATTARAY, P.; WALL, P.; TERZIJA, V.; MOHAPATRA, P.; YU, J. Impact of location and composition of dynamic load on the severity of ssr in meshed power systems. In: IEEE. 2017 IEEE Manchester PowerTech. [S.l.], 2017. p. 1–6. Citado na página 108.

DEPARTMENT, E. G. Grid Analysis Software. [S.l.], 2017. (*in Portuguese*). Citado 2 vezes nas páginas 109 and 142.

DÖRFLER, F.; JOVANOVIĆ, M. R.; CHERTKOV, M.; BULLO, F. Sparsity-promoting optimal wide-area control of power networks. IEEE Transactions on Power Systems, IEEE, v. 29, n. 5, p. 2281–2291, 2014. Citado na página 62.

DYNAMIC Models for TurbineGovernors in Power System Studies. [S.l.], 2013. Citado na página 108.

FARROKHIFARD, M. M.; HATAMI, M.; VENKATASUBRAMANIAN, V. M.; TORRESAN, G.; PANCIATICI, P.; XAVIER, F. Clustering of power system oscillatory modes using dbscan technique. In: IEEE. 2019 North American Power Symposium (NAPS). [S.l.], 2019. p. 1–6. Citado 2 vezes nas páginas 63 and 64.

FREEMAN, L. C. Centrality in social networks conceptual clarification. Social networks, North-Holland, v. 1, n. 3, p. 215–239, 1978. Citado na página 69.

FREY, B. J.; DUECK, D. Clustering by passing messages between data points. science, American Association for the Advancement of Science, v. 315, n. 5814, p. 972–976, 2007. Citado 4 vezes nas páginas 78, 79, 82, and 84.

GLOBAL Energy Review 2021. [S.l.], 2021. Citado 2 vezes nas páginas 8 and 20.

GOMEZ, O.; RIOS, M. A. Real time identification of coherent groups for controlled islanding based on graph theory. IET Generation, Transmission & Distribution, IET, v. 9, n. 8, p. 748–758, 2015. Citado na página 62.

GORBUNOV, A.; DYMARSKY, A.; BIALEK, J. Estimation of parameters of a dynamic generator model from modal pmu measurements. IEEE Transactions on Power Systems, IEEE, v. 35, n. 1, p. 53–62, 2019. Citado na página 96.

GORBUNOV, A.; PENG, J. C.-H.; BIALEK, J. W.; VOROBEV, P. Can center-of-inertia model be identified from ambient frequency measurements. IEEE Transactions on Power Systems, IEEE, 2022. Citado na página 96.

GORE, R.; KANDE, M. Analysis of wide area monitoring system architectures. In: 2015 IEEE International Conference on Industrial Technology (ICIT). [S.l.: s.n.], 2015. p. 1269–1274. Citado 2 vezes nas páginas 8 and 21.

GUO, J.; WANG, X.; OOI, B.-T. Online purely data-driven estimation of inertia and center-of-inertia frequency for power systems with vsc-interfaced energy sources. International Journal of Electrical Power & Energy Systems, Elsevier, v. 137, p. 107643, 2022. Citado na página 99.

Guo, T.; Milanovic, J. V. Online identification of power system dynamic signature using pmu measurements and data mining. IEEE Transactions on Power Systems, v. 31, n. 3, p. 1760–1768, 2016. Citado 3 vezes nas páginas 63, 64, and 66.

HATZIARGYRIOU, N.; MILANOVIC, J.; RAHMANN, C.; AJJARAPU, V.; CANIZARES, C.; ERLICH, I.; HILL, D.; HISKENS, I.; KAMWA, I.; PAL, B.; POURBEIK, P.; SANCHEZ-GASCA, J.; STANKOVIC, A.; CUTSEM, T. V.; VITTAL, V.; VOURNAS, C. Definition and classification of power system stability revisited and extended. IEEE Transactions on Power Systems, v. 36, n. 4, p. 3271–3281, 2021. Citado 2 vezes nas páginas 8 and 27.

Henneaux, P.; Ciapessoni, E.; Cirio, D.; Cotilla-Sanchez, E.; Diao, R.; Dobson, I.; Gaikwad, A.; Miller, S.; Papic, M.; Pitto, A.; Qi, J.; Samaan, N.; Sansavini, G.; Uppalapati, S.; Yao, R. Benchmarking quasi-steady state cascading outage analysis methodologies. In: 2018 IEEE International Conference on Probabilistic Methods Applied to Power Systems (PMAPS). [S.l.: s.n.], 2018. p. 1–6. Citado na página 62.

IEEE Standard for Synchrophasor Data Transfer for Power Systems. IEEE Std C37.118.2-2011 (Revision of IEEE Std C37.118-2005), p. 1–53, 2011. Citado na página 109.

JAMES, G.; WITTEN, D.; HASTIE, T.; TIBSHIRANI, R. An introduction to statistical learning. [S.l.]: Springer, 2013. v. 112. Citado na página 68.

KAMALI, S.; AMRAEE, T.; CAPITANESCU, F. Controlled network splitting considering transient stability constraints. IET Generation, Transmission & Distribution, IET, v. 12, n. 21, p. 5639–5648, 2018. Citado na página 62.

KAMWA, I.; PRADHAN, A. K.; JOÓS, G. Automatic segmentation of large power systems into fuzzy coherent areas for dynamic vulnerability assessment. IEEE Transactions on Power Systems, IEEE, v. 22, n. 4, p. 1974–1985, 2007. Citado 3 vezes nas páginas 63, 64, and 66.

KERDPHOL, T.; WATANABE, M.; NISHIKAWA, R.; TAMAKI, T.; MITANI, Y. Determining inertia of 60 hz japan power system using pmus from power loss event. In: IEEE. 2021 IEEE Texas Power and Energy Conference (TPEC). [S.l.], 2021. p. 1–5. Citado 4 vezes nas páginas 96, 98, 99, and 109.

KHALIL, A. M.; IRAVANI, R. A dynamic coherency identification method based on frequency deviation signals. IEEE Transactions on Power Systems, IEEE, v. 31, n. 3, p. 1779–1787, 2015. Citado 12 vezes nas páginas 63, 66, 75, 77, 78, 79, 82, 84, 92, 93, 94, and 144.

KHALIL, A. M.; IRAVANI, R. Power system coherency identification under high depth of penetration of wind power. IEEE Transactions on Power Systems, IEEE, v. 33, n. 5, p. 5401–5409, 2018. Citado 5 vezes nas páginas 63, 65, 66, 85, and 87.

Khan, M.; Ashton, P. M.; Li, M.; Taylor, G. A.; Pisica, I.; Liu, J. Parallel detrended fluctuation analysis for fast event detection on massive PMU data. IEEE Transactions on Smart Grid, v. 6, n. 1, Jan 2015. Citado na página 99.

KUNDUR, P.; BALU, N. J.; LAUBY, M. G. Power system stability and control. [S.l.]: McGraw-hill New York, 1994. v. 7. Citado 5 vezes nas páginas 18, 27, 28, 29, and 141.

LACKNER, C.; CHOW, J.; WILCHES-BERNAL, F.; DARVISHI, A. Voltage control performance evaluation using synchrophasor data. In: Proceedings of the 53rd Hawaii International Conference on System Sciences. [S.l.: s.n.], 2020. Citado 2 vezes nas páginas 73 and 140.

LIN, Z.; WEN, F.; DING, Y.; XUE, Y. Data-driven coherency identification for generators based on spectral clustering. IEEE Transactions on Industrial Informatics, IEEE, v. 14, n. 3, p. 1275–1285, 2017. Citado 4 vezes nas páginas 62, 63, 66, and 137.

LIN, Z.; WEN, F.; DING, Y.; XUE, Y. Wide-area coherency identification of generators in interconnected power systems with renewables. IET Generation, Transmission & Distribution, IET, v. 11, n. 18, 2017. Citado 4 vezes nas páginas 63, 65, 66, and 87.

LIN, Z.; WEN, F.; DING, Y.; XUE, Y.; LIU, S.; ZHAO, Y.; YI, S. Wams-based coherency detection for situational awareness in power systems with renewables. IEEE Transactions on Power Systems, IEEE, v. 33, n. 5, p. 5410–5426, 2018. Citado 2 vezes nas páginas 63 and 66.

LJUNG, L. System Identification: Theory for the User. [S.l.]: Prentice-Hall, 1999. Citado 5 vezes nas páginas 33, 35, 36, 39, and 41.

LUGNANI, L.; DOTTA, D. Monitoramento da constante inercial de see utilizando sincrofasores. In: Seminário Nacional de Produção e Transmissão de Energia Elétrica (XXV SNPTEE). [S.l.: s.n.], 2019. p. 1–9. Citado na página 122.

LUGNANI, L.; DOTTA, D.; LACKNER, C.; CHOW, J. Armax-based method for inertial constant estimation of generation units using synchrophasors. Electric Power Systems Research, Elsevier, v. 180, p. 106097, 2020. Citado 6 vezes nas páginas 61, 95, 96, 105, 107, and 121.

LUGNANI, L.; DOTTA, D.; PATERNINA, M. R.; CHOW, J. Real-time coherency identification using a window-size-based recursive typicality data analysis. In: 2022 IEEE International Conference on Smart Grid Synchronized Measurements and Analytics. [S.l.: s.n.], 2022. Citado na página 122.

LUGNANI, L.; JONES, M.; ALBERTO, L. F.; PEET, M.; DOTTA, D. Combining trajectory data with energy functions for improved region of attraction estimation. In: IEEE Control Systems Society Conference. [S.l.: s.n.], 2022. Citado na página 122.

LUGNANI, L.; JONES, M.; ALBERTO, L. F.; PEET, M.; DOTTA, D. Combining trajectory data with energy functions for improved region of attraction estimation (accepted). IEEE Control System Letters, 2022. Citado na página 121.

LUGNANI, L.; PATERNINA, M.; DOTTA, D.; CHOW, J.; LIU, Y. Power system coherency detection from wide-area measurements by typicality-based data analysis. IEEE Transactions on Power Systems, v. 37, n. 1, p. 388–401, 2022. Citado 8 vezes nas páginas 102, 104, 121, 137, 138, 140, 141, and 144.

LUGNANI, L.; PATERNINA, M. A. R.; DOTTA, D. Center of inertia and equivalent inertia estimation: A fully data-driven method and load contribution. Elsevier Electric Power Systems Research, 2022. Citado na página 122.

MAKOLO, P.; ZAMORA, R.; LIE, T.-T. Online inertia estimation for power systems with high penetration of res using recursive parameters estimation. IET Renewable Power Generation, Wiley Online Library, 2021. Citado 3 vezes nas páginas 96, 97, and 109.

MILANO, F. Rotor speed-free estimation of the frequency of the center of inertia. IEEE Transactions on Power Systems, IEEE, v. 33, n. 1, p. 1153–1155, 2017. Citado na página 96.

MILANO, F.; DÖRFLER, F.; HUG, G.; HILL, D. J.; VERBIČ, G. Foundations and challenges of low-inertia systems. In: IEEE. 2018 Power Systems Computation Conference (PSCC). [S.l.], 2018. p. 1–25. Citado na página 19.

MILANO, F.; ORTEGA, A. Frequency divider. IEEE Transactions on Power Systems, IEEE, v. 32, n. 2, p. 1493–1501, 2016. Citado na página 101.

NAGLIC, M. Evolving of ems scada with synchro-measurements: userneeds, challenges, and early-stage developments. In: Proceedings of The 2022 International Conference on Smart Grid Synchronized Measurements and Analytics SGSMA 2022. [S.l.: s.n.], 2022. Citado 2 vezes nas páginas 8 and 22.

NAGLIC, M.; POPOV, M.; MEIJDEN, M. A. van der; TERZIJA, V. Synchronized measurement technology supported online generator slow coherency identification and adaptive tracking. IEEE Transactions on Smart Grid, IEEE, v. 11, n. 4, p. 3405–3417, 2019. Citado 3 vezes nas páginas 63, 65, and 66.

ORTIZ-BEJAR, J.; PATERNINA, M. R. A.; ZAMORA-MENDEZ, A.; LUGNANI, L.; TELLEZ, E. Power system coherency assessment by the affinity propagation algorithm and distance correlation. Sustainable Energy, Grids and Networks, Elsevier, v. 30, p. 100658, 2022. Citado na página 121.

ORTIZ, J.; LUGNANI, L.; PATERNINA, M.; ZAMORA, A.; RAMIREZ, J.; REYES, R.; DOTTA, D.; TOLEDO, C.; ZARATE, J.; ZELAYA, F. Clustering Analytics for Power Systems Dynamics (CAPS-D). 2021. Eletronically. Disponível em: <http://148.216.38.78/cict/app/clusters/.> Citado na página 123.

PAL, B.; CHAUDHURI, B. Robust control in power systems. [S.l.]: Springer Science & Business Media, 2006. Citado 2 vezes nas páginas 75 and 108.

PAPIC, M.; EKISHEVA, S.; COTILLA-SANCHEZ, E. A risk-based approach to assess the operational resilience of transmission grids. Applied Sciences, Multidisciplinary Digital Publishing Institute, v. 10, n. 14, p. 4761, 2020. Citado na página 62.

PATERNINA, M. R. A.; ZAMORA-MENDEZ, A.; ORTIZ-BEJAR, J.; CHOW, J. H.; RAMIREZ, J. M. Identification of coherent trajectories by modal characteristics and hierarchical agglomerative clustering. Electric Power Systems Research, Elsevier, v. 158, p. 170–183, 2018. Citado 3 vezes nas páginas 63, 64, and 66.

PHURAILATPAM, C.; RATHER, Z. H.; BAHRANI, B.; DOOLLA, S. Measurement-based estimation of inertia in ac microgrids. IEEE Transactions on Sustainable Energy, IEEE, v. 11, n. 3, p. 1975–1984, 2019. Citado 3 vezes nas páginas 96, 97, and 109.

PINHEIRO, B.; LUGNANI, L.; DOTTA, D. A procedure for the estimation of frequency response using a data-driven method. In: 2021 IEEE Power Energy Society General Meeting (PESGM). [S.l.: s.n.], 2021. p. 01–05. Citado 3 vezes nas páginas 61, 105, and 122.

PINHEIRO, B.; LUGNANI, L.; DOTTA, D. Estimação da inércia regional utilizando dados ringdown e ambiente (under review). In: Congresso Brasileiro de Automática, CBA. [S.l.: s.n.], 2022. p. 1–7. Under review. Citado na página 122.

PODMORE, R. Identification of coherent generators for dynamic equivalents. IEEE Transactions on Power Apparatus and Systems, IEEE, n. 4, p. 1344–1354, 1978. Citado 2 vezes nas páginas 62 and 94.

Raak, F.; Susuki, Y.; Hikihara, T. Data-driven partitioning of power networks via koopman mode analysis. IEEE Transactions on Power Systems, v. 31, n. 4, p. 2799–2808, 2016. Citado 3 vezes nas páginas 63, 64, and 66.

RAHIM, A.; LALDIN, A. Aggregation of induction motor loads for transient stability studies. IEEE transactions on energy conversion, IEEE, n. 1, p. 55–61, 1987. Citado na página 108.

RODALES, D.; ZAMORA-MENDEZ, A.; SERNA, J. A. de la O.; RAMIREZ, J. M.; PATERNINA, M. R. A.; LUGNANI, L.; MEJIA-RUIZ, G. E.; DOTTA, D. Model-free inertia estimation in bulk power grids (under review). Elsevier Electic Power Systems Research, 2022. Citado na página 122.

SAUER, P. W.; PAI, M.; CHOW, J. Power system dynamics and stability. [S.l.]: John Wiley & Sons, 2016. Citado 3 vezes nas páginas 73, 103, and 136.

SAW, J. G.; YANG, M. C.; MO, T. C. Chebyshev inequality with estimated mean and variance. The American Statistician, Taylor & Francis, v. 38, n. 2, p. 130–132, 1984. Citado na página 70.

SCHIFFER, J.; ARISTIDOU, P.; ORTEGA, R. Online estimation of power system inertia using dynamic regressor extension and mixing. IEEE Transactions on Power Systems, IEEE, v. 34, n. 6, p. 4993–5001, 2019. Citado 3 vezes nas páginas 96, 97, and 109.

SIDDIQUI, S. A.; VERMA, K.; NIAZI, K.; FOZDAR, M. Real-time monitoring of post-fault scenario for determining generator coherency and transient stability through ann. IEEE Transactions on Industry Applications, IEEE, v. 54, n. 1, p. 685–692, 2017. Citado na página 62.

SIOSHANSI, F.; PFAFFENBERGER, W. Electricity market reform: an international perspective. [S.l.]: Elsevier, 2006. Citado na página 18.

SUSUKI, Y.; MEZIC, I. Nonlinear koopman modes and power system stability assessment without models. IEEE Trans. Power Syst., v. 29, n. 2, March 2014. ISSN 0885-8950. Citado 2 vezes nas páginas 63 and 64.

TAMRAKAR, U.; GURUWACHARYA, N.; BHUJEL, N.; WILCHES-BERNAL, F.; HANSEN, T. M.; TONKOSKI, R. Inertia estimation in power systems using energy storage and system identification techniques. In: IEEE. 2020 International Symposium on Power Electronics, Electrical Drives, Automation and Motion (SPEEDAM). [S.l.], 2020. p. 577–582. Citado 2 vezes nas páginas 96 and 98.

THAKALLAPELLI, A.; HOSSAIN, S. J.; KAMALASADAN, S. Coherency and online signal selection based wide area control of wind integrated power grid. IEEE Transactions on Industry Applications, IEEE, v. 54, n. 4, p. 3712–3722, 2018. Citado 3 vezes nas páginas 63, 64, and 66.

TUTTELBERG, K.; KILTER, J.; WILSON, D. H.; UHLEN, K. Estimation of power system inertia from ambient wide area measurements. IEEE Transactions on Power Systems, IEEE, 2018. Citado 3 vezes nas páginas 96, 98, and 107.

TYURYUKANOV, I.; POPOV, M.; MEIJDEN, M. A. V. D.; TERZIJA, V. Slow coherency identification and power system dynamic model reduction by using orthogonal structure of electromechanical eigenvectors. IEEE Transactions on Power Systems, IEEE, 2020. Citado na página 62.

TYURYUKANOV, I.; POPOV, M.; MEIJDEN, M. A. V. D.; TERZIJA, V. Slow coherency identification and power system dynamic model reduction by using orthogonal structure of electromechanical eigenvectors. IEEE Transactions on Power Systems, IEEE, 2020. Citado na página 62.

WALL, P.; TERZIJA, V. Simultaneous estimation of the time of disturbance and inertia in power systems. IEEE Trans. Power Del., v. 29, n. 4, 2014. Citado na página 96.

WANG, B.; YANG, D.; CAI, G.; MA, J.; CHEN, Z.; WANG, L. Online inertia estimation using electromechanical oscillation modal extracted from synchronized ambient data. Journal of Modern Power Systems and Clean Energy, v. 10, n. 1, p. 241–244, 2022. Citado 2 vezes nas páginas 96 and 98.

Wang, C. G.; Zhang, B. H.; Hao, Z. G.; Shu, J.; Li, P.; Bo, Z. Q. A novel real-time searching method for power system splitting boundary. IEEE Transactions on Power Systems, v. 25, n. 4, p. 1902–1909, 2010. Citado na página 62.

WANG, S.; LU, S.; ZHOU, N.; LIN, G.; ELIZONDO, M.; PAI, M. Dynamic-feature extraction, attribution, and reconstruction (dear) method for power system model reduction. IEEE transactions on power systems, IEEE, v. 29, n. 5, p. 2049–2059, 2014. Citado na página 62.

WILSON, D.; YU, J.; AL-ASHWAL, N.; HEIMISSON, B.; TERZIJA, V. Measuring effective area inertia to determine fast-acting frequency response requirements. International Journal of Electrical Power & Energy Systems, Elsevier, v. 113, p. 1–8, 2019. Citado 4 vezes nas páginas 96, 97, 109, and 116.

WU, X.; DÖRFLER, F.; JOVANOVIĆ, M. R. Input-output analysis and decentralized optimal control of inter-area oscillations in power systems. IEEE Transactions on Power Systems, IEEE, v. 31, n. 3, p. 2434–2444, 2015. Citado na página 62.

YANG, D.; WANG, B.; CAI, G.; CHEN, Z.; MA, J.; SUN, Z.; WANG, L. Data-driven estimation of inertia for multi-area interconnected power systems using dynamic mode decomposition. IEEE Transactions on Industrial Informatics, IEEE, 2020. Citado 3 vezes nas páginas 96, 97, and 109.

YANG, D.; WANG, B.; MA, J.; CHEN, Z.; CAI, G.; SUN, Z.; WANG, L. Ambient-data-driven modal-identification-based approach to estimate the inertia of an interconnected power system. IEEE Access, IEEE, v. 8, p. 118799–118807, 2020. Citado 2 vezes nas páginas 96 and 98.

YOU, H.; VITTAL, V.; WANG, X. Slow coherency-based islanding. IEEE Transactions on power systems, IEEE, v. 19, n. 1, p. 483–491, 2004. Citado na página 62.

YOU, S.; LI, H.; LIU, S.; SUN, K.; WANG, W.; QIU, W.; LIU, Y. Calculate center-of-inertia frequency and system rocof using pmu data. arXiv preprint arXiv:2010.12381, 2020. Citado na página 96.

ZENG, F.; ZHANG, J.; CHEN, G.; WU, Z.; HUANG, S.; LIANG, Y. Online estimation of power system inertia constant under normal operating conditions. IEEE Access, IEEE, v. 8, p. 101426–101436, 2020. Citado 2 vezes nas páginas 96 and 99.

ZHANG, J.; XU, H. Online identification of power system equivalent inertia constant. IEEE Transactions on Industrial Electronics, IEEE, v. 64, n. 10, 2017. Citado 2 vezes nas páginas 96 and 98.

ZHANG, Y.; MARKHAM, P.; XIA, T.; CHEN, L.; YE, Y.; WU, Z.; YUAN, Z.; WANG, L.; BANK, J.; BURGETT, J. et al. Wide-area frequency monitoring network (fnet) architecture and applications. IEEE Transactions on smart grid, IEEE, v. 1, n. 2, p. 159–167, 2010. Citado 2 vezes nas páginas 75 and 89.

ZHAO, J.; TANG, Y.; TERZIJA, V. Robust online estimation of power system center of inertia frequency. IEEE Transactions on Power Systems, IEEE, v. 34, n. 1, p. 821–825, 2018. Citado na página 96.

Znidi, F.; Davarikia, H.; Arani, M.; Barati, M. Coherency detection and network partitioning based on hierarchical dbscan. In: 2020 IEEE Texas Power and Energy Conference (TPEC). [S.l.: s.n.], 2020. p. 1–5. Citado na página 66.

ZNIDI, F.; DAVARIKIA, H.; IQBAL, K. Modularity clustering based detection of coherent groups of generators with generator integrity indices. In: IEEE. 2017 IEEE Power & Energy Society General Meeting. [S.l.], 2017. p. 1–5. Citado na página 63.

ZOGRAFOS, D.; GHANDHARI, M.; PARIDARI, K. Estimation of power system inertia using particle swarm optimization. In: IEEE. Intelligent System Application to Power

Systems (ISAP), 2017 19th International Conference on. [S.l.], 2017. Citado 3 vezes nas páginas 96, 97, and 109.

APPENDIX A – Appendix: Recursive TDA

A.1 Fundamentals

A.1.1 Coherency

Coherency is defined as the behavior of generators swinging together in response to a disturbance (CHOW, 2013), with minimal distances between their responses. This swing behavior can be observed in angle (δ) and frequency (f) measurements; likewise it can be derived from the linearized model analysis where the frequency of oscillatory modes and their participation factors indicate which generators are coherent to each other. Both approaches can be extended to non-generation buses and become less clear as the size of the system and the number of connections increase. In this scenario, a cut-off constant (γ) based on operator knowledge is used to determine the maximum distance that a bus must have to belong to a given group. This can be seen in (A.1) for frequency measurements:

$$f_i(t) - f_j(t) \leq \gamma \tag{A.1}$$

For a window of angle measurements or frequency signals, there are several ways to approach the assessment of coherency. One can calculate the difference at every instant, making the tuning of the cut-off constant much more sensible to transitory periods and noise. Or a distance metric can be also define as the best to represent the distance among two signals over a window length, making the tuning of γ easier. However, the determination of the window length becomes crucial as the distance will also alter as the window expands or contracts. For the determination of coherency over ringdown disturbances, the incorrect choice of the window length may impact the determination of coherent groups. Usually, windows are determined considering the slowest known inter-area mode of oscillation of the system, where the length of the window is set to twice the period of that mode. However, this means windows of at least 2.2 seconds, as the fastest inter-area mode has a 1.1 second period, up to 10 seconds, considering the slowest modes. This delay may be prohibitive for applications that would require fast action, such as area coordinated damping controls (SAUER et al., 2016).

The distance $d(i, j, t)$ between the frequency measurements f_i and f_j can be measured in several ways, such as the absolute distance, Euclidean distance, the Frechet distance, the cosine dissimilarity, among many others and a combination of more than one (LIN et al., 2017a). This is also a dependent choice on the operator knowledge and can impact the clustering of buses, specially regarding the sensitivity of the consequential clustering method. It deals with with appropriate filtering of signal to increase the signal-to-noise ratio (SNR) and the proper adjustment of the size of the data set, that is, the window length.

A.1.2 TDA

The TDA approach is a data-driven method derived from empirical data analysis (ANGELOV et al., 2017) that approximates the probability mass function (PMF) of the data exclusively from the data themselves and a distance metric in accordance with the type of data measured, without any previous assumption of the distribution type (e.g., Gaussian, Logistic, Weibull, etc), nor number of modes, i.e., how many distribution means the data possess. To approximate the PMF, some properties must be calculated, but first a distance metric between the points must be defined.

In (LUGNANI et al., 2022d), the TDA method is calculated for a fixed window T of frequency measurements. Here, the recursive form will be presented, where the following properties are calculated at every new measurement K. As the interest is the coherency between measured signals, in other words the distance between signals, the Euclidean distance is used:

$$d(i,j,t) = \sqrt{(f_i(t) - f_n)^2 - (f_j(t) - f_n)^2} \tag{A.2}$$

where $f_i(t)$ and $f_j(t)$ are frequency measurements at the time instant t, f_n is the system nominal frequency, and $d(i,j,t)$ is the distance metric between frequencies at the same time instant.

Next, three properties are calculated that lead to the value of the typicality τ, which as it approximates the PMF. These properties are: *i)* cumulative proximity; *ii)* eccentricity and *iii)* density. These properties are important as they are used for construction of the approximate PMF as equivalents to the statistical moments and at the clustering stage of the method, as the guarantee of the points, i.e. buses, belonging to a group is given by the Chebyshev inequality, where the eccentricity is used as a measure of anomaly within a group.

The first property, cumulative proximity $q(b_i)$, is given as follows:

$$q(b_i) = \sum_{j=1}^{N} d^2(f_i, f_j) \tag{A.3}$$

where N is the number of measuring points available. $q(f_i)$ is a scalar that represents the *total distance* of a point within a distribution based solely on the chosen metric or compound of metrics and b_i is a point in the data set, which can be for example the norm of the frequency at bus i for a given window of length T, or the vector of the norms of the distance between f_i to every other bus. However, $q(b_i$ can also be recursively calculated at every instant K as:

$$q_K(b_i) = q_{K-1}(b_i) + d^2(b_i, b_j) \tag{A.4}$$

in which case we can consider b_i solely as the measurement of angle or frequency at bus i at instant K. For the Euclidean distance, (ANGELOV; GU, 2019) shows that the recursive proximity can be calculated as:

$$q_K(b_i) = K(\|b_i - \mu_K\|^2 + X_K - \|\mu_K\|^2) \tag{A.5}$$

where μ_K and X_K are the means of the set b_K and $b^T b_K$, respectively, and both of them can be updated recursively as follows:

$$\mu_K = \frac{K-1}{K}\mu_{K-1} + \frac{1}{K}b_{\forall i,K} \tag{A.6}$$

$$X_k = \frac{K-1}{K}X_{K-1} + \frac{1}{K}\|b_{\forall i,K}\|^2 \tag{A.7}$$

Once this property is calculated recursively, all following properties can be updated at every new acquired measurement, in contrast to (LUGNANI et al., 2022d), where the properties are calculated once for the whole batch of measurements from the moment of disturbance up to $T = 10$. This recursive approach will become beneficial when we calculate the typicallity as K increases and we observe its values reaching stability earlier than $T = 10$.

The second property is the eccentricity, which is a measurement of anomaly within the data set. Here, we show the normalized form of the eccentricity, ϵ:

$$\epsilon_K(b_i) = \frac{2q_K(b_i)}{\frac{1}{K}\sum_{j=1}^{N} q_K(b_j)} \tag{A.8}$$

For the case where the distance matrix is Euclidean, the eccentricity can be calculated as:

$$\epsilon_K(b_i = 1 + \frac{\|b_i - \mu_K\|^2}{\sigma_K^2} \tag{A.9}$$

where σ_K is the standard deviation, $\sigma_K = \sqrt{X_K - \mu_K^2}$

The normalized eccentricity is a very important metric because it indicates the points that are away from the peak of the data distribution. Hence, it can be used to find the tails of each mode in the distribution, or in our case, the buses that are borderline part of a given coherent group. If we recall the Chebyshev inequality for the Euclidean distance:

$$P(\|\mu_K - b_i\|^2 > n^2\sigma_K^2) < \frac{1}{n^2} \tag{A.10}$$

where n is the number of times the standard deviation away from the global mean is being analyzed for b_i. Using the standardized eccentricity, the Chebyshev inequality can be reformulated of the form:

$$P(\epsilon_K(b_i) > n^2 + 1) < \frac{1}{n^2} \tag{A.11}$$

With this expression, it can be said that, there is a smaller than $\frac{1}{9}$ probability of $\epsilon_k(b_i \geq 10$, for $n = 3$, which is a widely used condition for anomaly/tail detection. Furthermore, if the data distribution is Gaussian (which is not imposed by the TDA method), the probability of $\epsilon_k(b_i \geq 10$, for $n = 3$ is less than 0.3%. This property is crucial for the clustering of buses without dependence on operator knowledge for setting a cut-off constant γ.

Next, we introduce the third property, the data density D_K, which is calculated as:

$$D_K(b_i) = \frac{1}{\epsilon_K(b_i)} \tag{A.12}$$

Data density is the inverse of the eccentricity and data points that are closer to the mean have higher density values. The value of the data density evaluated at a particular data sample indicates how strongly this particular data sample is influenced by the other data samples in the data space due to their mutual proximity and attraction. It is also inversely proportional to the square distance between these two data samples.

The last calculated property is the typicality τ, given as:

$$\tau_K(b_i) = \frac{D_K(b_i)}{\sum_{j=1}^{N} D_K(b_j)} \tag{A.13}$$

Analogously to the PMF, all points b_i have $\tau(b_i$ within $(0, 1]$, and the sum of all typicalities of the points of the distribution is equal to 1. However, since PMF

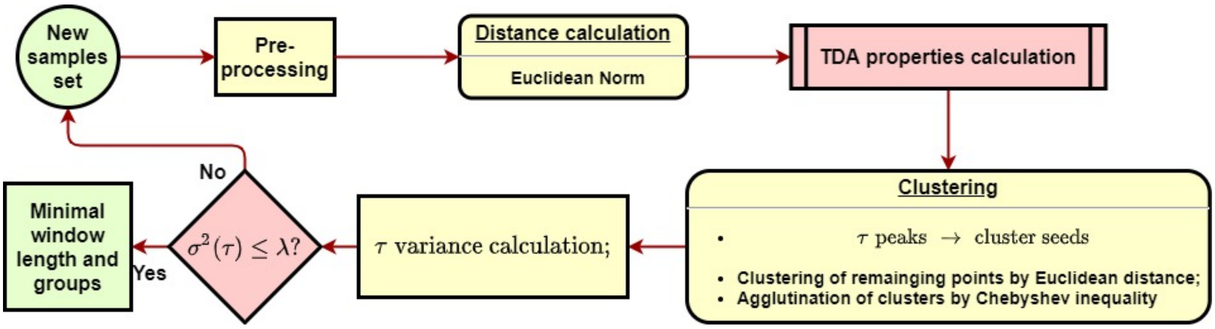

Figure A.1 – Recursive TDA methodology

is imposed to the data, it can have non-zero values for infeasible variable values (e.g., negative frequency), because characteristics of the variables are assumed prior to the data set. The points with higher typicality are the ones closer to the peak of the distribution, similar to PMFs like say, the tip of the bell curve for Gaussian distribution.

Once the properties are calculated, the clustering of buses is performed. With the recursive form of the TDA method, its properties and the clustering is done at every new measurement. The clustering process of the TDA method and more details of the method can be seen in (LUGNANI et al., 2022d). Next, the methodology for calculating the window length is presented, using the TDA method.

A.2 Methodology

The proposed methodology is presented in Fig. A.1. It is calculated for every new batch of PMU measurements received until the point where the variance condition is attended. The minimal data sample is $5 \times N$ due to the filtering process, where N is the number of PMUs available.

The first stage of the methodology is a pre-processing step to increase the SNR. As frequency measurements of PMUs are derived from voltage phasor angle measurements unrealistic spikes due to non-electromechanical phenomena may appear in both angle and frequency signals. To remove this effect, the first filter applied to the signals is a moving median filter, with a 5-sample window. Next, the DC offset is removed and the resulting signal is detrended with the dynamics separation algorithm (LACKNER et al., 2020).

The second step is the calculation of the distance, using (A.2) to form a metric of the measurements distribution. With the points and their distances, it is possible to the calculate the TDA cumulative proximity ($q(b_i)$ (A.3)), normalized eccentricity ($\epsilon_K(b_i)$ (A.8)), density ($D_K(b_i)$ (A.12)) and typicality ($\tau_K(b_i)$ (A.13)) properties. Starting at the second iteration of the methodology, $q(b_i)$ and $\epsilon_K(b_i)$ can be recursively calculated using (A.5), (A.6), (A.7) and (A.9), respectively.

The third step is the clustering algorithm which uses the Chebyshev algorithm as a cut-off proxy in substitution of an user dependent constant. The clustering algorithm firstly ranks the points' typicalities by their Euclidean distances, starting from the highest typicality value. This creates a global distribution of typicalities based on their proximity and peaks of typicality are formed, if the distribution is multi-modal, indicating the existence of those modes. The peaks in the typicalities distribution are addressed as seeds of clusters C_m. Each cluster seed/peak receives its closest points by Euclidean distance, where the mean and standard deviation of each cluster C_m are computed. If a point is equally distant from two clusters, the point is addressed to the most likely cluster by the Chebyshev criterion, using the eccentricity of the point. After all clusters are formed and their first statistical moments are known, each C_m is compared via Chebyshev inequality for a tail of 3σ with their mean values and the highest typicality of each cluster. If their means are closer than 2σ, the cluster with highest typicality agglutinates the other, repeating the process until the number of cluster remains the same. More details regarding this algorithm can be seen in (LUGNANI et al., 2022d).

At each iteration K, the variance of the typicalities var_k is also calculated as:

$$var_K(C_m) = \frac{\sum_{i=1}^{M}(\tau_i - \overline{\tau})^2}{M} \tag{A.14}$$

where $var_K(C_m)$ is the variance of cluster C_m at the instant K, M is the number of points in C_m and $\overline{\tau}$ is the mean of the typicalities at C_m. Finally, if $var_K(C_m)$, for every cluster, remains unaltered, say $\lambda = 0.5s$, then the method converged to the coherent groups/clusters, with a window of length K. Otherwise, the method is repeated for the next batch of samples at $t = K + 1$.

The proposed methodology generates a size controlled window iteration process, illustrated in Figure A.2 for bus 9 from Kundur 2-Area test system, where for new samples the method in Figure A.1 is repeated until the variance criteria is satisfied.

Next, we show the application of the proposed methodology to the Kundur test system, and discuss the characteristics of the work.

A.3 Results

The method is now applied to the 2-area Kundur system. The parameters of the system are the same as in (KUNDUR et al., 1994), shown in Figure A.3. This is a system with symmetrically well defined groups, due to its topology, and with a boundary bus (bus 8) that can be addressed to any group, depending on the tuning of the chosen coherency detection method. The groups are shown in Table A.1.

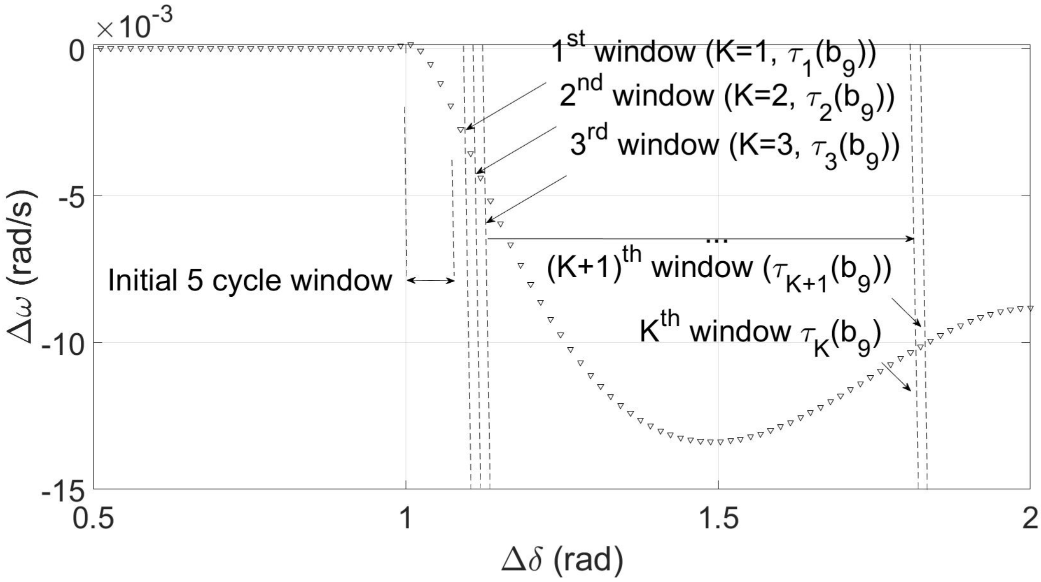

Figure A.2 – Size controlled window

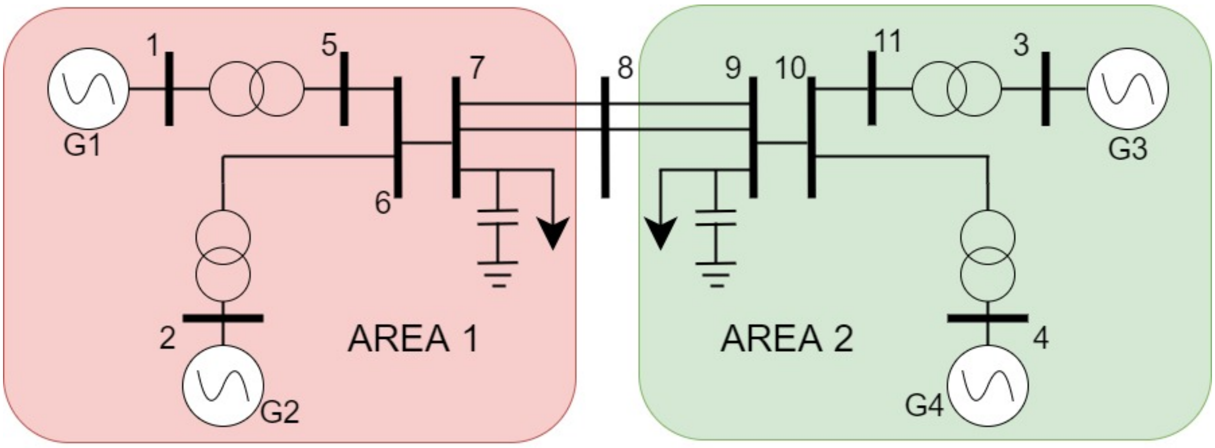

Figure A.3 – KundurTestSystem

Table A.1 – Groups in the 2-area Kundur system.

	Buses
Group 1	1,2,5,6,7,8
Group 2	3,4,9,10,11

The simulations were performed using the ANATEM software from CEPEL (DEPARTMENT, 2017), and the recursive TDA method was implemented with MATLAB R2018a, on an Intel Core i7-8850U 2.00 GHz processor with 8 GB of memory. To examine the proposed method, a 100 MW step is applied to bus 9 at 1 second which is the bus with highest load, in order to excite the ocillatory modes to be captured. The frequency response for all buses is presented in Fig. A.4.

The methodology is applied to the frequency signals starting with 5 cycles due to the move median filter. The first set of calculated typicalities is shown in Fig. A.5,

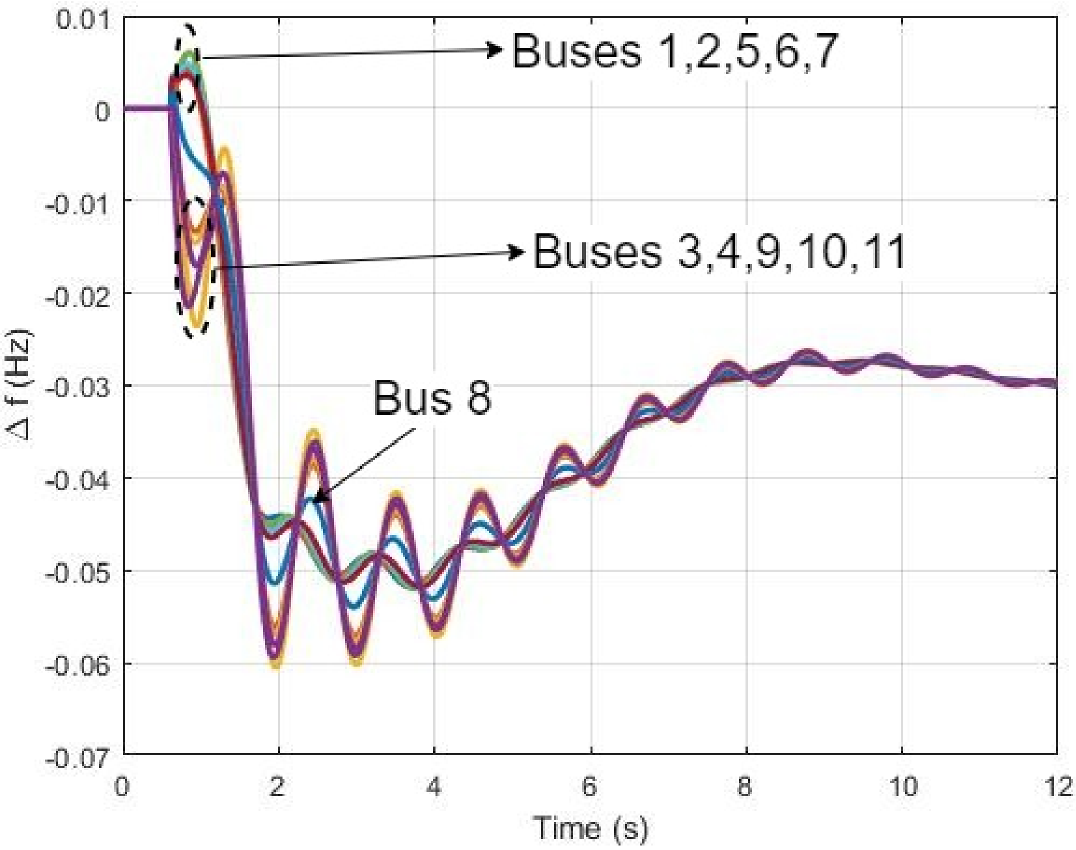

Figure A.4 – Frequency response of the Kundur test system to 100 MW step at bus 9.

where the blue group is the group of generators 1 and 2, as reference. Note that the initialization of the method and the lack of information as electromechanical phenomena takes seconds to develop, the groups are incoherent, according to the coherency concept and the system topology.

However, as time evolves and new samples are provided, the distribution of the data becomes more consistent with the coherent groups of the system, as shown in Fig. A.6. We can see that, even though the values of the typicalities oscillate, their values remain close to each other after a few seconds.

Figure A.6 also shows the highest values of typicality in each group, namely buses 5 and 10. As the highest value of typicality represents the point closest to the mean of the distribution in such group, this bus can be interpreted as the center of the coherent group, since the mean of the distribution would represent the mean of the coherent response observed in frequency signals of the group. It is also interesting to note that the center buses of each group are not symmetrically equivalent, as in Area 2 the center bus is closer to the point of the fault.

Furthermore, Figure A.6 reiterate the results corresponding to slow coherency

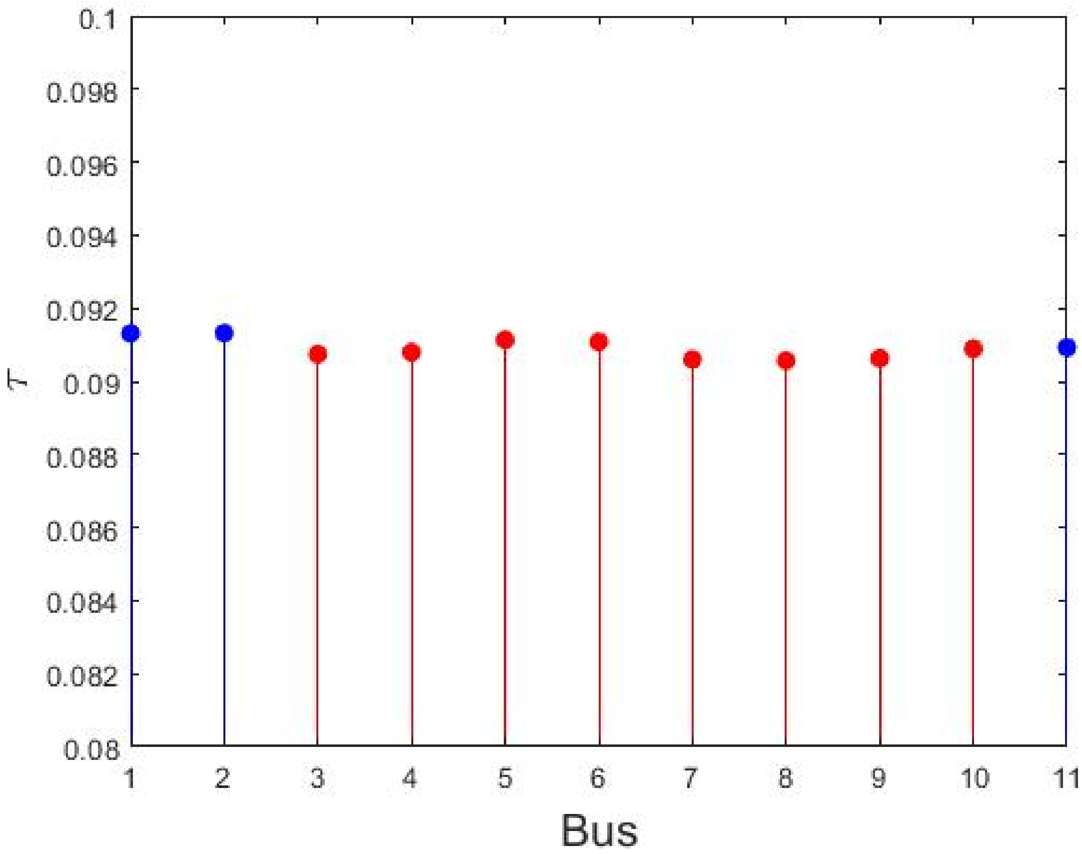

Figure A.5 – First set of typicalities.

clustering algorithm in (CHOW; SANCHEZ-GASCA, 2020), where eigenvectors associated with the inter-area frequency modes are computed and the mode shapes are used to form the slow coherency groups of generator and buses. However, due to the tail criterion of the TDA method, i.e. Chebyshev inequality, bus 8 is addressed to Area 1, whereas in (CHOW; SANCHEZ-GASCA, 2020) the bus is left outside any group. Note that, depending on the disturbance, the areas using recursive TDA may change, as the window length, contrary to slow coherency method, which considers the power system linear model, hence the areas remain constant for the same operating condition.

This behavior can be clearly seen in Fig. A.7, where after about 2.5 seconds, the variance of the groups remains stable. Considering that the disturbance is applied at 1 second, the resulting difference is of 1.5 seconds. This is in accordance with the frequency of the inter-area mode of the system, which is of 0.545 Hz, with a period of approximately 1.8 second. This points to the fact that a window length of two times the period of the the slowest known inter-area mode of the system, as used in (LUGNANI et al., 2022d; KHALIL; IRAVANI, 2015) may be overzealous. For this methodology, the window length necessary would be of 1.5 seconds, plus the additional 0.5 seconds for assertion of the variance criterion, that is, a window length of 2 seconds.

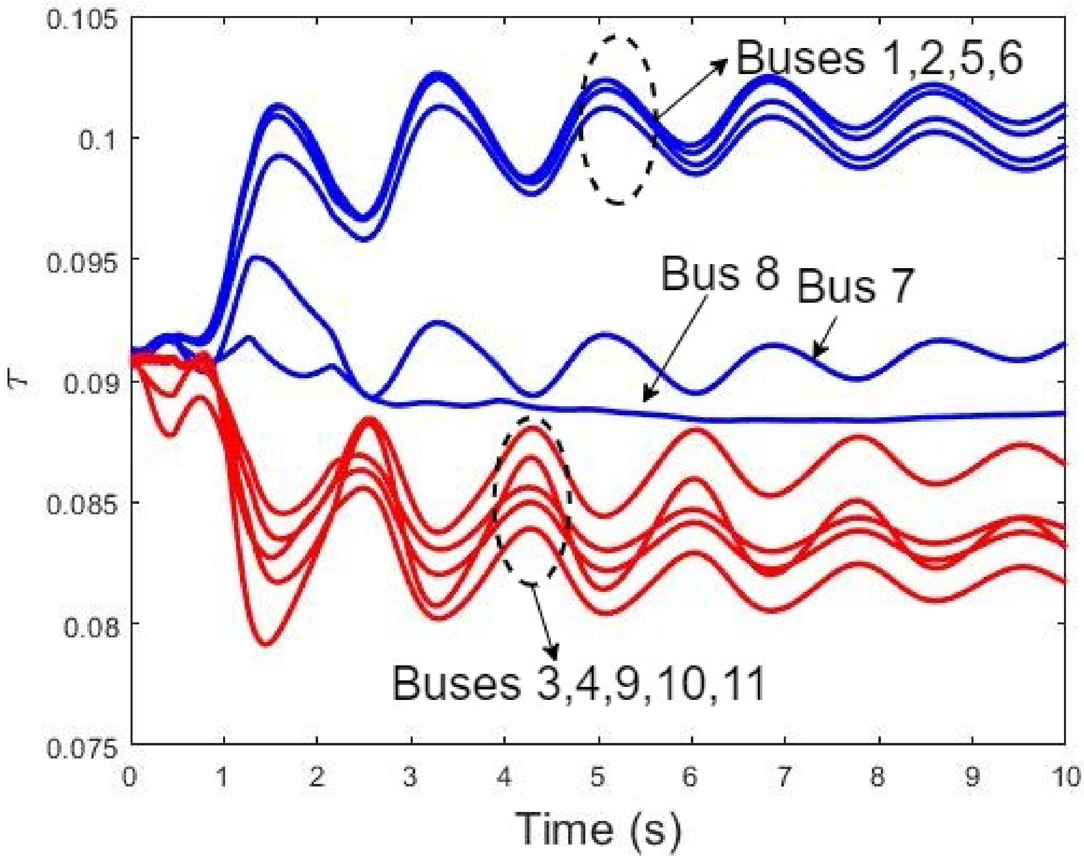

Figure A.6 – Evolution of typicalities.

It is important to note that the size of the window length may vary, according to the system or the system configuration itself. For instance, a bigger system with more modes, or a system with a slower mode may tend to have a different window length to accommodate the minimal information necessary in the signals.

A.4 Conclusion

This work has demonstrated that the recursive tipicality data analysis can be successfully implemented by using an adaptive window-size. Thus, the proposition of a recursive form of the TDA coherency detection method does not depend on an initial guess of the number of groups, its central points, neither an arbitrary cut-off constant. This is thanks to the recursive form removes the necessity of window length determination by the user, through the analysis of the variance of the typicalities within each group. The proposed method is applied to the Kundur test system to confirm its effectiveness and performance.

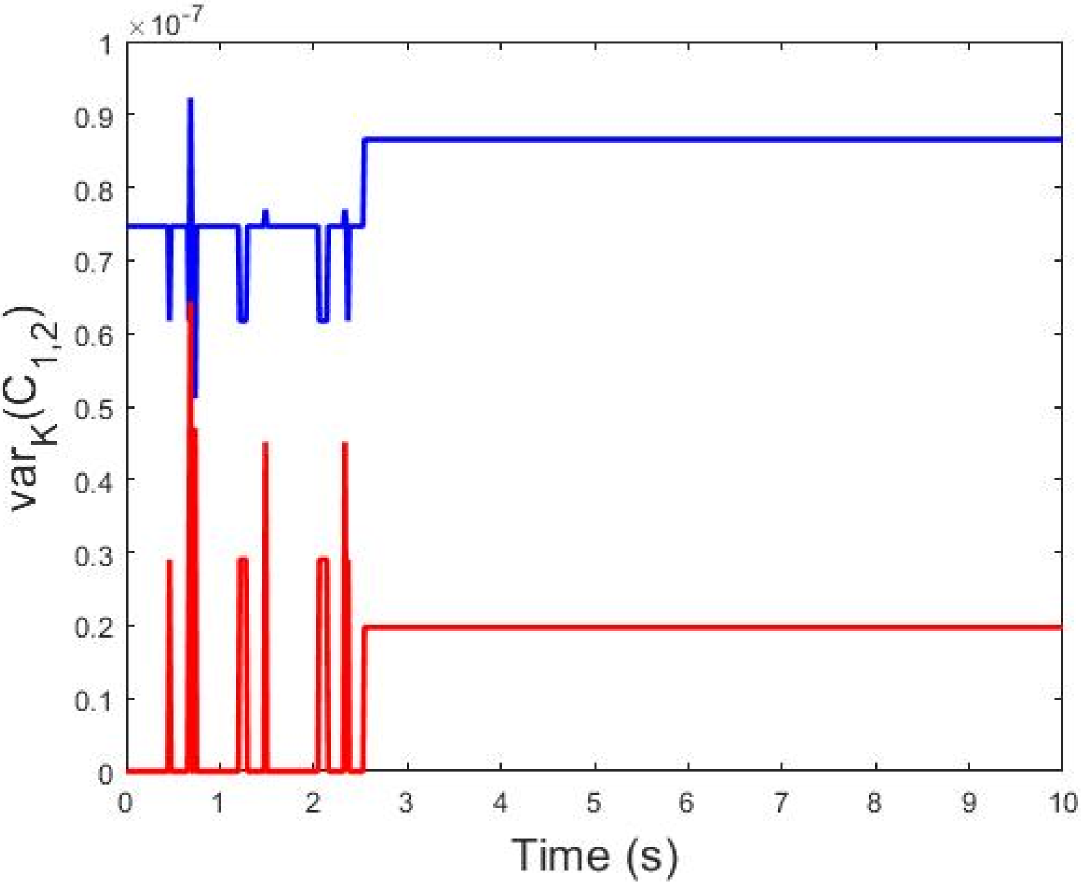

Figure A.7 – Variance of typicalities.